Sede Amministrativa: Università degli Studi di Padova

Dipartimento di Tecnica e Gestione dei Sistemi Industriali

SCUOLA DI DOTTORATO DI RICERCA IN:

INGEGNERIA INDUSTRIALE

INDIRIZZO: MECCATRONICA E SISTEMI INDUSTRIALI

XXII CICLO

EXPERIMENTAL AND NUMERICAL ANALYSIS OF WELDING AND HEAT TREATMENT OF DUPLEX STAINLESS STEELS

Direttore della Scuola: *Ch.mo Prof. Paolo F. Bariani*
Coordinatore d'indirizzo: *Ch.mo Prof. Alberto Trevisani*
Supervisore: *Ch.mo Prof. Franco Bonollo*

Dottorando: *Riccardo Cervo*

1 FEBBRAIO 2010

to my parents and to my grandfather

"Considerate la vostra semenza:
fatti non foste a viver come bruti,
ma per seguir virtute e canoscenza"

(Dante Alighieri, La divina commedia, L'inferno, Canto XXVI, vv. 118-120)

TABLE OF CONTENTS

PREFACE

This doctoral thesis is the result of three years full-time studies and researches at the University of Padova from January 2007 to December 2009. The experimental work was mostly carried out at the Department of Management and Engineering (DTG) in Vicenza. Some of the corrosion tests presented in the discussion were also performed at the "Corrosion Centre Aldo Daccò" in Ferrara during the period March-July 2009.

The principal supervisors were: Professor Franco Bonollo and Professor Alberto Tiziani.

The thesis is divided in two parts: an introduction ("State of the art"), which gives to the reader a literature and historical background on Duplex Stainless Steels and problems related to their welding processes; the second part presents a discussion of the work (with main results and conclusions) and also the following papers, referred in the text by their roman numerals:

Article I
"METALLURGICAL AND MECHANICAL CHARACTERIZATION OF UNS S32750 WELDED JOINTS WITH INNOVATIVE FILLER WIRE"
F. Bonollo, P. Ferro, R. Cervo, B. Vianello, M. Durante.
Published in "La Metallurgia Italiana", 10, 2009.

Article II
"STUDIO DELLA PRECIPITAZIONE DELL'AUSTENITE SECONDARIA E DELLA RESISTENZA A CORROSIONE IN CORDONI DI SALDATURA UNS S32750 TRATTATI TERMICAMENTE: INFLUENZA DELLA COMPOSIZIONE CHIMICA DEL MATERIALE D'APPORTO"
A. Tiziani, P. Ferro, R. Cervo, M. Bulla.
Proc. "32nd AIM National Conference", 24-26th September 2008, Ferrara, Italy.

Article III
"ANNEALING TEMPERATURE EFFECTS ON SUPER DUPLEX STAINLESS STEEL UNS S32750 WELDED JOINTS. I:MICROSTRUCTURE AND PARTITIONING OF ELEMENTS"
R. Cervo, P. Ferro, A. Tiziani.
Submitted to "Journal of Materials Science", 2009.

Article IV
"ANNEALING TEMPERATURE EFFECTS ON SUPER DUPLEX STAINLESS STEEL UNS S32750 WELDED JOINTS. II:PITTING CORROSION RESISTANCE EVALUATION"
R. Cervo, P. Ferro, A. Tiziani, F. Zucchi.
Submitted to "Journal of Materials Science", 2009.

Article V

"MODELING SIGMA PHASE PRECIPITATION IN 2205 AND 2507 DUPLEX STAINLESS STEELS - EXPERIMENTAL ANALYSIS AND NUMERICAL MODELS"
Expanded version of the paper:
"SET UP AND IMPLEMENTATION OF A NUMERICAL MODEL FOR THE SIMULATION OF HEAT TREATMENT OF DUPLEX STAINLESS STEELS"
P. Ferro, R. Cervo, F. Bonollo, R. Bertelli.
Proc. "Duplex 2007 International Conference & Expo", 18-20th June 2007, Grado, Italy.

The final part of the thesis contains other studies not mentioned above, but which have been elaborated during the PhD work, some of which are:

"CARATTERIZZAZIONE METALLURGICA E MECCANICA DI GIUNTI SALDATI IN ACCIAIO INOX UNS S32750 OTTENUTI MEDIANTE MATERIALE D'APPORTO INNOVATIVO" F. Bonollo, P. Ferro, R. Cervo, A. Lotteri, M. Durante (2008) in: Proc. "32nd AIM National Conference", 24-26th September 2008, Ferrara, Italy.

"INFLUENCE OF SOLUTION TEMPERATURE ON PITTING CORROSION RESISTANCE, MICROSTRUCTURE AND ELEMENTAL PARTITIONING OF UNS S32750 S.A. WELDED JOINTS" R. Cervo, P. Ferro, A. Tiziani, M. Bulla (2009) Oral Presentation at the "European Congress on Advanced Materials and Processes" (EUROMAT 2009), 7-10th September 2009, Glasgow, UK.

"EXPERIMENTAL AND NUMERICAL ANALYSIS OF LASER WELDING PROCESS ON ADVANCED HIGH STRENGTH STEELS" P. Ferro, A. Tiziani, R. Cervo, A. Zonato (2009) Poster Presentation at the "European Congress on Advanced Materials and Processes" (EUROMAT 2009), 7-10th September 2009, Glasgow, UK.

In addition, the following M.S. thesis have been supervised:

1. M. Beltrame, *Analisi sperimentale del trattamento termico post saldatura di acciai superduplex,* supervisors: A. Tiziani, R. Cervo, A.A. 2007/2008
2. N. Facchinelli, *Influenza della temperatura di trattamento termico su microstruttura e proprietà di resistenza alla corrosione di giunti in acciaio inossidabile SAF 2507 saldati ad arco sommerso,* supervisors: A. Tiziani, R. Cervo, A.A. 2007/2008
3. M. Pontarollo, *Studio della cinetica di precipitazione della fase sigma in laminati di acciaio inossidabile superduplex UNS S32750,* supervisors: F. Bonollo, R. Cervo, A.A. 2009/2010.

SUMMARY

Duplex and Super Duplex Stainless Steels (DSS and SDSS) are high-strength and corrosion-resistance alloys, which found application in chemical, petrolchemical, pulp, paper industries, offshore and desalination plants. Their localized corrosion behavior is an all-important facet, and is deeply altered by the thermal cycles produced by the welding operations.

The aim of this doctoral dissertation is to study experimentally and numerically the influence of welding and heat treatments on DSS and SDSS microstructure and corrosion performance, in order to optimize all the materials and processes involved in these operations. The techniques used in this work include: LOM (Light Optical Microscopy), ESEM (Environmental Scanning Electron Microscopy), EDS (Energy Dispersive Spectroscopy), optical spectroscopy, tensile tests, microhardness measurements, anodic polarization curves, weight losses corrosion tests, and finally numerical models developed in SYSWELD 11.0®.

On the base of a literature review of previously published results on DSS and SDSS welding, heat treatment and corrosion studies, new researches were carried out, and the main topics discussed in the PhD work were:

- In duplex welding, filler metals are nickel-rich to assure a more balanced microstructure. What is the impact of an innovative filler wire enriched in nickel on microstructure, mechanical and corrosion properties of SDSS welded joints?
- A post welding heat treatment is generally performed to restore the optimal corrosion properties of a SDSS welded joint; what is the impact of this annealing treatment on microstructure and pitting corrosion properties of SDSS? What is the influence of different filler metals used during welding in relation to this treatment, on microstructure and pitting corrosion properties of SDSS welded joints?
- The pitting corrosion performance of DSS and SDSS welded joints depends on some microstructural features, like ferrite/austenite ratio and chemical composition of phases (to calculate the PREN -*pitting resistance equivalent number*- of ferrite and austenite). What is the most important factor which determines the final pitting corrosion behavior? Does a more balanced microstructure gives a better pitting corrosion behavior or does it depend on chemical composition of the phases?
- The phase compositions depend on the temperature. In which manners does the post welding treatment temperature influence the pitting corrosion performance of a SDSS welded joint? Development of a correlation between microstructure and experimental pitting behavior.
- SDSS are more corrosion-resistant but also more prone to precipitation of detrimental phases than DSS. What is the tendency of these alloys to secondary phases formation in relation to isothermal and continuos cooling treatments? Setting-up of a numerical model to predict the final microstructure of DSS and SDSS in relation to these treatments.

For future stainless steels development, the availability of satisfactory correlations between composition, microstructure and properties are essential to optimize alloy design.

The study of welding of Duplex Stainless Steels has lead, during the PhD work, to the experimental and numerical analysis of welding on other materials. These activities are illustrated in the final part of the thesis.

SOMMARIO

Gli acciai Duplex e Super Duplex sono leghe inossidabili caratterizzate da elevata resistenza meccanica e alla corrosione. Essi trovano applicazione soprattutto nell'industria chimica, petrolchimica, della carta e negli impianti offshore e di desalinizzazione. La loro resistenza alla corrosione localizzata è un aspetto essenziale, ed è profondamente alterato dai cicli termici imposti dalle operazioni di saldatura.

Lo scopo della presente tesi di dottorato è lo studio, sperimentale e numerico, dell'influenza di diversi processi di saldatura e trattamento termico sulla microstruttrura e il comportamento a corrosione di acciai Duplex e Super Duplex, in modo da ottimizzare tutti i materiali e i processi coinvolti in queste operazioni. Le tecniche utilizzate in questo lavoro prevedono: microscopia ottica (LOM), microscopia elettronica a scansione (ESEM), spettroscopia a dispersione di energia (EDS), spettroscopia ottica, test di trazione, misure di microdurezza, curve di polarizzazione anodica, test di corrosione gravimetrici, e modelli numerici sviluppati in SYSWELD 11.0®.

Sulla base di una recensione dei risultati pubblicati in letteratura riguardo saldatura, trattamento termico e proprietà di resistenza alla corrosione di acciai Duplex e Superduplex, sono state condotte nuove ricerche, cercando di approfondire i seguenti argomenti:

- Nella saldatura di acciai Duplex, i metalli d'apporto utilizzati sono arricchiti in nichel, per garantire una microstruttura finale più bilanciata. Qual è l'impatto di un filo innovativo arricchito in nichel sulla microstruttura, sulle proprietà meccaniche e di resistenza alla corrosione di giunti in acciaio Super Duplex?
- Per ristabilire le ottime proprietà di resistenza alla corrosione dei giunti saldati in acciaio Super Duplex, è generalmente previsto un trattamento post-saldatura; qual è l'impatto di questo trattamento sulla microstruttura e sulle proprietà di resistenza alla corrosione per pitting di giunti in Super Duplex? Qual è l'influenza di diversi metalli d'apporto utilizzati in saldatura, sulla microsrtuttura e sulla resistenza alla corrosione per pitting, in relazione a questo trattamento?
- Il comportamento a corrosione per pitting degli acciai Duplex e Super Duplex dipende da alcune caratteristiche microstrutturali, quali il rapporto ferrite/austenite e la composizione chimica delle singole fasi (che permette di calcolare il PREN - *pitting resistance equivalent number*). Qual è il fattore determinante per le proprietà di resistenza alla corrosione per pitting? Può una microstruttura più bilanciata garantire una miglior prestazione a pitting o il comportamento a corrosione dipende dalla composizione chimica delle fasi?
- La composizione delle fasi dipende dalla temperatura. In che modo la temperatura di trattamento termico post-saldatura influenza le proprietà di resistenza a pitting dei giunti saldati in acciaio Super Duplex? Sviluppo di una correlazione tra microstruttura e comportamento a pitting ricavato sperimentalmente.

- Gli acciai Super Duplex, avendo un maggior contenuto di elementi in lega degli acciai Duplex, garantiscono un miglior comportamento a corrosione, ma allo stesso tempo sono più inclini alla precipitazione di fasi secondarie dannose. Qual è la tendenza di queste leghe alla formazione di fasi secondarie in relazione a trattamenti isotermi e a raffreddamento controllato? Implementazione di un modello numerico per predire la microstruttura finale di acciai Duplex e Super Duplex in relazione a questi trattamenti.

Per lo sviluppo futuro degli acciai inossidabili, risulta essenziale disporre di correlazioni tra microstruttura, composizione chimica e proprietà, in modo ottimizzare la progettazione delle suddette leghe.

Lo studio della saldatura su acciai inossidabili Duplex, ha condotto, durante lo svolgimento del Dottorato di Ricerca, allo studio sperimentale e numerico della saldatura anche su altri tipi di materiali. Queste attività non sono riportate nel corpo della tesi, ma sono illustrate nella parte finale.

AIM OF THE WORK

The aim of the present work has been to study experimentally the impact of welding and heat treatment processes of Duplex Stainless Steels on their microstructure and pitting corrosion properties, in order to optimize all the materials and processes involved in welding of austenitic/ferritic stainless steels. A numerical model describing the microstructural evolution of DSS and SDSS due to isothermal and anisothermal (continuos cooling) heat treatments, has been also developed in SYSWELD 11.0® to predict the precipitation risk in these alloys. The reference material for most of the work has been the UNS S32750 (SAF 2507).

The following diagram represents the leading thread of the doctoral thesis and it describes the relationships between microstructure, final properties, processes and applications of Duplex Stainless Steels:
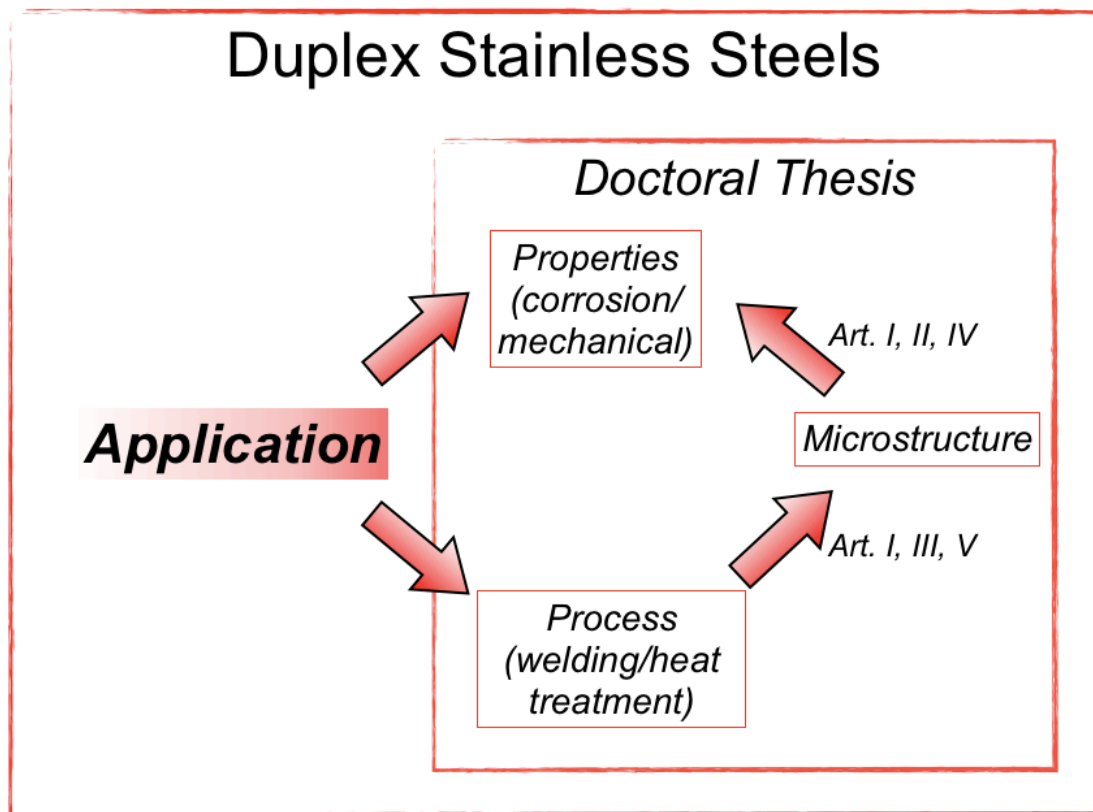
Scheme of the doctoral thesis

In particular, the scheme reported expresses the following concepts: the starting point is the type of application (i.e. where the component will be applied), which requires specific properties (project requirements) and implies a given process for the fabrication of the part (for example, offshore structures or pipes for oil or chemical products transport are generally subjected to welding processes). At the same time, the process (welding or heat treatment) influences the DSS microstructure (i.e. ferrite/austenite balance, phase composition, presence of precipitates) which in turn determines their final properties (in terms of corrosion and mechanical features).

The articles presented in this thesis, go into more depth on two main aspects illustrated in the previous diagram: the influence of the process (welding or heat treatment) on microstructure and final properties of DSS (in particular pitting corrosion properties) and the study of the relationship between microstructure and pitting corrosion properties of austenitic/ferritic stainless steels.

In detail, the issues discussed in this thesis can be summarized as:

- evaluation of the effects of an innovative filler wire for Gas Tungsten Arc Welding (GTAW) of SDSS on their microstructure, mechanical properties and corrosion behavior. Comparison with a traditional filler wire in order to optimize the materials used in SDSS welding to obtain a more balanced microstructure and better properties (Article I);
- study of influence of filler metal composition on the precipitation kinetic of secondary austenite related to post welding heat treatment and on pitting corrosion properties of SDSS solution treated GTA welded joints, in order to optimize the materials used in SDSS welding in relation to post-welding heat treatment (Article II);
- study of the influence of post welding heat treatment temperature on microstructure of SDSS Submerged Arc welded joints, in particular on the ferrite/austenite balance, phase compositions and dissolution of detrimental phases precipitate during welding (Article III);
- analysis of the effect of post welding heat treatment temperature on pitting corrosion properties of SDSS welded joints, in order to optimize the process parameters of post welding heat treatment; development of a relationship between microstructure and experimental pitting corrosion behavior of SDSS submerged-arc welded joints (Article IV);
- experimental study of isothermal and anisothermal heat treatments on DSS and SDSS in critical temperature range, to analyze and compare the tendency of secondary phases formation. Setting up of a numerical model, based on the Avrami equation, describing the microstructural evolution of DSS and SDSS due to isothermal and anisothermal heat treatments (which can simulate a cooling resulting from a welding operation in the HAZ -Article V).

STATE OF THE ART

1. The origins of "stainlessness" and general classification of stainless steels

It is without a doubt that stainless steels are an important class of alloys [1]. Their importance is manifested in the plenitude of applications that rely on their use. From low-end applications, like cooking utensils and furniture, to very sophisticated ones, such as space vehicles, the use of stainless steels is indispensable. In fact, the omnipresence of stainless steels in our daily life makes it impossible to enumerate their applications.

The word 'steel' means that iron constitutes the bulk of the material, while the use of the adjective 'stainless' implies absence of staining, rusting or corroding in environments where 'normal' steels are susceptible (for instance, in relatively pure, dry air). In order to impart 'stainlessness' to steels, chromium must be added to at least about 11 wt%. At this Cr level, an adherent, self-healing chromium oxide can form on the steel surface in relatively benign environments. However, to guard against pitting and rusting in more hostile environments (say, in moist atmospheres or polluted environments) or in the presence of elements like carbon, higher Cr contents must be added.

While the Fe–Cr system forms the basis, modern stainless steels, besides Cr, also contain a host of other alloying elements whose presence enhances specific properties. Mo is added for enhancing resistance against pitting and Ni for obtaining austenite, for instance. It is not uncommon for some grades, e.g., the superferritics and superaustenitics, to contain very generous amounts of these alloying elements. When the contents of Cr and Ni are added in substantial amounts, the resulting alloy is called heat-resisting alloy. Although a jumble of alloying elements may be present in stainless steels, their total content is usually kept below the iron content, for the sake of maintaining the resulting alloy to be a steel.

Three main types of microstructures exist in stainless steels, i.e., ferritic, austenitic and martensitic. These microstructures may be obtained by properly adjusting steel chemistry. Out of these three main microstructures, stainless steels may be categorized into several main classes [2,3]. These are :

(1) ferritic stainless steels,
(2) austenitic stainless steels,
(3) martensitic stainless steels,
(4) duplex stainless steels,
(5) precipitation hardening stainless steels and
(6) Mn-N substituted austenitic stainless steels.

The different classes of stainless steels possess different properties. For instance, fully austenitic stainless steels are non-magnetic, but their martensitic and ferritic counterparts possess ferromagnetism. The different properties of the various stainless steels have been studied extensively for a very long period and thus are very well

documented in the literature. An early handbook on stainless steels, which contains a series of informative articles, is a very good source on this topic [4].

Fig. 1 contains the most popular diagram experimentally developed for a weld metal by Schaeffler, which enables to identify the different stainless steels categories on the base of chemical composition (cfr. section 2.2).
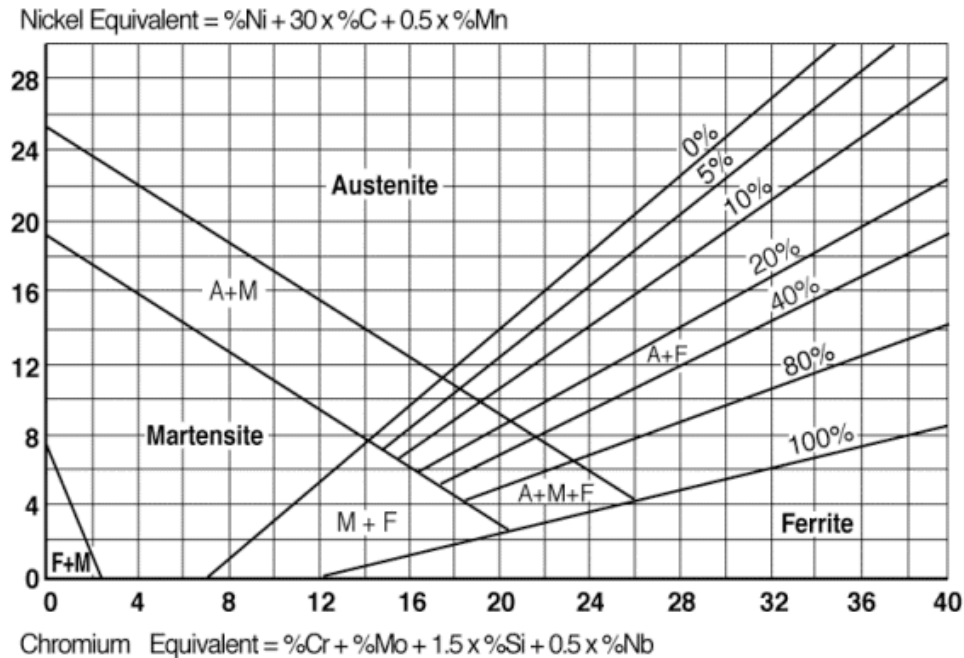
Fig. 1 - The Schaeffler constitution diagram for stainless steel weld metal

2. Duplex stainless steels

2.1. A brief history

The discovery of a duplex microstructure was first described by Bain and Griffiths in 1927 but it was not until the 1930's that duplex stainless steels (DSS) became commercially available [5,6]. The early grades were alloys of chromium, nickel and molybdenum, and the constant vertical section of the ternary phase diagram (70% iron) of the metallurgical behavior is shown in Fig. 2. This phase diagram illustrates that these alloys solidify as ferrite, some of which then transforms to austenite as the temperature falls to about 1000°C depending on alloy composition. There is little further change in the equilibrium ferrite-austenite balance at lower temperatures. Thermodynamically, because the austenite is forming from the ferrite, it is impossible for the alloy to go past the equilibrium level of austenite. The main problem with Duplex is that it forms very easily brittle intermetallic phases, such as Sigma, Chi, Chromium Nitrides, R and Alpha Prime [7,8]. The TTT diagram for a UNS 32750 (Super Duplex Stainless Steel 2507) is shown in figure 3.

| Fig. 2 - The constant (70% wt. Fe) vertical section of the Fe-Cr-Ni system [9] | Fig. 3 - TTT diagram for UNS 32750. Curves indicates 1% volume fraction of precipitates [9] |
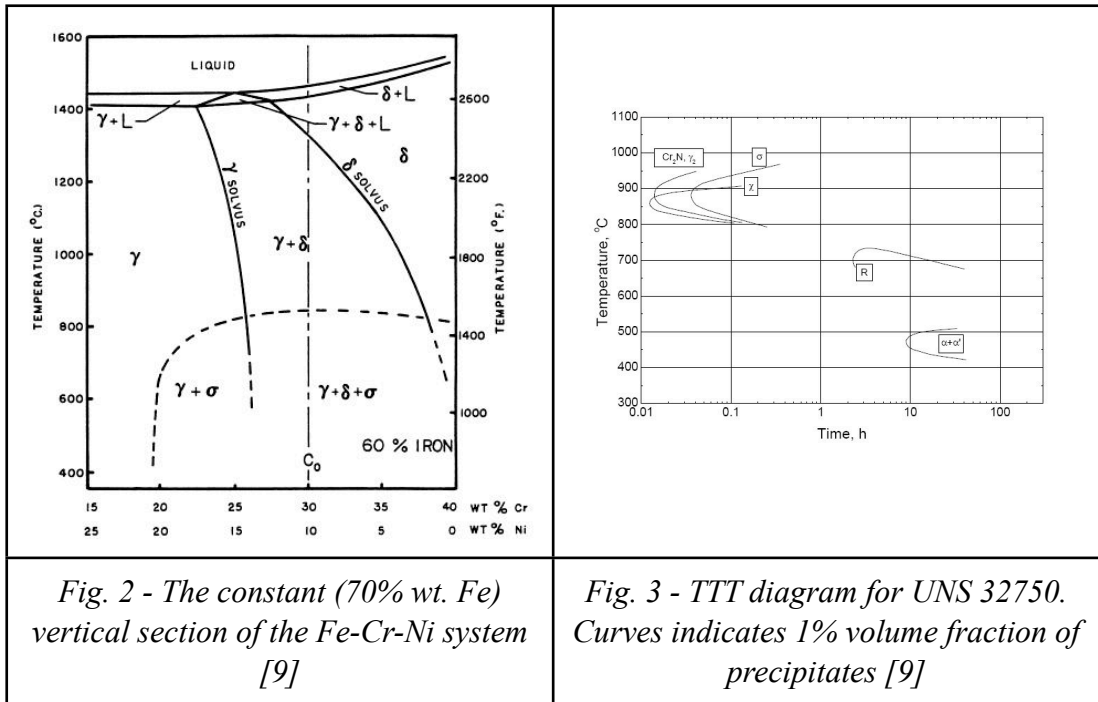
The first wrought duplex stainless steels were produced in Sweden in 1930 and were used in the sulfite paper industry. These grades were developed to reduce the intergranular corrosion problems in the early high-carbon austenitic stainless steels. Duplex castings were produced in Finland in 1930, and a patent was granted in France in 1936 for the forerunner of what would eventually be known as Uranus 50. It became obvious that a balance of ferrite and austenite had better resistance to chloride stress-corrosion cracking than a fully austenitic microstructure. Engineers have exploited this advantages of duplex over austenitic steels ever since. In France, the UR 50 grade with 20-35% ferrite (UNS S32404) was marketed in various product forms, including forging, for such industries as oil refinement, food processing, pulp and paper, and pharmaceutical. These steels were produced in high-frequency induction furnaces using precisely weighed alloying additions. Partial vacuum ensured carbon removals, rudimentary deoxidation and restricted nitrogen ingress.

One of the first duplex grades developed specifically for improved resistance to chloride stress corrosion cracking (SCC) was 3RE60. AISI Type 329 became well established after World War II and was used extensively for heat exchanger tubing for nitric-acid service. In subsequent years, both wrought and cast duplex grades have been used for a variety of processing industry applications including vessels, heat exchangers and pumps. These first-generation duplex stainless steels provided good performance characteristics but had limitations in the as-welded condition. The heat-affected zone (HAZ) of welds had low toughness because of excessive ferrite and significantly lower corrosion resistance than that of the base metal. These limitations confined the use of the first-generation duplex stainless steels, usually in the non-welded condition, to a few specific applications.

During the late 1960s and early 1970s, there were two main factors which advanced the development and use of duplex alloys. First, there was a nickel shortage that pushed up the price of austenitic steels, in combination with increased activity in the

offshore oil industry which demanded a stainless steel material to handle aggressive environments. Second, steel production techniques improved dramatically with the introduction of the vacuum and argon oxygen decarburization (VOD and AOD) practices. These techniques made it possible to produce much cleaner steels with a very low carbon level and well controlled nitrogen content. In the 70's, the introduction of continuous casting in stainless steel production has contributed to lower production costs and higher quality. From 1970 onwards, the addition of nitrogen and lowering of carbon content improved corrosion resistance and high temperature stability of the duplex structure, e.g. the HAZ, by stabilizing the austenite.

The last two decades have seen the introduction of the "super" stainless steels. Super-ferritic grades with very low interstitial levels and high chromium and molybdenum contents have superior corrosion resistance compared to standard ferritic grades. However, although these steels have found certain applications, their success has been limited. The highly alloyed super-austenitic and superduplex stainless steels, with excellent corrosion resistance and weldability than the ferritic steels, have found a more widespread use and are today important engineering alloys. The hot workability and rolling experience was greatly improved, making possible the production of wide sheets and coils [7].

Modern Development

In the early 1980's, a second generation of duplex steels was introduced with improved welding properties mainly through nitrogen alloying. The most common duplex grade today is EN 1.4462 or 2205 (UNS S31803), which has a nominal composition of 22% Cr, 5%Ni, 3% Mo, and 0.16% N. This steel is used in a great number of applications in a wide variety of product forms. Many of the grades have become commonly known by a number that reflects their typical chromium and nickel contents, e.g. 2205 with 22% Cr and 5%Ni. The 2205 alloy is a nitrogen-enhanced duplex stainless steel alloy. The nitrogen serves to significantly improve the corrosion resistance properties of the alloy, which also exhibits a yield strength that is more than double that of conventional austenitic stainless steels; especially in the welded condition. Earlier duplex alloys have had moderate resistance to general corrosion and chloride stress-corrosion cracking, but suffered a substantial loss of properties when used in the as-welded condition. The 2205 duplex stainless steel provides corrosion resistance in many environments that is superior to the AISI Type 304, 316 and 317 austenitic stainless steels. This duplex stainless steel is often used in the form of welded pipe or tubular components, as well as a formed and welded sheet product in environments where resistance to general corrosion and chloride stress corrosion cracking is important. The increased strength creates opportunities for reduction in tube wall thickness and resists handling damage.

Nevertheless, the extraordinary corrosion resistance (and other properties) of 2205 may be greater than is required in some applications. In certain SCC applications, while 2205 would provide an acceptable technical solution, it may not be an economical replacement alloy for Type 304, 316 or 317 stainless steel. The higher cost of 2205 is due primarily to the amounts of the alloying elements nickel (nominal 5.5%) and molybdenum (nominal 3%). Thus, it is desirable to provide a weldable, formable duplex stainless steel that has greater corrosion resistance than the Type

304, 316 or 317 austenitic stainless steels, and has a lower production cost than the commonly used 2205 duplex stainless steel.

The success of the 2205 grade led to the development of an entire family of duplex alloys, which range in corrosion resistance depending on their alloy content. The modern duplex stainless steels can be divided into four groups [10]:

• lean duplex as 2304, with 0.05-0.6 wt% of Mo
• 2205, the work-horse grade accounting for more than 80% of duplex use
• 25Cr duplex as Alloy 255 and DP-3
• super duplex, with 25-26 Cr and increased Mo and N compared with the 25 Cr grades, including grades such as 2507, Zeron 100, UR52N+, and DP-3W.

Table 1 lists the chemical composition of the modern wrought duplex stainless steels and includes also the first generation of duplex stainless steels as a point of reference.

Grade	UNS	C	Cr	Ni	Mo	Mn	N	Cu	W
First generation DSSs									
329	S329000	0.08	23-28	2.5-5.0	1.0-2.0	1.0	-	23-28	2.5-5.0
3RE60	S31500	0.03	18-19	4.3-5.2	2.5-3.0	1.2-2.0	0.05-0.10	18.0-19.0	4.3-5.2
UR50	S32404	0.04	20.5-22.5	5.5-5.8	2.0-3.0	20	-	1-2	-
Modern DSSs									
2304	S32304	0.03	21.5-24.5	3.0-5.5	0.0-0.6	2.5	0.05-0.20	-	-
2205	S31803	0.03	21.0-23.0	4.5-6.5	2.5-3.5	2.0	0.08-0.20	-	-
DP-3	S31260	0.03	24.0-26.0	5.5-7.5	5.5-7.5	1.0	0.10-0.30	0.20-0.80	0.10-0.5
UR52N	S32520	0.03	24.0-26.0	5.5-8.0	3.0-5.0	1.5	0.20-0.35	0.50-3.00	-
255	S32550	0.04	24.0-27.0	4.5-6.5	2.9-3.9	1.5	0.10-0.25	1.50-2.50	-
DP-3W	S39274	0.03	24.0-26.0	6.8-8.0	2.5-3.5	1.0	0.24-0.32	0.20-0.80	1.50-2.5
2507	S32750	0.03	24.0-26.0	6.0-8.0	3.0-5.0	1.2-2.0	0.24-0.32	0.50	-
Zeron 100	S32760	0.03	24.0-26.1	6.0-8.1	3.0-4.0	1.0	0.20-0.30	0.50-1.00	0.50-1.0

Table 1 - Chemical composition in wt. % of wrought Duplex Stainless Steel grades with the corresponding Unified Numbering System and European Norm [1]

2.2. Effect of alloying elements and temperature on phase balance of duplex stainless steels

An important aspect related to duplex stainless steels is the phase balance control, because it has a direct impact on corrosion and mechanical properties. For instance, delta ferrite has long been known to affect the low-temperature toughness [11,12], creep strength [13] and propensity to hot cracking [14,15] of austenitic stainless steel welds.

Regarding duplex stainless steels, the phase balance control results to be crucial and it is mainly related to two important factors: the alloy chemistry and the temperature.

Effects of alloying elements on phase balance
Traditionally, the effects of different alloying elements on phase balance have been quantified by using the nickel and chromium equivalent numbers. Several formulae for these two equivalent numbers, as proposed by Schaeffler [16], DeLong [17] and Hull [18], have been in use for a very long time. Equations (1) and (2) show the formulas reported by Datta et al. [19], as a reference:

$$Cr_{eq} = (Cr) + 2(Si) + 1.5(Mo) + 5(V) + 5.5(Al) + 1.75(Nb) + 1.5(Ti) + 0.75(W) \quad (1)$$

$$Ni_{eq} = (Ni) + (Co) + 0.5(Mn) + 0.3(Cu) + 25(N) + 30(C) \quad (2)$$

While the effects of major alloying elements like Cr and Ni have been well-studied, the effect of Mn is still under investigation, because its role on phase stability is still controversial and the Mn–Cr–(N) stainless steels have been gaining importance in recent years.

Regarding the interplay between Mn and other alloying elements, Raghavan [20] has found that the phase-stabilizing effect of Mn depends on the contents of other alloys, not just on its own content. In his study, Raghavan has also reported that Mn becomes a ferritiser if the content of Cr is high. The composition-dependent role of Mn on phase stability has been supported by several other workers (Chen et al. [21], Schino et al. [22] and Milititsky [23]).

Besides the effects of common alloying elements like Cr, Ni and Mn, effects of other elements have also been assessed recently. Kolman et al. [24] have concluded that Ga should be a weak ferritiser. Balan et al. [25] have suggested that the potency factor, i.e., the coefficient of Co in the formula for Ni_{eq}, is about 0.64, whereas early studies suggested that it should either be 1 [19, 26] or in the range of 0.6–0.8 [27]. Titanium, while taken as a ferritiser by Pickering [28] in an early study, has been found to increase the retained austenite content of ferritic stainless steel weld metals [29].

Furthermore, newer versions of expressions for the chromium and nickel equivalent numbers have been suggested, with consideration to the effects of alloying elements that were not analyzed by early workers.

Effect of temperature on phase balance
In addition to steel chemistry, temperature also influences phase balance in DSS. A study by Hertzman et al. [30] gives a formula to obtain the austenite volume fraction at equilibrium in function of chemical composition of the alloy and temperature. The relationship has been obtained starting from experimental data considering various duplex stainless steels:

$$f_\gamma = 0.01 \left[75 - 6.8 \times 10^{-15} \times T^5 + 190 \left(C_C - 0.03 \right) + 6 \left(22 - Cr_C \right) + 9 \left(Ni_C - 5 \right) + 6.5 \left(3 - Mo_C \right) + 160 \left(N_C - 0.15 \right) \right]$$

$$(3)$$

where C_c, Cr_c, Ni_c, Mo_c, N_c are respectively the carbon, chromium, nickel, molybdenum and nitrogen content of the alloy.

A first empirical formula to calculate T_δ (the temperature at which the structure is completely ferritic) in function of Ni_{eq} and Cr_{eq} in super duplex stainless steels has been proposed by Sharafi [31] in his doctoral thesis:

$$T_\delta = 1201 + 30.59 \text{ x } Ni_{eq} - 3.62 \text{ x } Cr_{eq} \qquad (4)$$

A more recent statistical regression study [32] using a large number of data in the literature has shown that the temperature T_δ (in this case, the temperature corresponding to the phase boundary of $(\gamma/\gamma + \delta)$) in austenitic stainless steels could be calculated by the following empirical relationship:

$$T_\delta \text{ (°C)} = T_4 - 21.2 \text{ x } Cr_{eq} + 15.8 \text{ x } Ni_{eq} - 223 \qquad (5)$$

where T_4 is the $\gamma \rightarrow \delta$ transformation temperature for pure iron and Cr_{eq} and Ni_{eq} are respectively the chromium and nickel equivalent values, considering the following coefficients:

Ni_{eq} coefficients: C, 25-30; N, 20-30; Cu, 0.3-0.5; Mn, 0.5.

Cr_{eq} coefficients: Si 0.5-2.5; Mo, l-2: Nb, 0.5-2.0; Ti, 2-5; V, 1.5-5.0; Al, 2.5-5.5; W, 0.7.

In addition, this study has also shown that the volume fraction of delta ferrite varies exponentially with temperature around T_δ:

$$V_\delta \text{ (\%)} = 0.715 \exp [0.015(T - T_\delta)] \qquad (6)$$

Furthermore, precipitation of carbides/carbonitrides may alter steel chemistry and so Ni_{eq} and Cr_{eq} may change accordingly. The effects of carbides/carbonitrides on T_δ have been given in another study by the same authors [33].

For the estimation of ferrite contents in stainless steel weld metals, the Schaeffler diagram [16] and the DeLong [17] diagram are arguably the most popular. These diagrams are basically iso-ferrite content maps.

2.3. Precipitates

Inevitably, a lot of stainless steel components are used or processed at elevated temperatures.

In contrast to austenitic stainless steels, which are often used in high temperatures applications, DSS are not recommended in applications where temperatures exceed 250°C, the reason being the thermal instability of ferrite. In the temperature range 250-500°C spinodal decomposition of ferrite termed 475°C embrittlement may occur after long term exposure, whereas various types of precipitate may form at temperature in the range 550-1000°C: σ, χ, ε, R phases, carbides and nitrides (cf. fig. 3).

Although DSS most commonly used at temperatures below 250°C and, therefore, the effects mentioned above are not expected during service, the producer and

manufacturer of these steels has to be aware of these phase transformations because they may occur either during production or during welding when the material is exposed to elevated temperature for shorter or longer times.

This section introduces recent results on the various types of precipitates that may form in duplex stainless steels upon thermal ageing, considering two ranges of temperatures:

- low range (250-500°C) where the most important precipitate is alfa prime (α'_{Cr})
- high range (550-1000°C) where the possible precipitates are σ, χ, secondary austenite, ε, R phases, carbides and nitrides.

While spinodal decomposition of ferrite in low range temperature leads to reduced toughness, precipitation in the higher temperature regime may lead to a reduction in corrosion resistance and/or a reduction in toughness.

Phase	Chemical formula	Temperature interval, °C	Crystallographic structure	Lattice parameter, nm
sigma	Fe-Cr-Mo	600-1000	P4$_2$/mnm	a = 0.879 ; c = 0.454
chromium nitride	Cr$_2$N	700-1000	P31m	a = 0.480 ; c = 0.447
chi	Fe$_{36}$Cr$_{12}$Mo$_{10}$	700-900	143m	a = 0..892
R	Fe-Cr-Mo	550-700	R3	a = 1.090 ; c = 1.934
pi greco	Fe$_7$-Mo$_{13}$-N$_4$	550-600	P4,32	a = 0.647
tau	-	550-650	Fmmm	a = 0.405; b = 0.484; c = 0.286
M$_7$C$_3$	-	950-1050	Pnma	a = 0.452; b = 0.699; c = 1.211
M$_{23}$C$_6$	-	600-950	Fm3m	a = 1.056 - 1.065

Table 2 - Secondary phases observed in DSS/SDSS [34]

alfa prime (α'_{Cr})

Spinodal decomposition of ferritic stainless steels is a subject that was studied by a lot of early workers [35–38]. It is generally accepted that thermal ageing below roughly about 550°C may cause spinodal decomposition.

Early workers concretely established that when spinodal decomposition occurs, the ferrite would decompose into α and α'_{Cr} domains that are enriched in Fe and Cr, respectively. The lattices of both α and α'_{Cr} are body-centered cubic and both are of extremely fine scales.

While it has long been known that both fully ferritic stainless steels and the ferrite phase of duplex stainless steels will undergo spinodal decomposition, a study by Miller et al. [39] has shown that the ferrite phase of the duplex stainless steels decomposes more rapidly. The importance of this study lies in the fact that it raises

doubt on the validity of modeling the behavior of the ferrite phase in duplex steels by using the binary Fe–Cr system.

It is generally accepted that 475°C-embrittlement is due to the formation of the α'_{Cr} phase, which forms either through nucleation and growth or spinodal decomposition. Interestingly, Vitek et al. [40] have shown that both mechanisms can occur simultaneously. Also, an early work by Grobner [41] mentioned that α'_{Cr} forms through nucleation and growth if the Cr content is less than 17%, otherwise it will form through spinodal decomposition. Nevertheless, a very recent work of Hattestrand et al. [42] has shown that α'_{Cr} may form in the ferrite phase in SAF 2507 duplex stainless steel (%Cr > 17%) either through nucleation and growth or spinodal decomposition, depending on both ageing temperature and whether the material is plastically deformed. Plastic deformation encourages spinodal decomposition because dislocations may break down coherency strains, which act as barriers to the spinodal process [42].

σ (sigma) phase

Sigma phase is usually the most important of the secondary phases since it can be present at the highest volume fractions and clearly devastates the toughness and corrosion properties of DSS [43]. The precipitation occurs between 600 and 1000 °C [9] and often starts at triple junctions or grain boundaries (ferrite/ferrite or ferrite/ austenite) and grows into the adjacent ferrite grains. The formation can be suppressed by a high solution temperature, due to dilution of σ formation elements in the ferrite [44,45].

Cr, Mo and Si are the main elements which increase the susceptibility to σ phase precipitation. The "sigma equivalent" (σ_{eq}) is a parameter proposed by Ramirez-Londoño [46] to measure the tendency of a DSS or SDSS to σ precipitation:

$$\sigma_{eq} = X_{Cr(\delta)} + 4.5 X_{Mo(\delta)} + 1.5 X_{Si(\delta)} \tag{7}$$

where, $X_{Cr(\delta)}$, $X_{Mo(\delta)}$ and $X_{Si(\delta)}$ are the amounts of Cr, Mo and Si in the ferritic matrix. Therefore, it can be easily noted that super duplex stainless steels with high additions of Cr and Mo are more prone to sigma precipitation. A study of DSS 2205 [47] indicated the following stoichiometry, independent of temperature: $(Fe_{0.95}Ni_{0.04}Mn_{0.01})_{0.61}(Cr_{0.88}Mo_{0.09}Si_{0.03})_{0.39}$.

χ (chi) phase

Chi (χ) phase precipitates in the temperature range 700-900°C [9,48] and has a similar effect on the material as σ, but occurs mainly at somewhat lower temperatures, where the diffusion is slower. Moreover, χ needs large amount of Mo to form [49]. This can explain why the precipitated volume fraction of χ is significantly lower compared to σ in commercial DSS. χ phase is more unstable than σ phase and might eventually transform into σ phase during aging [50]. The stoichiometry of chi phase is $Fe_{36}Cr_{12}Mo_{10}$ [51], its composition is similar to that of the sigma phase, but chi is richer in molybdenum, so it could be distinguished from sigma using electron backscattered diffraction [52]. In addition, in contrast to sigma,

carbon can dissolve in the χ-phase. Due to this property, the χ-phase was defined [53] as a carbide-type $M_{18}C$ in the past.

Cr₂N

Chromium nitrides precipitate between 700 and 900°C during rapid cooling (i.e. in heat affected zones of welding [54,55]) or isothermal heat treatment. Slow cooling rates reduce the amount of Cr_2N due to increasing austenite formation, where nitrogen can dissolve [56]. The precipitation decreases the pitting corrosion resistance due to depletion of chromium and nitrogen [55,56,57].

Secondary austenite (γ₂)

Austenite precipitations in duplex steel created as a result of reheating to a temperature lower than the solvus line temperature (cf. fig. 2) after fast cooling are considered as the secondary austenite [58].

Intragranular secondary austenite in a DSS could be found in heat affected zones or reheated passes of welded components [59,60,61,62,63], resulting in a $\delta+\gamma \rightarrow \delta+\gamma+\gamma_2$ transformation.

There appear to be three mechanisms (in addition to the direct transformation of ferrite to austenite occurring at very high temperatures) by austenite can precipitate in δ-ferrite:

- as a result of the eutectoid reaction $\delta \rightarrow \sigma + \gamma_2$ in the temperature range 700–900°C (at the ferrite/austenite grain boundaries)
- a diffusive transformation at a temperature above 650 °C resulting in a Widmanstätten precipitates (intragranular)
- a non-diffusive isothermal transformation at a temperature lower than 650°C analogous to a martensitic transformation [64].

Nilsson et al. [62] reported that intragranular secondary austenite has a lower chromium, molybdenum and nitrogen content compared to the primary austenite, therefore it is more susceptible to pitting attack (cf. section 2.4).

Other phases (carbides, R phase, epsilon phase)

M₂₃C₆ carbides have high mobility and can form prior to other phases at the grain boundaries, acting as nucleation sites for later formed secondary austenite and σ. Modern duplex stainless steels have low contents of C and carbide precipitation is unlikely to occur [9].

R phase is Mo rich and can be found between 550-650°C, uniformly distributed throughout the ferrite grains [65]. The corrosion and toughness properties are reduced due to R phase precipitation.

For steels containing relatively high contents of copper, the *ε(Cu) phase* that forms during spinodal decomposition of ferrite will further lower pitting corrosion resistance [66,67,68].

2.4. Pitting corrosion properties

The most common types of corrosion phenomenon in stainless steels are intragranular, crevice and pitting corrosion, which is introduced in this section.

The pitting corrosion of stainless steels is a stochastic event [69], and it is generally associated to a local breakdown of the protective passive layer and their susceptibility to a such damage can be evaluated by using different methods: critical pitting temperature measurements [70], gravimetric tests after immersion in high-aggressive solutions [71], and electrochemical measurements [72]. It is generally accepted that pitting initiates when the pitting potential reaches a critical value (E_p), which depends on the chemical composition of the alloy and on the environment (temperature and chloride concentration). E_p is often measured by potentiodynamic anodic polarization tests. In these measurements the onset of pitting corrosion is observed as an irreversible increase in current density (Fig. 4). The higher the E_p value, the more resistant is the alloy to pitting corrosion in the environment considered [73].
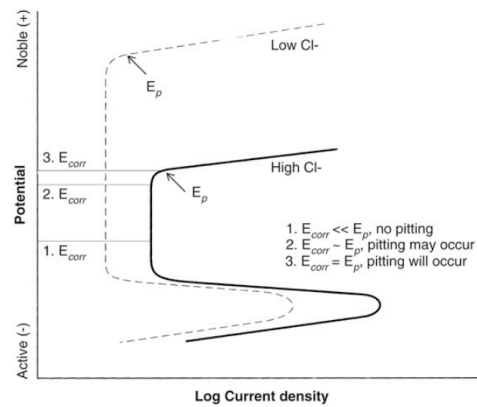

Fig. 4 - Schematic representation of a polarization curve, determining the pitting corrosion risk [73]

It is common to define the pitting corrosion resistance of stainless steels by their *Pitting Resistance Equivalence Number* [74] (PREN) as defined by the following equations:

$$PREN = \%Cr + 3.3\%Mo + 16\%N \tag{8}$$
$$PREN = \%Cr + 3.3\%Mo + 20\%N \tag{9}$$
$$PREN = \%Cr + 3.3\%Mo + 30\%N \tag{10}$$

Equation 8 is generally used for austenitic stainless steels, while eq. 9 and 10 are used for Duplex and Super Duplex grades in order to emphasize the importance of nitrogen in the behavior of the alloy.

While PREN does not provide an absolute value for corrosion resistance and is not applicable in all environments, it provides an overview of the expected resistance to pitting corrosion in an aqueous chloride solution. Some alloys contain an addition of tungsten, which is another element that acts to increase the pitting resistance of stainless steels. For these alloys, the pitting resistance is expressed as PREW, according to Eq. 11:

$$PREW = \%Cr + 3.3\%Mo + 1.65\%W + 16\%N \tag{11}$$

The PREN or PREW number is commonly used to classify the family to which an alloy belongs. In a work of Dolling et al. [75], also the negative influence of phosphorus and sulphur in the calculation of PREN in SDSS has been evaluated.

When considering austenitic/ferritic stainless steels the difficult is that there are two phases with different compositions and with the three key elements (Cr, Mo and N) partitioned between them in different ways. Berhnardsson [76] supposed for first that austenite and ferrite have different PRE numbers and the pitting resistance of the alloy is given by the PREN of the weaker phase [77-80].

In general, materials having a pitting resistance number in the low 30's or lower are classified as lean duplex grades, those with PRE's in the mid 30's such as 2205, are classified as standard duplex, and those with PRE's of 40 or more are known as super duplex alloys [81].

The super duplex grades with a pitting index PREN/W>40, contain 25% Cr, 6.8% Ni, 3.7% Mo and 0.27% N, with or without Cu and/or W additions (UNS S32750, UR52N, DP3W, Zeron 100). This is the most highly alloyed grade for wrought products, and is specially designed for marine, chemical and oil engineering applications, requiring both high mechanical strength and resistance to corrosion in extremely aggressive environments (chloride-containing acids etc.).

An exponential relationship between PREN and experimental pitting potential (E_p) has been founded by Merello et al. [82].

In the following table, as a conclusion, the effect of the typical alloying elements of DSS on pitting corrosion resistance is illustrated.

POSITIVE		NEGATIVE	
Element	*Effect*	*Element*	*Effect*
Si	Stabilizes the passive film	C	Increases the risk of chromium carbides precipitation
Cr	Stabilizes the passive film	Mn	Destabilizes the passive film Tends to form sulphurs which can act as pitting onset
Mo	Stabilizes the passive film	S	Forms sulphurs which can act as pitting onset
W	Stabilizes the passive film	Ni	Impoverishes the nickel content of austenite decreasing its PREN
N	Increases the PREN of austenite		

Table 3 - Effect of main alloying elements of DSS on pitting corrosion resistance

2.5. Applications

Modern DSSs have been on the market for many years, including the super duplex grade, which was developed about 10 years ago. Due to the very fine-grained structure, nitrogen alloying, and ferrite and austenite mixture, the mechanical strength of DSSs is very high. DSSs may be used in many corrosive environments

within the temperature range of approximately 50°C to less than 300°C. Chloride containing process media or cooling water is common in the refining and petrochemical industry. Even at very low concentrations, the aggressive chloride ions may cause rapid failure if an improper material is selected.

Chloride stress-corrosion cracking is a rapid form of corrosion, and can cause severe problems of hydrocarbon processing plants when occurring in equipment such as heat exchangers. Standard austenitic stainless steels of the AISI 300 series are sensitive to SCC in chloride-containing environments above approximately 60°C. This limits the use of these steels since many heat exchangers in the process industries are working at higher temperatures. It was observed that heat exchangers are by far the most critical piece of equipment and that DSSs in most cases are chosen as the first countermeasure to combat this form of corrosion. As regards pitting corrosion resistance, duplex alloys are as resistant as austenitic alloys with comparable PRE numbers.

At the Sixth Conference of Duplex Stainless steels, Charles [83] provides a paper which outlines the high number of applications where DSS and SDSS were extensively used, in particular:

- Pulp and paper industry (chip preparation and chip presteaming vessels, bleaching pulp storage tank, pulp batch digester- sulfite and sulfate processes, chlorine dioxide bleach water drums);
- Chemical and petrolchemical industries [84,85] (PVC stripper columns and heat exchangers, pressure vessel for organic products, reactors for the oxo alcohol production);
- Hydrometallurgy;
- Chemical fertilizer industry (phosphoric acid production, urea industry);
- Organic and caustic media;
- Pollution control equipments;
- Chemical tankers;
- On/Offshore applications;
- Seawater and chloride containing water [86,87] (hot water tanks and drums, seawater applications, reverse osmosis desalination, industrial and domestic water storage tanks and pipings);
- Architecture;
- Transports [88].

Life Cycle Costing [89]

The selection of a material for a given application requires a compromise between optimum corrosion resistance, required mechanical properties, workability, availability and cost.

The selection of materials is being made not simply on what is immediately the cheapest technically acceptable option, but on a longer term view of the costs incurred for the duration of a project.

The Life Cycle Costing (LCC) approach utilizes established accounting methods to compare the costs of alternative materials selections by calculating the *present day value* of future costs associated with the chosen materials. By using LCC it can often be demonstrated that paying out more at the start for corrosion resistant alloys,

including duplex stainless steels, rather than an apparently much cheaper material, results in substantial savings in operating, maintenance and repair costs in the future.

Duplex stainless steels in the future [90]
Some new duplex grades have been introduced in the market or are concerned by R&D activities. Nowadays the main target is the development of so-called lean duplex having much less alloying elements than the standard 2205 duplex grade; there targets is the replacement of 316 and even 304 grades. Chromium contents are in the range 20/22 while Ni additions are reduced by further increase of Mn contents. For some more corrosion resistance applications molybdenum, copper and tungsten contents are considered; those developments may boost the developments of duplex grades in the future. Duplex grades, particularly the lower alloying grades are know to have poor hot workability properties, and then, production of wide hot coils free of defects remains a technical challenge.

3. The welding of Duplex Stainless Steels

The study of weldability of DSS and SDSS is a fundamental issue for their proper industrial application. During welding of these alloys, two main problems may arise, due to the evolution of microstructure during cooling: the achievement of a not well-balanced austenite-to-ferrite ratio and the precipitation, in the Fusion Zone (FZ) and Heat Affected Zone (HAZ), of secondary phases which generally decrease the corrosion resistance and the toughness of the alloy. The FZ and HAZ microstructures could be very different from that of the base material as a function of both chemical composition and thermal history.

In this section, the metallurgy, the welding processes, and the effect of welding on microstructure and properties of DSS and SDSS welded joints are presented. The attention is focused on the microstructure and pitting corrosion properties of the FZ and the HAZ.

3.1. Metallurgy

The favorable combination of corrosion resistance and mechanical properties of DSS and SDSS is directly connected to their balanced microstructure, which depends on their thermal history.

However, the welding operations can locally upset the DSS optimal microstructure in two manners:
- by altering the ferrite/austenite ratio (and phases composition),
- by causing the precipitation of undesired secondary phases.
In particular, the FZ and HAZ can be affected by these problems [91,92].

Weld metal structure
The weld metal structure is the result of chemical composition [93] and thermal history [94]. The thermal weld cycle has a substantial effect on DSS microstructure that can result in a large deviation from the parent material (Fig. 5).
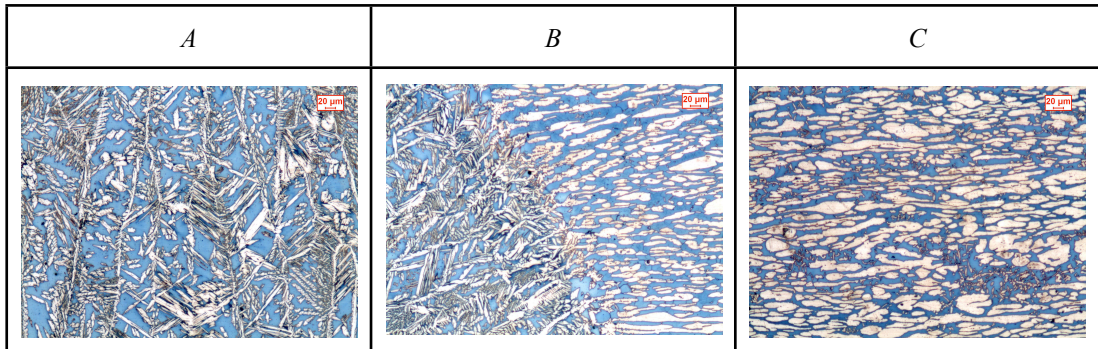
Fig. 5 - Typical DSS microstructures (100x): A - fused zone, B - heat affected zone C - as-rolled material (UNS S32750)

In the weld metal a ferritic solidification involves an epitaxial growth from parent material at the fusion boundary [95]. The dendrite growth is oriented in relation to the thermal gradient [96]. The cooling rate through the two-phase region in welding is often too fast to allow sufficient formation of austenite and the equilibrium fraction of austenite is never achieved in the weld. Low cooling rates result in a more austenite formation while high cooling rates give less austenite. Generally, weld metals of duplex stainless steels have ferrite contents in the range of about 30-70% depending on composition and cooling rates.

Consequently, welding consumables generally have a more austenitic composition than the parent steel for improved mechanical and corrosion properties. The fillers are today normally made with 2-4% more nickel than the base metal [94].

In addition to phase balance, the diffusion controlled transformation $\delta \rightarrow \delta + \gamma$ involves partitioning of elements between the two phases. At high cooling rates substitutional elements (Cr, Ni, Mo etc.) are almost equal in both phases [92] whereas the interstitial elements (N) controlling the reaction are heavily concentrated to the austenite. Therefore, the partitioning of elements in the as-welded condition is always much different than the partitioning in the solutioned conditions [95].

HAZ transformations

For duplex stainless steels it may be appropriate to consider the so-called high temperature heat affected zone (HTHAZ) and low temperature heat affected zone (LTHAZ). The former could be defined as the zone with a thermal cycle resulting in almost complete ferritization while the latter is the zone where the phase balance has remained substantially duplex.

The resulting microstructure in HTHAZ for a given steel composition is subject to the imposed thermal history [54,58,59,60,61,97]. Reformation of austenite occurs largely as described above for the weld metal. Thus, heat input, multipass welding, preheat and interpass temperatures can influence the microstructure. The diffusion controlled austenite reformation, which in principle is a nitrogen redistribution, has been well described by Sieurin et al. [98] using a numerical model for submerged arc welding of DSS UNS S31803.

The LTHAZ is located further away from the fusion boundary and has a thermal history that may cause the formation of intermetallic phases.

Thus it is apparent that the welding parameters should be specified to ensure overall cooling conditions slow enough to allow adequate austenite formation at high temperatures and fast enough to avoid deleterious precipitation at low temperatures. Traditional guidelines provide recommended heat input ranges and maximum interpass temperatures. Better practical guideline is given by the cooling times between 800 and 500°C, $\Delta t_{8/5}$, or rather between 1200 and 800°C, $\Delta t_{12/8}$, which is more linked to the temperature range where austenite formation occurs. Preferred cooling times lie in the range 8 to 30 seconds for $\Delta t_{8/5}$ which correspond to approximately 4 to 15 seconds for $\Delta t_{12/8}$.

Secondary phases precipitation

Above, the major transformation sequences have been discussed. As the diffusion controlled process has not reached full equilibrium, also other reactions might occur. Although there is a high diffusion rate of nitrogen, the solubility in the ferrite is quite low with decreasing temperature. Formation of hexagonal chromium nitride (Cr_2N) might therefore take place in the supersaturated ferrite of the HAZ in the temperature range 700-900°C [54,55,99]. Nitride precipitation occurs particularly in welds with rapid cooling resulting in a high ferrite content and providing long distances to the austenite islands that act as nitrogen sinks (Fig. 6).
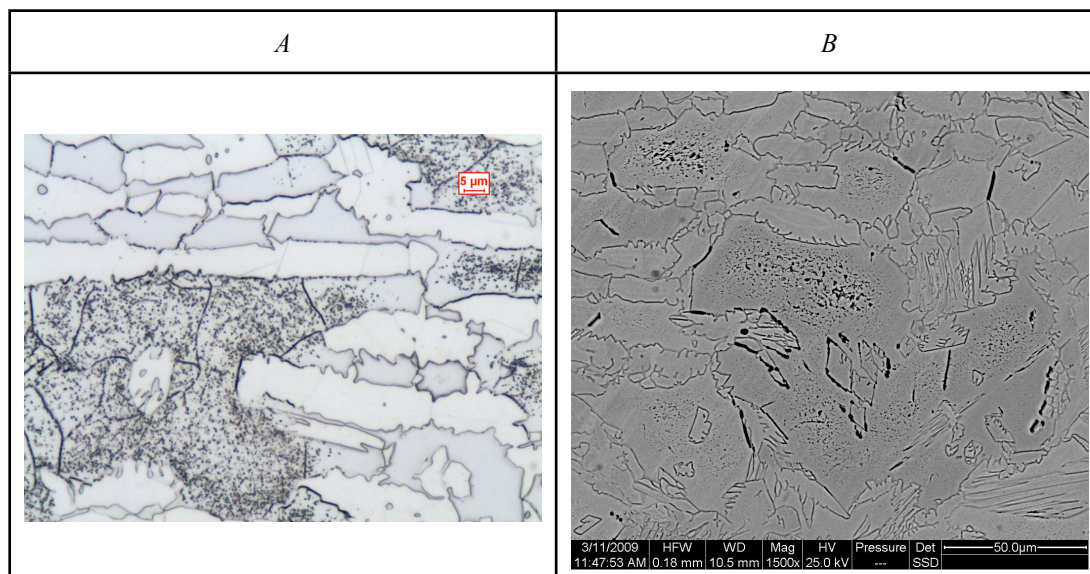
Fig. 6 - Precipitation of chromium nitrides in the heat affected zone of SAW of UNS S32750: A - LOM micrography (500x), B - SEM micrography (1500x)

The as welded, non-equilibrium weld metal structure might be affected by additional thermal treatments such as multipass welding and post weld heat treatments. In both cases secondary austenite can precipitate from the supersaturated ferrite. It has been shown that the secondary austenite precipitated in an interpass region contains lower chromium, molybdenum and nitrogen than does the primary ferrite formed at higher temperatures [62].

Precipitation of other intermetallic phases (like σ and χ phases) can occur during welding in the weld metal as well as in the HAZ, particularly for the highly alloyed SDSS.

3.2. Processes

At the 4th International Conference on Duplex Stainless Steels, Koteeki et al. [100] classified the welding processes currently applied in 1994 to DSS and SDSS in two categories: mature and immature. All the traditional arc-welding processes belonged to the first category, while the technologies included in the second category were slightly unformed at that time: resistance welding, laser welding, electron beam welding, friction welding, and electroslag welding.

Nowadays, all the conventional welding processes are applicable to austenitic-ferritic stainless steels, considering proper materials and process parameters:

- Gas Tungsten Arc Welding (GTAW) [101,102,103]
- Gas Metal Arc Welding (GMAW) [95]
- Shielded Metal Arc Welding (SMAW) [103]
- Flux-Cored Arc Welding (FCAW) [104]
- Plasma Arc Welding (PAW) [105,106,107]
- Submerged Arc Welding (SAW) [108,109]
- Electron Beam Welding (EBW) [105]
- Laser Welding (LW) [105,106,110,111]
- Friction Stir Welding (FSW) [112]
- Resistance Spot Welding (RSW) [113]

Another classification of the above mentioned processes applied to austenitic-ferritic stainless steels, has been proposed in a review by Bonollo et al. [114]. They divided the different welding processes on the base of the welding heat input transferred to the material, which is the most important parameter that affects the microstructure and consequently the properties of a DSS welded joint. Therefore, the classification using this convention becomes:

- traditional arc-welding processes: GTAW, SAW, GMAW, FCAW, SMAW, characterized by a quite high heat input distributed on a large surface (the applied power is 1×10^2 W/cm^2);
- innovative processes: PAW, LW, EBW, characterized by a concentrated and high heat input (1×10^6 W/cm^2 in EBW and LW)

The processes pertaining to the first category involve a lower cooling rate, while the the innovative processes with high density power allow to weld thick components (up to 10-12 mm) with one pass, but produce high cooling rates. The final microstructure of FZ and HAZ is strictly connected to the type of process and the cooling rate involved.

Recently, some experiments are in progress to improve the productivity of GTAW process applied to DSS using the so-called Activate TIG [115] or Keyhole TIG [116].

3.3. Effect of welding on corrosion properties and PWHT (Post Welding Heat Treatment)

Since stainless steels are applied in very aggressive environments, their corrosion performance is critical, especially in terms of localized corrosion (pitting and crevice).

It is well known that the welding operations deteriorate the pitting corrosion properties of stainless steels welded joints, due to microsegregation, unfavorable phase content, presence of secondary phases and porosities, solidification cracking [71,103,117,118,119].

In the case of DSS and SDSS the pitting corrosion performance may be connected to the PREN, which is generally different for the two constituents phases, austenite and ferrite [76-80].

The phase, microstructural and compositional changes of DSS after welding depend on the peak temperature, heat input, preheat temperature, interpass temperature and cooling rate. In general, the weld of a DSS exhibits higher ferrite contents, coarser grain size and extensive precipitation of Cr_2N.

Therefore, the severe thermal cycles involved in welding processes could affect the pitting corrosion properties of DSS and SDSS in different manners:
- by altering the austenite/ferrite balance and phase compositions, and consequently modifying the PRE number of single phases (cf. section 2.4);
- by inducing the precipitation of secondary phases in the FZ [62] or in the HAZ [2], like chromium nitrides or secondary austenite, which are deleterious for pitting corrosion resistance [120]. It has been reported that the deleterious effects of Cr_2N on pitting corrosion were associated with the formation of Cr-depletion zone adjacent to Cr_2N precipitates [121,122], while secondary austenite is deleterious for pitting because of its lower chromium, molybdenum and nitrogen content [62].

Therefore, to restore the optimum microstructure and corrosion properties of welded DSS, it may be necessary to subject the component to post-weld heat treatment (PWHT) (ASTM A928/A928M [123]). Any solubilization heat treatment of a duplex stainless steel, should be a full solution annealing in the temperature range 1050-1120°C, followed by water quenching to avoid the formation of undesired phases.

The main purposes of the PWHT are:
- to restore the optimum ferrite/austenite ratio (1:1) in the FZ and HAZ;
- to homogenize the altered phase compositions in the FZ;
- to dissolve possible precipitates formed during welding in the FZ or in the HAZ.

The effects of the PWHT on simulated HAZ of DSS have been studied by Nowacki et. al [61], but the data regarding the entire welded joint are still lacking.

In addition, since in DSS and SDSS welding the filler metal has a different composition if compared with the base material, the entire welded joints is constituted by two different materials. Therefore, the effects of PWHT on microstructure of fusion zone or base material could be different.

Ferro et al. [71] studied the effect of PWHT on microstructure and pitting corrosion properties of DSS welded joints, connecting the pitting corrosion behavior with the morphology of secondary austenite precipitated in the fusion zone.

A particular PWHT were tested on laser welded DSS [110,124]: to counterbalance the typical excess of ferrite of the laser welded joints, they were surface treated by using the same laser source adopted during welding. The experimental results reported in these studies, demonstrated that both microstructure and elemental distribution between ferrite and austenite could be restored to values close to those of the solution treated parent metal, through an optimized selection of laser parameters for the post-weld surface treatment.

Further researches for a better understanding of the effect of PWHT on SDSS welded joints, and the relation between microstructure and pitting corrosion behavior of the components are presented in this thesis.

REFERENCES

[1]   K.H. Lo, C.H. Shek, J.K.L. Lai, "Recent developments in stainless steels", Materials Science and Engineering R 65 (2009), 39.

[2]   R.A. Lula, Stainless Steel, American Society for Metals, 1986.

[3]   J. Beddoes, J.G. Parr, Introduction to Stainless Steels, 3rd edition, ASM International, Materials Park, OH, USA, 1999.

[4]   D. Peckner, I. M. Bernstein (Eds.), Handbook of Stainless Steels, McGraw-Hill Inc.,1977.

[5]   Iris Alvarez-Armas "Duplex Stainless Steels: Brief History and Some Recent Alloys", Recent Patents on Mechanical Engineering 1 (2008) 51.

[6]   J. Olsson J. Liljas M. "60 years of DSS applications" NACE Corrosion 94, Baltimore, MD, 1994.

[7]   Gunn RN. Duplex Stainless Steels: Microstructure, properties and applications. Ed. by Gunn R.N., Abington Publishing, Cambridge England, 1997.

[8]   Herzman S, Pettersson R, Frisk K, Jerwin T. "The relation between alloy composition and kinetics of intermetallics phase formation" In: Proc Duplex 2000 Int. Conf. & Expo, Venice, Italy. AIM 2000; 347.

[9]   J.O. Nilsson, "Super duplex stainless steels", Materials Science and Technology 8 (1992) 685.

[10]   Practical Guidelines for the Fabrication of Duplex Stainless Steels, International Molybdenum Association (IMAO), Pennsylvania, USA, 2001.

[11]   E.R. Szumachowski, H.F. Reid, Welding Journal 57 (1978) 325.

[12]   V. Muthupandi, P. Bala Srinivasan, V. Shankar, S.K. Seshadri, S. Sundaresan, Materials Letters 59 (2005) 2305.

[13]   Y. Cui, D. Carl, C.D. Lundin, Materials Science and Engineering A 452–453 (2006) 284.

[14]   C.D. Lundin, C.P.D. Chou, WRC Bulletins 289 (1983) 1.

[15]   T. Ogawa, E. Tsunetomi, Welding Journal 61 (1982) 82.

[16]   A.L. Schaeffler, Metal Progress 56 (1949) 680.

[17]   C.J. Long, W.T. DeLong, Welding Journal 52 (1973) 281.

[18]   F.C. Hull, Welding journal 52 (1973) 183.

[19]   P. Datta, G.S. Upadhyaya, Materials Chemistry and Physics 67 (2001), 234.

[20]   V. Raghavan, Metallurgical and Materials Transactions 26 (1995) 237.

[21]   S.R. Chen, H.A. Davies, W.M. Rainforth, Acta Materialia 47 (1999) 4555.

[22]   A. Di Schino, M.G. Mecozzi, M. Barteri, J.M. Kenny, Journal of Materials Science 35 (2000) 375.

[23]   M. Mililitsky, B.C. DeCooman, J.G. Speer, N. De Wispelaere, N. Akdut, Metallurgical and Materials Transactions A 37 (2006) 2117.

[24]   D.G. Kolman, J.F. Bingert, R.D. Field, Metallurgical and Materials Transactions A 35 (2004) 3445.

[25]   K.P. Balan, K.V. Rama Rao, A. Venugopal Reddy, D.S. Sarma, Materials Science and Technology 15 (1999) 798.

[26]   H. Schneider, Foundry Trade Journal 108 (1960) 562.

[27]   C.M. Hammond, STP 369, ASTM, Philadelphia, PA, 1965, 47.

[28]   F.B. Pickering, International Metals Review 21 (1976) 227.

[29]   T. Mohandas, G.M. Reddy, M. Naveed, Journal of Materials Processing Technology 94 (1999) 133.

[30]   S. Hertzman, W. Roberts, M. Lindenmo, Proceedings of Duplex Stainless Steels 86, The Hague, The Netherlands; 1986, 257.

[31]   Shahriar Sharafi "Microstructure of Superduplex Stainless Steels", Doctoral Thesis, Department of Materials Science and Metallurgy, Cambridge, 1993.

[32]   D. Qixun, Y. Ruzeng, Materials Characterization 38 (1997) 129.

[33]   Y. Ruzeng, D. Qixun, Materials Characterization 38 (1997) 143.

[34]   J.-O. Nilsson, "The physical metallurgy of duplex stainless steels", Proc. Conf. Duplex Stainless Steels '96, 1996.

[35]   R.O. Williams, Transactions of the TMS-AIME 212 (1985) 497.

[36]   T. De Nys, P.M. Gielen, Metallurgical Transactions 2 (1971) 1423.

[37]   T.J. Nochol, A. Datta, G. Aggen, Metallurgical Transactions A 11 (1980) 573.

[38]   A.Hendry, Z.F. Mazur, K.H. Jack, Metal Science 13 (1979) 482.

[39]   M.K. Miller, J.M. Hyde, A. Cerezo, G.W.D. Smith, Applied Surface Science 87/88 (1995) 323.

[40]   J.M. Vitek, S.A. David, D.J. Alexander, J.R. Keiser, R.K. Nanstad, Acta Metallurgica et Materialia 39 (1991) 503.

[41]   P.J. Grobner, Metallurgical Transactions A 4 (1973) 251.

[42] M. Hattestrand, P. Larsson, G. Chai, J.-O. Nilsson, J. Odqvist, "Study of decomposition of ferrite in a duplex stainless steel cold worked and aged at 450-500°C", Materials Science and Engineering A 499 (2009) 489.

[43] J.O. Nilsson, A. Wilson, "Isothermal phase transformations on toughness and pitting corrosion of super duplex stainless steel SAF 2507", Materials Science and Technology, 9 (1993), 545.

[44] Josefsson B., Nilsson J.-O., Wilson A., "Phase transformations in duplex steels and the relation between continuous cooling and isothermal heat treatment", Duplex Stainless Steels '91, Beaune, France, 1 (1991) 67.

[45] Chen T. H., Yang J. R., "Effects of solution treatment and continuous cooling on σ-phase precipitation in a 2205 duplex stainless steel", Mater. Sci. Eng. A, 311 (2001) 28.

[46] A.J. Ramirez Londoño, "Estudo da precipitação de nitreto de cromo e fase sigma por simulação térmica da zona afetada pelo calor na soldagem multipasse de aços inoxidáveis duplex", M.Sc. Thesis 1997, University of São Paulo (USP).

[47] A. Redjaimia, G. Metauer, M. Gantois, "Decomposition of delta ferrite in a Fe-22Cr-5Ni-3Mo-0.03C Duplex stainless steel. A morphological and structural study", Proc. Duplex Stainless Steels '91, Beaune, France, 1 (1991) 119.

[48] D.M. Escriba, E. Materna-Morrisb, R.L. Plauta, A.F. Padilha, "Chi-phase precipitation in a duplex stainless steel", Materials characterization 60 (2009), 1214

[49] L.Duprez, De Cooman B. C., Akdut N., "Microstructural changes in duplex stainless steel during isothermal annealing", Proc. Duplex 2000 Int. Conf. & Expo, Venice, Italy, (2000) 355.

[50] T.H. Chen, K.L. Weng, J.R. Yang, "The effect of high-temperature exposure on the microstructural stability and toughness property in a 2205 duplex stainless steel", Mater. Sci. Eng. A, 338 (2002) 259.

[51] Cortie M. B., Jackson E. M. L. E. M., "Simulation of the precipitation of sigma phase in duplex stainless steels", Metall. Mater. Trans. A, 28 (1997) 2477.

[52] J. Dobranszky, P.J. Szabo, T. Berecz, V. Hrotko, M. Portko "Energy-dispersive spectroscopy and electron backscatter diffraction analysis of isothermally aged SAF 2507 type superduplex stainless steel", Spectrochimica Acta Part B 59 (2004) 1781.

[53] H.J. Goldschmidt, Interstitial Alloys. London: Butterworths (1967) 126.

[54] Horng-Yih Liou, Rong-Iuan Hsieh, Wen-Ta Tsai "Microstructure and pitting corrosion in simulated heat-affected zones of duplex stainless steels", Materials Chemistry and Physics 74 (2002) 33.

[55] J. Liao, "Nitride Precipitation in Weld HAZs of a Duplex Stainless Steel", ISIJ International, Vol. 41 (2001), N°5, 460.

[56] H. Hoffmeister, G. Lothongkum, "Quantitative effects of nitrogen contents and cooling cycles on δ-γ transformation, chromium nitride precipitation and pitting corrosion after weld simulation of duplex stainless steels", Proc. of the Duplex Stainless Steels 94, Glasgow, Scotland 1994.

[57] J.O. Nilsson, B. Wilson, B. Josefsson, T. Thorvaldsson, "Relationship between pitting corrosion, toughness and microstructure for isothermally heat treated super duplex stainless steel", Applications of Stainless Steel '92, Stockholm, Sweden, 1 (1992) 280.

[58] A. Lukojc, J. Nowacki, "The influence of welding thermal cycle on properties of a duplex steel heat affected zone" Acta Metall Slovaca, April (2004) 741.

[59] A. J. Ramirez, S. D. Brandi and J. C. Lippold, "Secondary austenite and chromium nitride precipitation in simulated heat affected zones of duplex stainless steels", Science and Technology of Welding and Joining, Vol. 9, N°4 (2004) 301.

[60] C.M. Garzon, A.J. Ramirez, "Growth kinetics of secondary austenite in the welding microstructure of a UNS S32304 duplex stainless steel", Acta Materialia 54 (2006) 3321.

[61] J. Nowacki , A. Lukojc , "Microstructural transformations of heat affected zones in duplex steel welded joints", Materials Characterization 56 (2006) 436.

[62] Nilsson J.O., Karlsson L., Anderson J.O., "Secondary austenite formation and its relation to pitting corrosion in duplex stainless steel weld metal", Mater Sci. Technol. 11 (1995) 276.

[63] J. Nowacki, A. Lukojc, "Structure and properties of the heat-affected zone of duplex steels welded joints", Journal of Materials Processing Technology 164-165 (2005) 1074.

[64] B. Josefsson, J.O. Nilsson, A.Wilson "Phase transformation in duplex stainless steels" Proc. Duplex Stainless Steels '91, Beaune, France, 1 (1991).

[65] Redjaimia A., Metauer G., Gantois M., "Decomposition of delta ferrite in a Fe-22Cr-5Ni-3Mo-0.03C Duplex stainless steel. A morphological and structural study", Proc. Duplex Stainless Steels '91, Beaune, France, 1 (1991).

[66] A.M. do Nascimento, M.C.F. Ierardi, A.Y. Kina, S.S.M. Tavares, "Pitting corrosion resistance of cast duplex stainless steels in 3.5%NaCl solution", Materials Characterization 59 (2008) 1736.

[67] T. Otarola, S. Hollner, B. Bonnefois, M. Anglada, L. Coudreuse, A. Mateo, "Embrittlement of a superduplex stainless steel in the range of 550–700°C", Engineering Failure Analysis 12 (2005) 930.

[68] J. Charles, M. Verneau, "How to improve duplex stainless steels properties with copper additions" Proc. of the conference in duplex stainless steels 2000, Venezia, Italy, AIM, 2000.

[69] L. Lazzari, M. Ormellese, S. Ravasio "Modello a matrici di Markov per la previsione dell'innesco del pitting di acciai inossidabili", Proc. Giornate Nazionali sulla Corrosione e Protezione 2009, Udine, Italy, AIM, 2009.

[70] Bo Deng, Yiming Jiang, Jia Gong, Cheng Zhong, Juan Gao, Jin Li, "Critical pitting and repassivation temperatures for duplex stainless steel in chloride solutions", Electrochimica Acta 53 (2008) 5220.

[71] P. Ferro, A. Tiziani, F. Bonollo, "Influence of induction and furnace post welding heat treatment on corrosion properties of SAF 2205 (UNS 31803)", Welding Journal. 87 (2008) 298.

[72] G. Lothongkum, P. Wongpanya S. Morito, T. Furuhara, T. Maki "Effect of nitrogen on corrosion behavior of 28Cr–7Ni duplex and microduplex stainless steels in air-saturated 3.5wt %NaCl solution" Corrosion Science 48 (2006) 137.

[73] P. Pohjanne, L. Carpén, T. Hakkarainen, P. Kinnunen (2008) "A method to predict pitting corrosion of stainless steels in evaporative conditions", Journal of Constructional Steel Research 64, 1325.

[74] Gunn RN. Duplex Stainless Steels: Microstructure, properties and applications. Ed. by Gunn R.N., Abington Publishing, Cambridge England, 1997.

[75] R. Dölling, V.Neubert and P. Knoll, "Corrosion behavior of super duplex steel cast alloys with a PREN>41", Proc. Duplex Stainless Steels 91, Beaune, France, 1991

[76] S. Bernhardsonn "The corrosion resistance of duplex stainless steels", Proc. of the Duplex Stainless Steels Conference, Beaune, France 1991, 185.

[77] H. Vannevik, J.O. Nilsson, J. Frodigh, P. Kangas, "Effect of Elemental Partitioning on Pitting Resistance of High Nitrogen Duplex Stainless Steels", ISIJ Int. 36 (7) (1996), 807.

[78] L. Weber, P.J. Uggowitzer, "Partitioning of chromium and molybdenum in super duplex stainless steels with respect to nitrogen and nickel content", Material Science and Engineering A 242 (1998) 222.

[79] Tan Hua, Jiang Yiming, Deng Bo, Sun Tao, Xu Ju- liang, Li Jin, "Effect of annealing temperature on the pitting corrosion resistance of super duplex stainless steel UNS S32750",Materials Characterization (2009), doi: 10.1016/j.matchar.2009.04.009

[80] L.F. Garfias-Mesias, J.M. Sykes, C.D. Tuck "The effect of phase composition on the pitting corrosion of 25 Cr duplex stainless steel in chloride solutions", Corrosion Science (1996), Vol. 38, No. 8, 1319.

[81] D.S. Bergstrom "Benchmarking of Duplex Stainless Steels versus Conventional Stainless Steel Grades" Proc. Duplex 2007 Int. Conf & Expo, Grado, Italy, AIM 2007.

[82] R. Merello, F.J. Botana, J. Botella, M.V. Matres, M. Marcos "Influence of chemical composition on the pitting corrosion resistance of non-standard low-Ni high-Mn–N duplex stainless steels", Corrosion Science 45 (2003) 909.

[83] J. Charles "10 years later, obviously duplex grades in industrial applications look like a success store" Proc. Duplex 2000 Int. Conf. & Expo, Venice, Italy, AIM 2000.

[84] M. Holmquist "Consider duplex stainless steels for corrosive exchangers's service" Hydrocarbon Processing October 2001.

[85] T. Cassagne, F. Busschaerth, "Experience in duplex stainless steel in oil and gas production" Proc. Duplex 2007 Int. Conf & Expo, Grado, Italy, AIM 2007.

[86] J. Olsson, M. Snis "Duplex - A new generation of stainless steels for desalination plants" Desalination; 205, (2007) 1-3: 104.

[87] S. Jacques, J. Peultier, P. Soulignac "Desalination plants: why using duplex stainless steels" Proc. Duplex 2007 Int. Conf. & Expo, Grado, Italy, AIM 2007.

[88] E. Johansson, F. Colombari, R. Pettersson "Gli acciai inossidabili Duplex nei trasporti" Proc. Giornate Nazionali sulla Corrosione e Protezione 2009, Udine, Italy, AIM 2009.

[89] L. M. Smith, M. Celant "Life cycle costing - are duplex stainless steels the cost-effective choice?", Proc. of the Duplex Stainless Steels 94, Glasgow, Scotland 1994.

[90] J. Charles "Past, present and future of the Duplex Stainless Steels" Proc. Duplex 2007 Int. Conf. & Expo, Grado, Italy, AIM 2007.

[91] M Liljas, "The welding metallurgy of duplex stainless steels", Proc. of the Duplex S t a i n l e s s Steels 94, Glasgow, Scotland 1994.

[92] F. Bonollo, A. Tiziani, P. Ferro, "Advances in Duplex Stainless Steels" - Chapter 4, ISTE LTD. London, 2009.

[93]   J.-O. Nilsson, T. Huhtala, P. Jonsson, L. Karlsson, A. Wilson, "Structural stability of super duplex stainless weld metals and its dependence on Tungsten and Copper", Metall. Mater. Trans. A 27A (1996), 2196.

[94]   V. Muthupandi, P. Bala Srinivasan, S.K. Seshadri, S. Sundaresan, "Effect of weld metal chemistry and heat input on the structure and properties of duplex stainless steel welds", Materials Science and Engineering A358 (2003), 9.

[95]   S. Atamert, J.E. King, "Elemental partitioning and microstructural development in duplex stainless steel weld metal", Acta Metall. Mater. 39 (1991), 273.

[96]   L. Van Nassau, H. Meelker, J. Hilkes , Proc. of the Duplex Stainless Steels Conference, Beaune, France 1991, 303.

[97]   S. Atamert, J.E. King.,"Superduplex stainless steels Part 1. Heat affected zone microstructures", Mater. Sci. Technol. 8 (1992), 896.

[98]   H. Sieurin, R. Sandstrom "Austenite reformation in the heat-affected zone of duplex stainless steel 2205", Materials Science and Engineering A 418 (2006) 250.

[99]   J. Hochmann, A. Desestret, P. Jolly P, Mét. Corro Industrie, 2 (591-592), 1974, 390.

[100] D. J. Koteeki, J. L. P. Hilkes "Welding processes for duplex stainless steels", Proc. of the Duplex Stainless Steels 94, Glasgow, Scotland 1994.

[101] V. Muthupandi, P. Bala Srinivasan, S. K. Seshadri and S. Sundaresan   "Effect of nitrogen addition on formation of secondary austenite in duplex stainless steel weld metals and resultant properties", Science and Technology of Welding and Joining 9, N°1 (2004) 47.

[102] P. Sathiya, S. Aravindan, R. Soundararajan, A. Noorul Haq, "Effect of shielding gases on mechanical and metallurgical properties of duplex stainless steel welds", Journal of Material Science 44 (2009) 114, DOI 10.1007/s10853-008-3098-8

[103] S.S.M. Tavares, J.M. Pardal, L.D. Lima, I.N. Bastos, A.M. Nascimento, J.A. de Souza "Characterization of microstructure, chemical composition, corrosion resistance and toughness of a multipass weld joint of superduplex stainless steel UNS S32750", Materials Characterization 58 (2007) 610

[104] T. Kannan, N. Murugan, "Effect of flux cored arc welding process parameters on duplex stainless steel clad quality", Journal of Materials Processing Technology 176 (2006) 230.

[105] F. Bonollo, A. Gregori, A. Tiziani, "Saldatura di acciai superduplex mediante processi non convenzionali: confronto tra Laser, Fascio Elettronico e Plasma", Proc. "1° Conferenza Nazionale sulla Saldatura e le Costruzioni Saldate", Genova, Italy 1996.

[106] A. Urena, E. Otero, M.V. Utrilla, C.J. Munez "Weldability of a 2205 duplex stainless steel using plasma arc welding", Journal of Materials Processing Technology 182 (2007) 624.

[107] Emel Taban "Toughness and microstructural analysis of superduplex stainless steel joined by plasma arc welding", Journal of Mater Science 43 (2008) 4309 DOI 10.1007/ s10853-008-2632-z

[108] N.A. McPherson, K. Chi, T.N. Baker "Submerged arc welding of stainless steel and the challenge from the laser welding process", Journal of Materials Processing Technology 134 (2003) 174.

[109] Jerzy Nowacki, Pawel Rybicki "The influence of welding heat input on submerged arc welded duplex steel joints imperfections", Journal of Materials Processing Technology 164 (2005) 1082.

[110] E. Capello, P. Chiarello, B. Previtali, M. Vedani "Laser welding and surface treatment of a 22Cr5Ni3Mo duplex stainless steel", Materials Science and Engineering A351 (2003) 334.

[111] F. Bonollo, A. Tiziani, A. Zambon, M. Penasa, "Laser beam welding of superduplex stainless steels", Proc. of the Duplex Stainless Steels 94, Glasgow, Scotland 1994.

[112] Y.S. Sato, T.W. Nelson, C.J. Sterling, R.J. Steel, C.-O. Pettersson "Microstructure and mechanical properties of friction stir welded SAF 2507 super duplex stainless steel", Materials Science and Engineering A 397 (2005)   376.

[113] J.Linder, A. Melander, M. Larsson, Y. Bergengren, "Fatigue design of spot-welded austenitic and duplex stainless sheet steels", Fatigue & fracture of engineering materials & structures 21 N°6 (1998) 673.

[114] F. Bonollo, A. Tiziani, P. Ferro, "Evoluzione microstrutturale di acciai duplex e superduplex in relazione ai processi di saldatura", La Metallurgia Italiana 2 (2005) 27.

[115] J. Dobránszky, T. Sándor, A. Nagy-Hinst, A. Géza Eichhardt, L. Gyur "Weld pool characteristics of the ATIG-welded joints" Proc. Duplex 2007 Int. Conf. & Expo, Grado, Italy, AIM 2007.

[116] J.O. Smith, S.M. Mueller, L.M. Volpone "Weldability of an austenitic-ferritic 1.4462 (SAF 2205) steel on tubular products using GTAW in keyhole-modality (K-TIG)", Proc. Duplex 2007 Int. Conf. & Expo, Grado, Italy, AIM 2007.

[117] Horng-Yih Liou, Rong-Iuan Hsieh, Wen-Ta Tsai "Microstructure and pitting c o r r o s i o n i n simulated heat-affected zones of duplex stainless steels", Materials Chemistry and Physics 74 (2002) 33.

[118] C.T. Kwok, S.L. Fong, F.T. Cheng, H.C. Man, "Pitting and galvanic corrosion behavior of laser- welded stainless steels", Journal of Materials Processing Technology 176 (2006) 168.

[119] C. Garcia, F. Martin, P. de Tiedra, Y. Blanco, M. Lopez "Pitting corrosion of welded joints of austenitic stainless steels studied by using an electrochemical minicell", Corrosion Science 50 (2008) 1184.

[120] HeonYoung Ha, HyukSang Kwon "Effects of Cr_2N on the pitting corrosion of high nitrogen stainless steels", Electrochimica Acta 52 (2007) 2175.

[121] L.R. Scharfstein, "Effects of composition, structure and heat treatment on the corrosion resistance of stainless steel" in: D. Peckner, I.M. Bernstein (Eds.), Handbook of Stainless Steels, McGraw Hill, 1977, Chapter 15.

[122] Z.L. Zhang, T. Bell, "Structure and corrosion resistance of plasma nitrided stainless steel", Surf. Eng. 1 (1985) 131.

[123] ANNUAL BOOK OF ASTM STANDARDS, ASTM A928/A928M - 09 Standard Specification for Ferritic/Austenitic (Duplex) Stainless Steel Pipe Electric Fusion Welded with Addition of Filler Metal.

[124] F. Bonollo, A. Tiziani, P. Lazzarin, R. Tovo "Effetto dei trattamenti termici sulle caratteristiche microstrutturali di acciai inossidabili superduplex (UNS S32750) saldati laser", La Metallurgia Italiana vol. 87, N°11 (1995) 551.

RESULTS AND DISCUSSION

Duplex Stainless Steels (DSS) and Super Duplex Stainless Steels (SDSS) are austenitic/ferritic stainless steels which take advantage of their favorable microstructure (about 50% ferrite and 50% austenite) and combine the optimum characteristics of the two structures. In particular, they have good mechanical properties, excellent resistance to pitting corrosion and stress-corrosion cracking. Consequently, they found several applications in fields where the corrosion resistance is fundamental: chemical, petrolchemical, pulp, paper industries, offshore and desalination plants. They could often replace the employment of others stainless steels because of their more favorable life cycle costing.

However, welding and heat treatment processes on these type of steels are generally a crucial operation because they alter the microstructure and, as a consequence, the properties of the examined component.

For example, the most common effects of a welding process on DSS are:
  - local alteration of the ferrite/austenite balance
  - precipitation of detrimental phases in reheating passes of the fusion zone and in the heat-affected zone
  - local decay of the mechanical and corrosion properties.

The literature about this argument is widespread: several studies on welding, heat treatments, mechanical and corrosion properties of DSS have been carried out by many researchers and material scientists and has been presented in detail in the part "State of the art" of this thesis.

Nevertheless, the interest on welding operations and on the development of new relationships between microstructure and corresponding properties of DSS and SDSS is continuously growing.

The present doctoral dissertation is aimed to analyze in detail the problems and recent developments related to welding and heat treatments of Duplex Stainless Steels. In particular, type of process, materials involved and post welding heat treatment in relation to corrosion properties have been analyzed, and the relationships between process, final microstructure and properties has been investigated.

The reference material for most of the work has been the Super Duplex UNS S32750 (SAF 2507), but also the Duplex grade UNS S31803 (SAF 2205) has been examined. Nowadays, all the most popular welding technologies are successfully applied to austenitic/ferritic stainless steels (cf. §3.2 of section "State of the art"): in particular, *gas tungsten arc welding* (GTAW, Article I, Article II) and *submerged arc welding* (SAW, Article III, Article IV) on UNS S32750 has been considered in this work.

It must be keep in mind that in DSS or SDSS welding processes, the filler metal, when used, differs in composition if compared with the base material (cf. §3.1 of "State of the art").
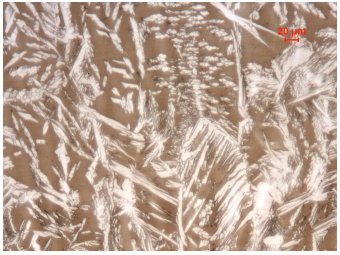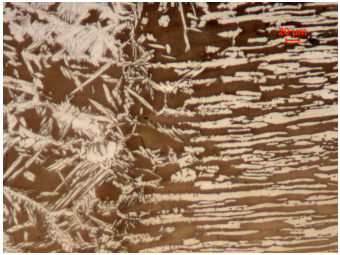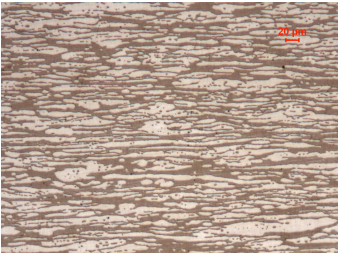
In this section, by collecting the main results presented in the papers and following the leading scheme reported in the section "Aim of the work", the foremost conclusions of the thesis are summarized.
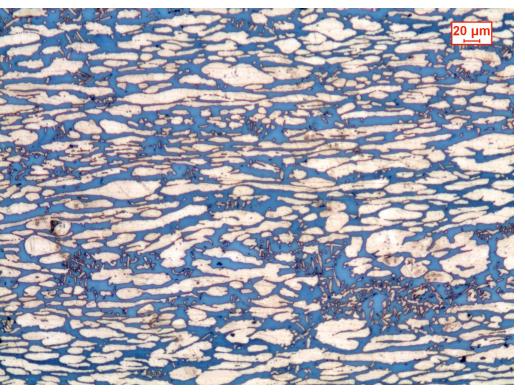
1. Influence of the process on microstructure

1.1 Welding

First of all, the effects of the considered welding processes on microstructure of UNS S32750 SDSS have been analyzed (Article I, Article III).

The phase balance of UNS S32750 results upset in the fusion zone (FZ) and in the heat affected zone (HAZ) respect to the parent metal (PM); the experimental results for both the studied welding technologies are summarized in the following tables:
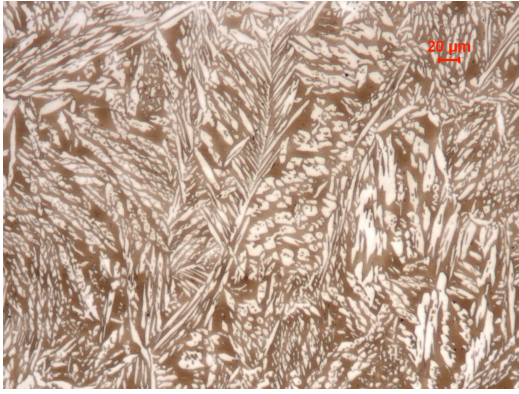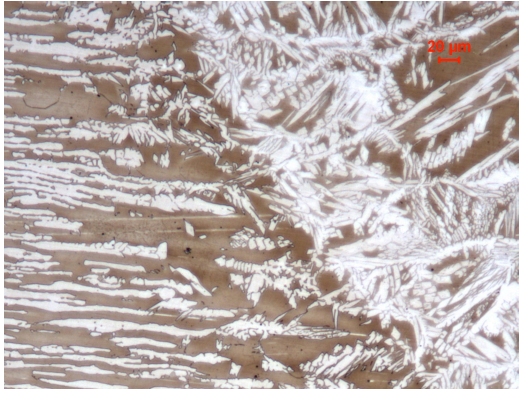
GTAW		
FZ - 100x	*HAZ - 100x*	*PM - 100x*
% vol. Austenite		
42.5 ± 2.4	44 ± 3.7	57.2 ± 3.3

Table 1 - Results of microstructural analysis on UNS S32750 GTA welded

SAW	
FZ - 100x	*PM - 100x*
% vol. Austenite	
48.1 ± 1.9	53 ± 2.0

Table 2 - Results of microstructural analysis on UNS S32750 SA welded

If an innovative nickel-rich filler metal is used in GTAW of UNS S32750, a greater austenite amount in the fusion zone is guaranteed:

GTAW	
FZ - 100x	*PM - 100x*
% vol. Austenite	
52.5 ± 3.1	46.2 ± 3.8

Table 3 - Results of microstructural analysis on UNS S32750 GTA welded joints with innovative filler wire

Another important microstructural feature which is affected by the welding operation on SDSS and DSS is the partitioning of elements in the fusion zone.

In fact, the rapid cooling induced by the welding thermal cycles, inhibits the diffusion and tends to make the austenite and ferrite composition homogeneous, regarding the substitutional elements (Cr, Mo, Ni etc.). Nevertheless, interstitial elements controlling the reaction (N) are heavily concentrated to the austenite.

The experimental data concerning the partitioning of elements obtained in the fusion zone of UNS S32750 GTA and SA welded joints are reported in table 4:

	GTAW						SAW		
Element	δ Innovative filler	γ Innovative filler	Partitioning ratio δ/γ Innovative filler	δ Traditional filler	γ Traditional filler	Partitioning ratio δ/γ Traditional filler	δ	γ	Partitioning ratio δ/γ
Mo	4.18	3.46	**1.21**	4.08	3.29	**1.24**	3.73	3.47	**1.07**
Cr	25.94	24.89	**1.04**	25.87	24.54	**1.05**	23.67	23.59	**1.00**
Ni	8.51	9.51	**0.89**	8.30	9.14	**0.91**	8.41	8.81	**0.95**
N*	0.05	0.46	**0.11**	0.05	0.49	**0.10**	0.05	0.42	**0.12**

*Table 4 - Partitioning of elements in the fusion zone of UNS S32750 GTA and SA welded joints (* = Calculated, cf. <u>Article III</u>)*

The partitioning of elements in the parent metal (UNS S32750) is reported in the following table for comparison:

| Element	PM		
	δ	γ	Partitioning ratio δ/γ
Mo	4.62	2.93	**1.58**
Cr	25.61	23.24	**1.10**
Ni	5.12	7.87	**0.65**
N*	0.06	0.46	**0.13**

*Table 5 - Partitioning of elements in UNS S32750 base material (* = Calculated, cf. Article III)*

It can be seen that GTA welding of UNS S32750 guarantees a slightly better partitioning of the substitutional elements if compared with SA welding: the values of partitioning ratios of Chromium, Molybdenum and Nickel in the fusion zone of GTA welded joints are closer to the corresponding values of the base material than the partitioning ratios obtained in the fusion zone of SA welded joints. It can be concluded that the GTAW probably assures a slower cooling and a better diffusion in the fusion zone than SAW.

It is known that DSS and SDSS welded joints could be affected by the precipitation of detrimental phases in the fusion zone or in the heat affected zone (cf. §2.3 or §3.1 of section "State of the art").

In particular, it has been reported that in SDSS, which are characterized by higher nitrogen content than DSS, the precipitation of chromium nitrides could take place in the heat-affected zone.

The experimental results show that the oxalic etchant (100 ml H_2O, 10 g oxalic acid, electrolytic 6V) results more efficient to reveal the presence of precipitates than the traditional Beraha's etchant. The following figures report some optical micrographs and scanning electron microscope images of the chromium-rich precipitates detected in the HAZ of the weldings experimentally examined, which have been identified as chromium nitrides.
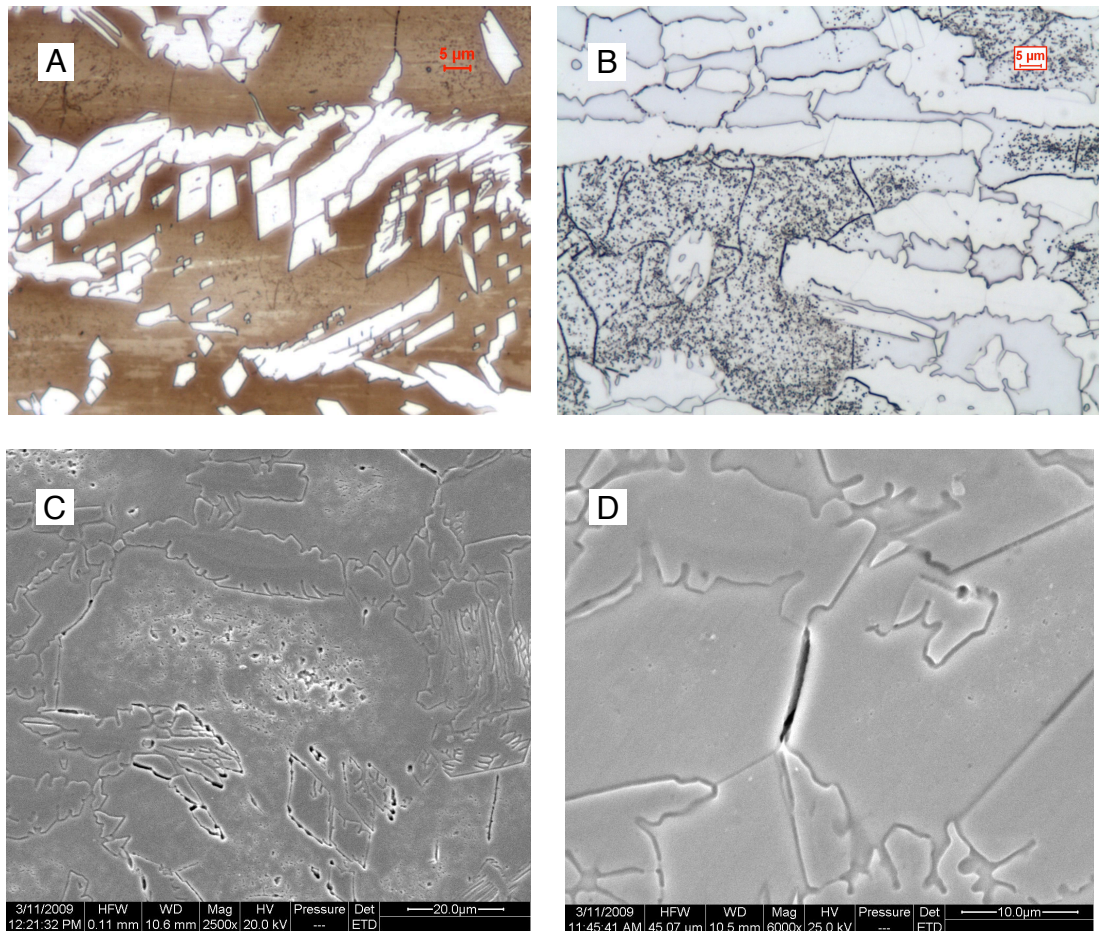
Fig. 1 - Images of precipitates detected in the HAZ of the analyzed welded joints:
A - Optical micrography of GTA welded joints, Beraha's etchant (500x)
B - Optical micrography of SA welded joints, Oxalic etchant (500x)
C - Scanning electron microscope image of SA welded joints, Oxalic etchant (2500x)
D - Scanning electron microscope image of SA welded joints, Oxalic etchant (6000x)

The presence of these intermetallic phases could affect negatively the corrosion and mechanical properties of the welded joints.

1.2 Post welding heat treatment (PWHT)

Post welding heat treatment on DSS and SDSS is a full solution anneal generally performed in the range 1050-1120°C, in dependence of the chemical composition of the considered alloy. For major details on PWHT see §3.3 of section "State of the art".

The effects of PWHT on microstructure of UNS S32750 GTA and SA welded joints have been studied in this work (Article II, Article III) and the results found could be summarized as:

- PWHT increases the austenite content in the fusion zone. Both intragranular austenite precipitates and grows on ferrite grains, and Widmanstätten-type austenite grows inside the ferrite grains after solution treatments (fig. 2).
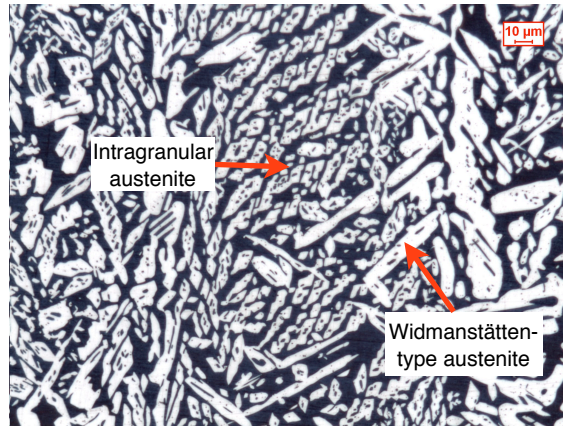
Fig. 2 - Optical micrograph of the fusion zone of solution treated sample (SAW of UNS S32750, annealed at 1100°C for 1 hour, 200x); Beraha's etchant (dark phase-ferrite, white phase-austenite)

The austenite content content slightly increases with holding time but decreases with the annealing temperature, in particular if it exceed 1100°C. The experimental results are summarized in the following tables:

PWHT Temperature [°C]	-	1050					1075					1100				
PWHT Time [min]	-	1	4	11	18	27	1	4	11	18	27	1	4	11	18	27
% vol. Austenite - Fusion zone	27	42	41	42	44	42	43	42	41	44	46	42	43	44	45	47

Table 6 - Experimental austenite volume fractions detected in the fusion zone of annealed UNS S32750 GTA welded joints

PWHT Temperature [°C]	-	1050	1100	1150
PWHT Time [min]	-	60	60	60
% vol. Austenite - Fusion zone	48.3 ± 3	65.8 ± 1.6	62.3 ± 3	51.8 ± 2
% vol. Austenite - Base material	53 ± 3.3	55.6 ± 1.2	49.3 ± 2	47.8 ± 2.3

Table 7 - Experimental austenite volume fractions detected in the fusion zone and in the base material of annealed UNS S32750 SA welded joints

- The composition of ferrite and austenite (i.e. the partitioning of elements) in the fusion zone of UNS S32750 SA welded joints reaches the equilibrium values after PWTH. In particular ferrite enriches in Chromium and Molybdenum and austenite enriches in Nickel if compared with the as-welded conditions, like reported in table 8:

SAMPLE	AUSTENITE				FERRITE				PARTITIONING RATIOS (δ/γ)		
	Cr	Ni	Mo	N*	Cr	Ni	Mo	N*	Cr	Ni	Mo
AS - WELDED	23.6	8.8	3.5	0.42	23.7	8.4	3.7	0.05	1.0	1.0	1.1
ST 1050°C	22.7	9.8	2.8	0.33	25.4	6.4	5.1	0.05	1.1	0.7	1.8
ST 1100°C	22.7	9.9	2.7	0.35	25.1	6.7	5.0	0.05	1.1	0.7	1.8
ST 1150°C	22.5	10.1	2.7	0.38	25.0	6.8	4.7	0.05	1.1	0.7	1.7

Table 8 - Chromium, Nickel, Molybdenum and Nitrogen (* = Calculated, cf. Article III) content in ferrite and austenite of the fusion zone of UNS S32750 SA welded joints (ST = solution treated)

- The chromium-rich precipitates detected in the as-welded HAZ dissolve after PWHT and transform in austenite, like demonstrated by the following figure:

Fig. 3 - Optical micrograph of HAZ of the solution treated specimen at 1100°C. SAW of UNS S32750, Oxalic etchant (200x)

1.3 Isothermal and anisothermal heat treatments in the range 800-950°C

It is well known that DSS and SDSS are prone to formation of secondary phases in the range 600-1000°C, which are generally deleterious for corrosion and mechanical behavior.
In this work (Article V), some isothermal heat treatments in the range 800-950°C for various holding times and some anisothermal heat treatments with different cooling
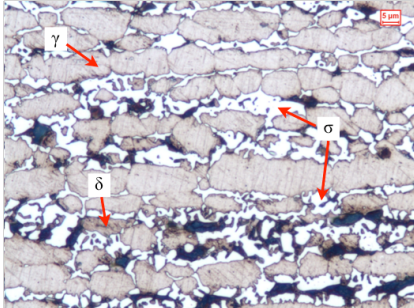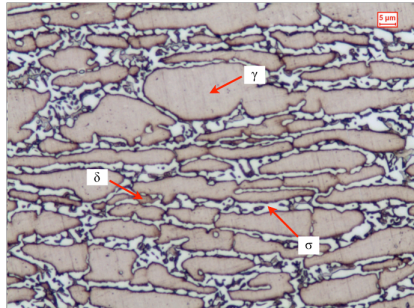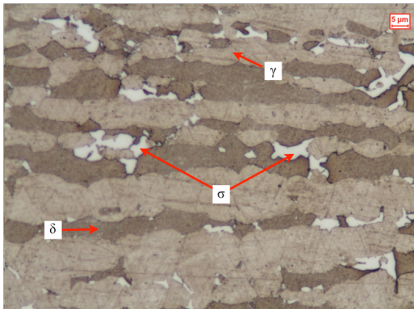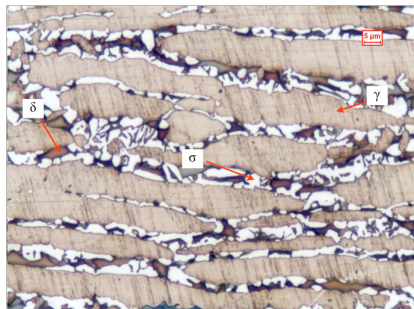
rates have been performed on Duplex and Super Duplex Stainless Steels to study the kinetic of sigma phase precipitation.

The collected data have been used to set up a numerical model to calculate and visualize the Temperature-Time-Transformation (TTT) curves and the Continuos Cooling Transformation (CCT) curves relatively to sigma phase precipitation.

In particular, the SDSS analyzed (UNS S32750) results to be more prone to sigma phase formation than the DSS (UNS S31803) both for isothermal (fig. 4) and anisothermal (fig. 5) treatments.

The experimental critical cooling rates for sigma phase precipitation results to be equal to 0.3°C/s in the case of Duplex grade and 0.5 °C/s for the Super Duplex one. These results are useful to define the welding parameters (which determines the cooling rate) to avoid the formation of deleterious phases in the HAZ of welded components made in DSS and SDSS.

In conclusion, even if the Super Duplex grade is more corrosion-resistant than the Duplex one (the pitting resistance equivalent number, PREN, is higher), it results to be more prone to deleterious phase precipitation.

Heat treatment	UNS S31803	UNS S32750
850°C, 420 min		
900°C, 30 min		

Fig. 4 - Optical micrographs of isothermally treated specimens, Beraha's etchant (500x)
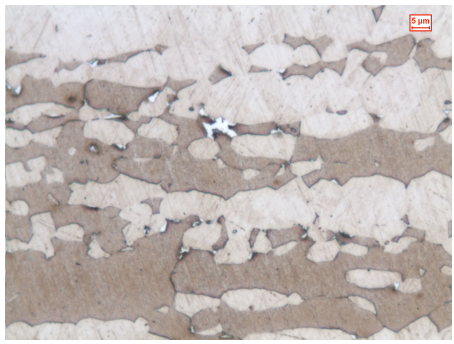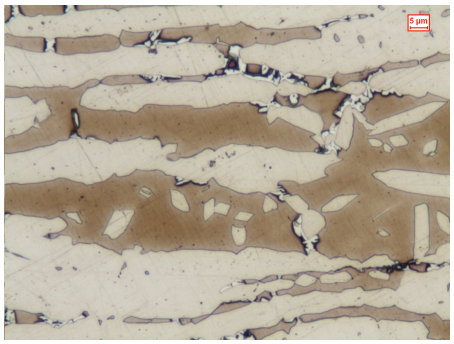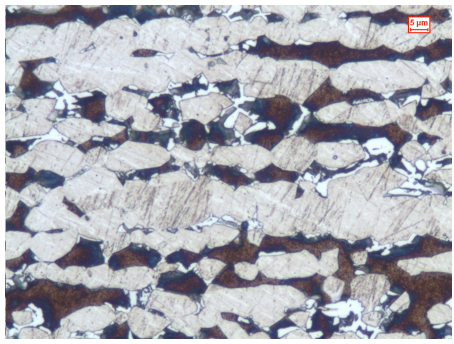
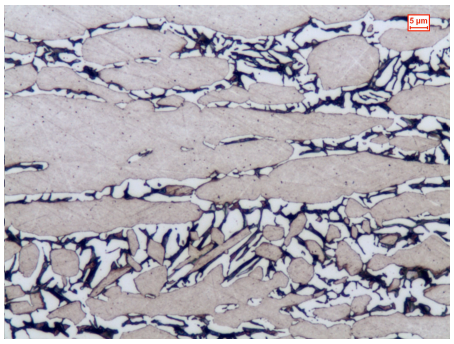| Cooling rate	UNS S31803	UNS S32750
0.3°C/s		
0.033°C/s		

Fig. 5 - Optical micrographs of heat treated specimens (continuos cooling), Beraha's etchant (500x); dark phase: ferrite, white phase: austenite, light white phase: sigma phase.

2. Influence of the process on properties

In §3.3 of section "State of the art" the literature concerning the influence of welding on corrosion properties of DSS has been presented.

In this work, the effects of GTAW (Article II) and SAW (Article IV) on pitting corrosion resistance of UNS S32750 welded joints have been analyzed.

The experimental methods used for pitting corrosion evaluation have been: gravimetric tests according ASTM G48 standards (24 h test in 6% $FeCl_3$ solution at 50°C) and electrochemical measurements (anodic polarization curves in 3.5% NaCl solution at 80°C, open to air).

The results concerning the ASTM G48 test of annealed GTA welded joints at various temperatures and holding times are reported in the following figure:
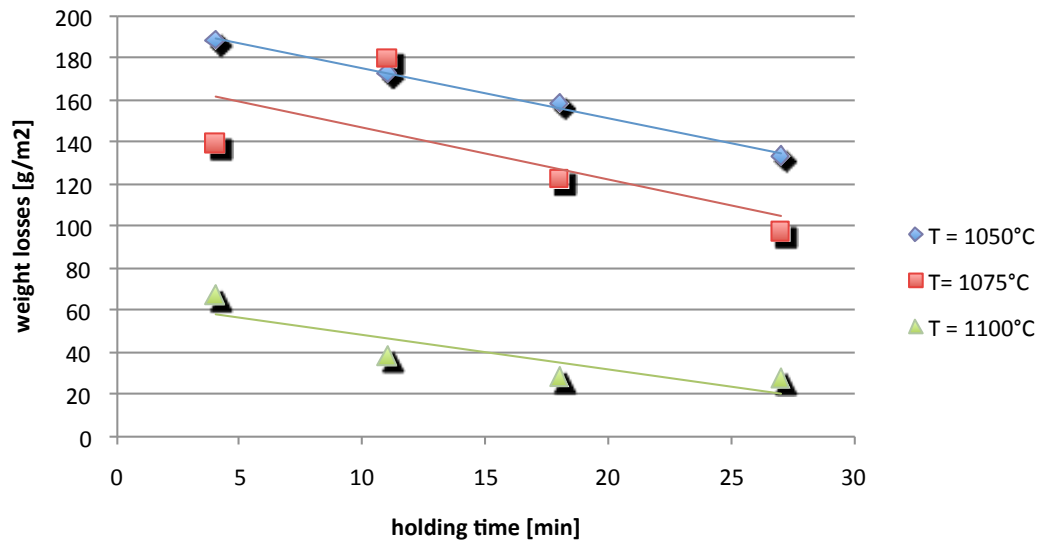
Fig. 6 - Weight losses after 24h ASTM G48 test on annealed UNS S32750 GTA welded joints

The corresponding value of the as welded joint results to be 170 g/m². It can be seen that the weight losses after PWHT decrease with increasing the annealing temperature (in the range 1050-1100°C) and holding times. In this case the optimum annealing temperature results to be equal to 1100°C.

To express the pitting resistance of stainless steels, the parameter PREN (*pitting resistance equivalent number)* = %Cr + 3.3%Mo + 16 ÷ 30%N, could be used (cf. §2.4 of section "State of the art"). Since DSS and SDSS are constituted by two phases with different compositions (depending on annealing temperature) PREN of weaker phase must be considered to define the behavior of the entire alloy.

In general, PREN of the as-welded fusion zone corresponds to the PREN of ferrite, which is very poor in nitrogen and corresponds to the weaker phase (cf. Table 8). In fact, the experimental tests on the fusion zone of UNS S32750 SA welded joints shows a deep pitting attack in this phase, like showed in figure 7.
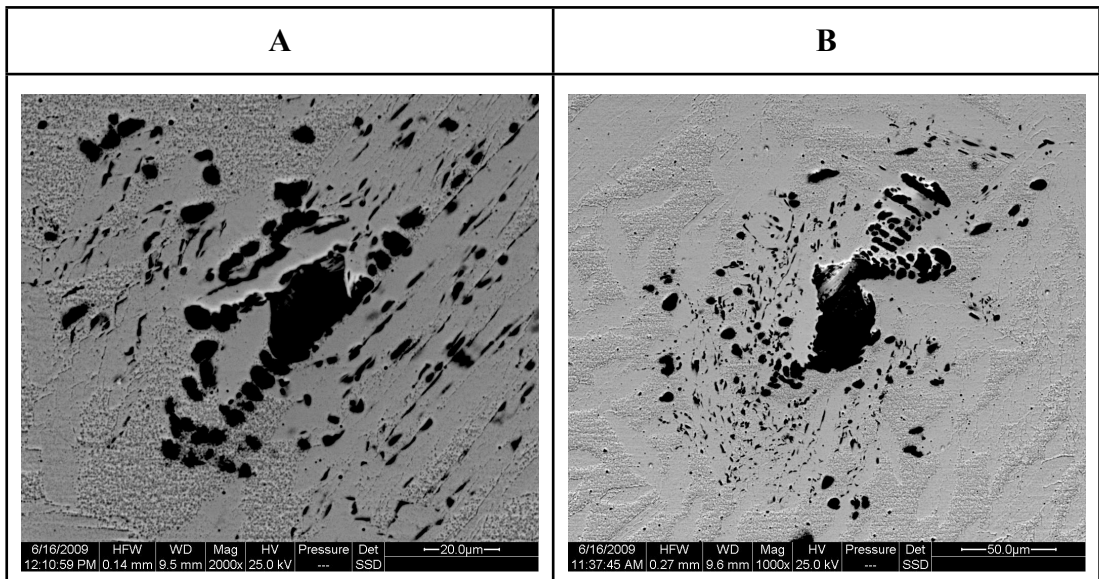
A	B

Fig. 7 : Aspect of the pitting attack revealed in the fusion zone of the as-welded specimen after potentiodynamic test in 3.5% NaCl at 80°C (A - 2000x, B - 1000x)

After PWHT the phase compositions in the fusion zone change (cf. Table 8), and consequently the calculated PREN of single phases depends on the annealing temperature, like showed by the following figures:
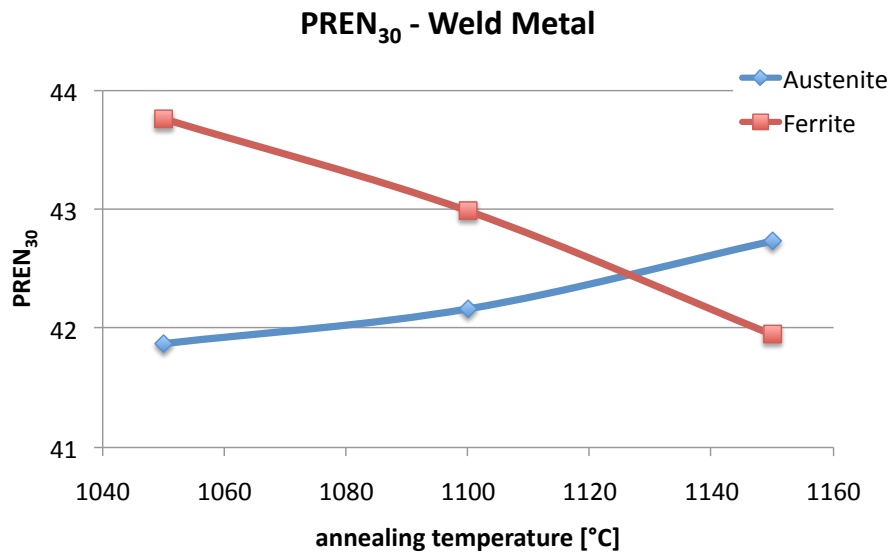

Fig. 8 - Calculated $PREN_{30}$ for austenite and ferrite phase concerning the weld metal (fusion zone) of UNS S32750 SA welded joints (as welded specimen : $PREN_{30}$ (austenite) = 47.6 $PREN_{30}$ (ferrite) = 37.5)
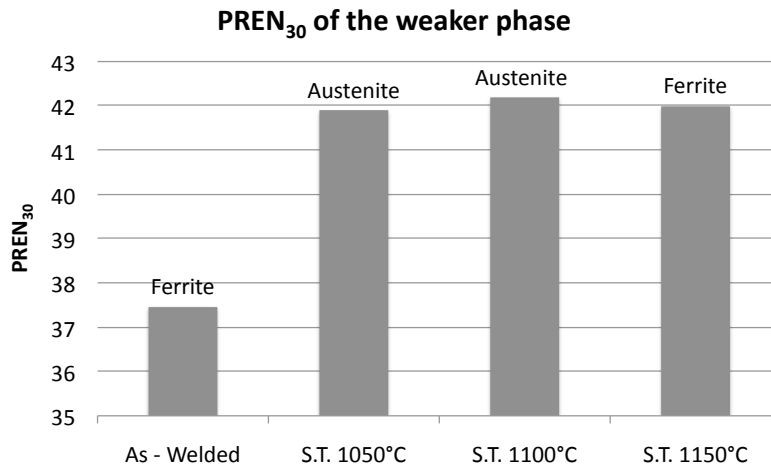
PREN$_{30}$ of the weaker phase

Fig. 9 : Calculated values of PREN$_{30}$ of the weaker phase in UNS S32750 SA welded joints

Like showed in figure 9, PREN$_{30}$ of weaker phase shows an abrupt increase after PWHT. In particular, the best pitting corrosion behavior corresponds to the highest value of PREN, i.e. at the temperature at which the two curves of figure 8 cross each other.

The experimental results regarding the electrochemical measurements (pitting potentials of parent and weld metal) and ASTM G48 tests of UNS S32750 SA welded joints are summarized in the following figures (in this case PWHT has been carried out at 3 temperatures - 1050, 1100, 1150°C - for a holding time of 1 hour):
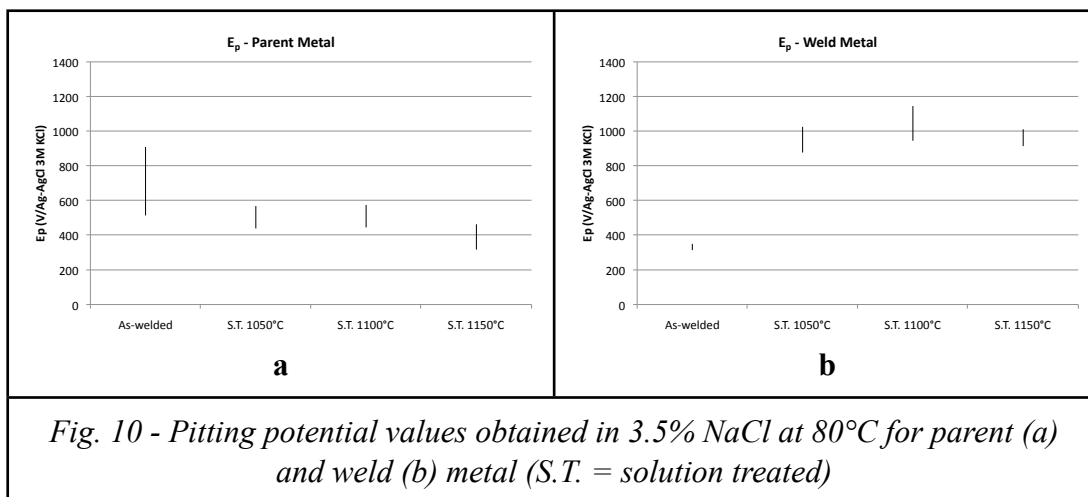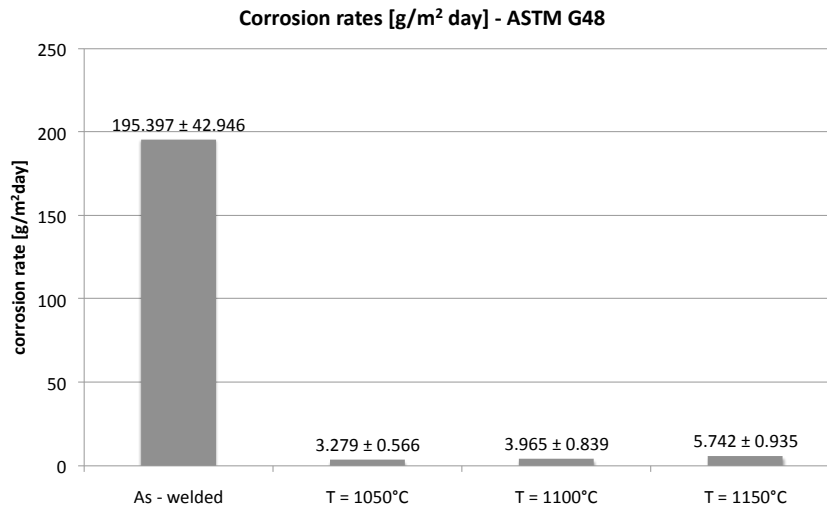

Fig. 10 - Pitting potential values obtained in 3.5% NaCl at 80°C for parent (a) and weld (b) metal (S.T. = solution treated)

Fig. 11 - Histogram showing the corrosion rates of considered specimens after pitting corrosion test in 6% FeCl$_3$ solution, 24 h

By examining figure 10 it can be noted that, after PWHT, the pitting potential (which represents the resistance to pitting corrosion) of weld metal show an abrupt increase. In particular, at an annealing temperature of 1100°C, the pitting resistance of weld metal reaches the highest value. This fact is confirmed by the histogram reported in figure 11, which contains the weight losses after ASTM G48 test: PWHT increases the pitting corrosion resistance of the entire welded joint by increasing the resistance of the fusion zone.

3. Relationship between microstructure and properties

Since DSS and SDSS microstructure is strictly connected to their properties, the knowledge of correlations between microstructure and resulting properties is essential to optimize future alloy design.
In particular, in this thesis the relationship between microstructure and pitting corrosion properties of SDSS has been deeply investigated, with reference to welding and heat treatment processes.

3.1 Relationship between as-welded microstructure and properties: effects of filler wire

The results of a first study concerning the effects on microstructure and properties of an innovative filler wire for GTAW of UNS S32750 are here presented (Article I).
Regarding the microstructure of the welded joints, it has been demonstrated that a nickel-rich filler metal guarantees a higher austenite content in the fusion zone (cf. Table 1-3). The study also analyzes the influence of the innovative filler on mechanical and corrosion properties in comparison with a traditional filler wire, chosen as a reference.
The resulting properties regarding the innovative filler (called A) and the traditional one (called B) are summarized in the following table:
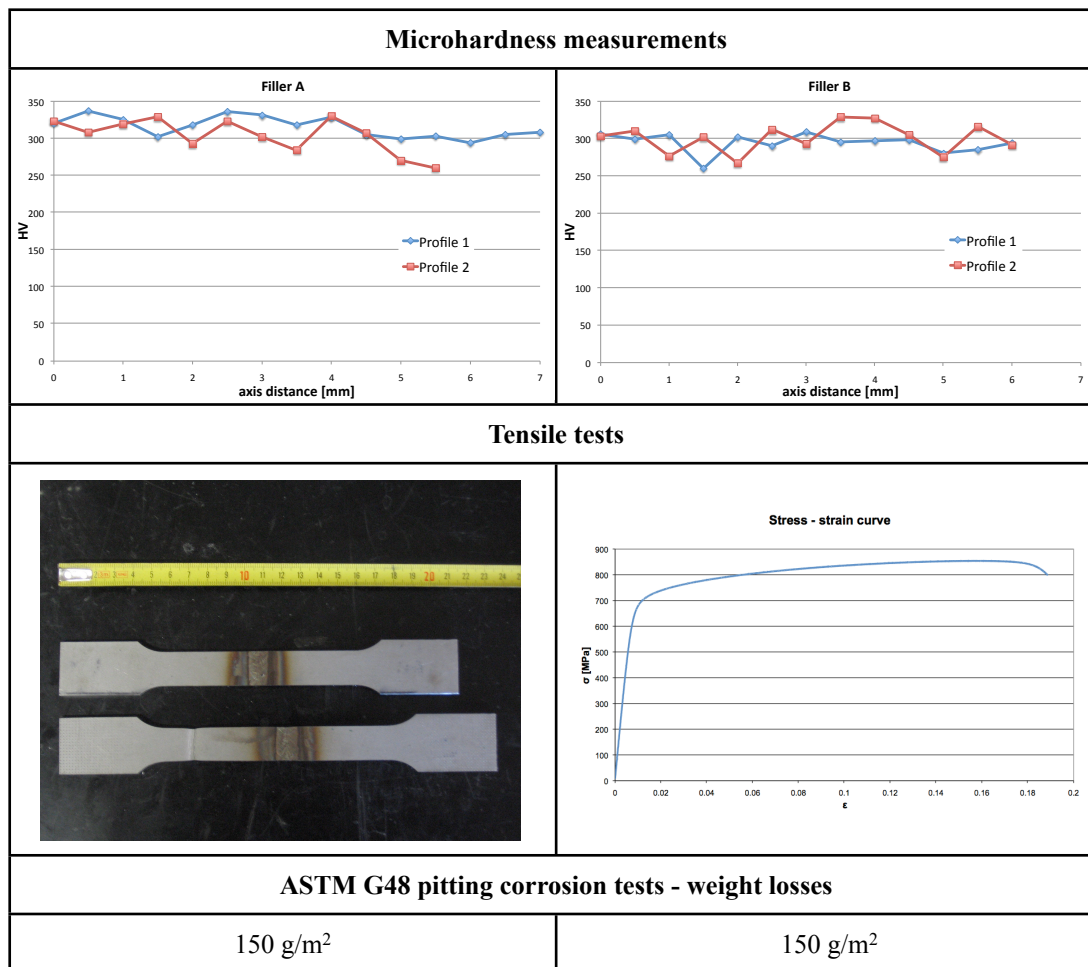
Microhardness measurements	
Filler A	**Filler B**
Tensile tests	
ASTM G48 pitting corrosion tests - weight losses	
150 g/m^2	150 g/m^2

Table 9 - Comparison of resulting properties of GTAW welded joints with two different filler metals

By examining Table 9, it can be noted that:
- a significant difference in the phase distribution between the two welded joints, doesn't imply an appreciable variance of mechanical properties (in terms of microhardness profiles and tensile properties, in fact the fracture affects the base material for both the fillers and the two stress-strain curves agree);
- the pitting corrosion resistance of the as-welded joints, expressed as weight losses after ASTM G48 test, is comparable for each filler metal.

Considering that the pitting corrosion resistance of the welded joints results comparable, but at the same time they have different austenite volume fractions (cf. Tables 1-3), it can be supposed that the pitting corrosion resistance of the welded joints isn't influenced by the corresponding austenite volume fraction of the fusion zone.

3.2 Relationship between PWHT microstructure and resulting properties

The influence of PWHT on corrosion properties of UNS S32750 GTA welded joints has been investigated in Article II.

It has be seen that PWHT increases the austenite content in the fusion zone, and the austenite content slightly increases with holding time (cf. Tables 6-7). Nevertheless, the precipitation of austenite (called "secondary austenite") is very quick: after 1 minute of permanence at PWHT temperature, the austenite fraction is close to the equilibrium value, and increasing the holding time, the corresponding austenite volume fraction doesn't show significant variations (cf. Table 6). The fact is well-illustrated in figure 12, where the experimental secondary austenite fractions (i.e. the austenite fractions precipitates in the fusion zone after PWHT) are reported in function of PWHT holding time, and interpolated using an Avrami equation to study the precipitation kinetics of secondary austenite.
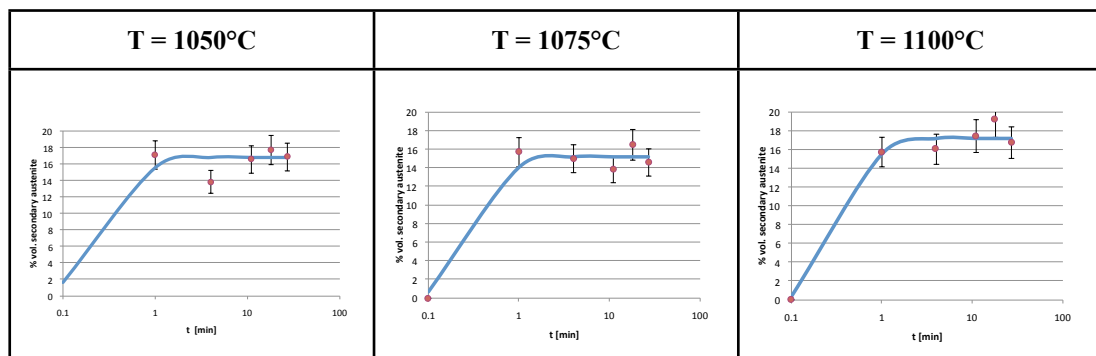

Figure 12 - Secondary austenite fractions precipitates in function of PWHT holding times in the fusion zone of UNS S32750 GTA welded joints

Since the corresponding pitting corrosion tests have showed that increasing the PWHT holding time, the weight losses tend to decrease (cf. Fig. 11), the pitting corrosion resistance of welded joints increases with increasing the PWHT holding time.

In conclusion, increasing the PWHT holding time, while the austenite volume fraction of fusion zone remains almost constant or undergoes slight variations, the pitting corrosion resistance of the welded joints increases. Therefore, pitting corrosion resistance isn't just connected to the austenite volume fraction of fusion zone, but others microstructural factors must be considered.

Starting from these consideration, Article IV takes a deeper look into the relationship between the microstructure of SDSS welded joints in relation to PWHT and resulting pitting corrosion properties, considering another important factor: the evolution of phase composition. In particular, UNS S32750 SA welded joints annealed at 3 different temperatures (1050, 1100, 1150°C) for one hour has been analyzed.

The evolution of ferrite and austenite composition in relation to PWHT is summarized in Table 8, while the corresponding values of PREN of the weaker phase is illustrated in Figure 9. The evolution of pitting corrosion properties (in terms of pitting potentials) of the fusion zone and the entire welded joint (in terms of weight losses) are shown in Figure 10 and 11.

It is easy to assume that the experimental pitting corrosion behavior of the fusion zone is strictly connected to the corresponding PREN of weaker phase: in fact, while the as-welded sample has a low PREN (which is due to the low Nitrogen content of the as-welded ferrite phase), PWHT changes the phase composition in the fusion

zone increasing the Chromium and Molybdenum content of ferrite (i.e. the PREN) and at the same time the corresponding pitting potential of the fusion zone.

The available literature on the argument, reports an exponential relationship between the pitting potential and the PREN for several stainless steels (cf. §2.4 of section "State of the art").

In this case, the analytical relationship between the experimental pitting potential (E_p) and $PREN_{30}$ of the weaker phase regarding the fusion zone of UNS S32750 SA welded joints is illustrated in the following figure:
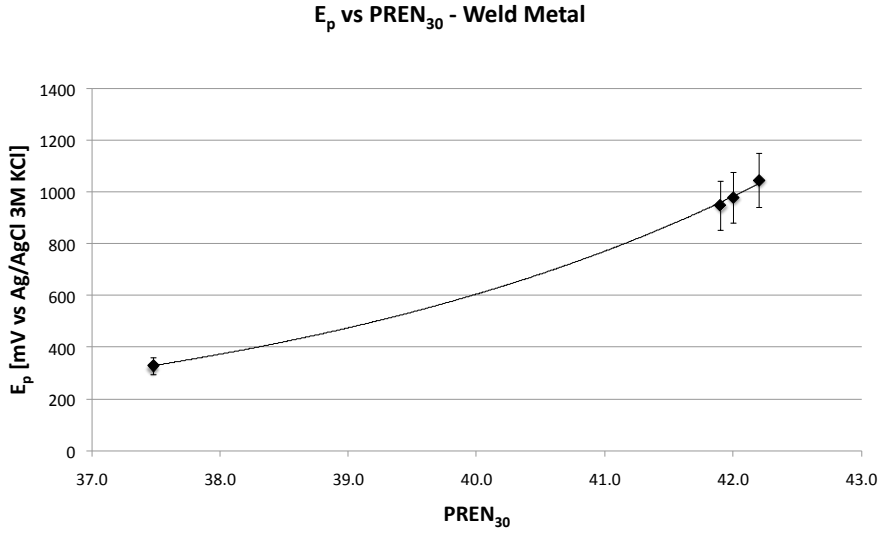
E_p vs $PREN_{30}$ - Weld Metal

Fig. 13 - Pitting potential vs $PREN_{30}$ of the weaker phase (i.e. alloy) regarding the weld metal

as reported in the literature, an exponential relationship between calculated $PREN_{30}$ of weaker phase and experimental pitting potentials of fused zone could be observed:

$$E_p = 0.035 \exp (0.243 PREN_{30}) \tag{1}$$

where the units of the coefficient 0.035 are (mV vs Ag/AgCl 3M KCl).

For the first time, a relationship between pitting potential and PREN has been proposed for a weld metal, referring to post-welding heat treatment.

CONCLUSIONS

The present doctoral dissertation allows to draw the following conclusions:

- When Super Duplex Stainless Steels are welded their local microstructure results upset.
In the fusion zone, the phase balance is altered as a consequence of the rapid cooling involved in welding; the austenite amount decreases if compared with base material and its morphology changes to grain boundary austenite and side plates Widmanstätten austenite.
The phase composition is deeply modified: the severe welding thermal cycles, inhibits the diffusion and tends to make the austenite and ferrite composition homogeneous, regarding the substitutional elements (Cr, Mo, Ni etc.). Nevertheless, interstitial elements (N) are heavily concentrated to the austenite. The experimental partitioning ratios of the substitutional elements in the fusion zone of UNS S32750 GTA and SA welded joints result to be close to 1, even tough GTAW assures a better partitioning than SAW, probably for the more flat cooling rate induced.
The presence of Chromium-rich precipitates, which has been identified as chromium nitrides, has been observed in the heat-affected zone (HAZ) of UNS S32750 SA and GTA welded joints; the oxalic etchant is excellent to highlight their presence. These precipitates can be deleterious for the corrosion behavior of the welded joints.

- The use of an innovative Nickel-rich filler wire in GTAW of UNS S32750 guarantees a higher austenite fraction in the fusion zone than the corresponding use of a traditional one; nevertheless, this significant difference in the phase distribution doesn't imply an appreciable variation in terms of mechanical and corrosion properties.
In particular, the pitting corrosion behavior of a SDSS welded joint isn't directly connected with the austenite volume fraction of the fusion zone.

- Post Welding Heat Treatment (PWHT) in the range 1050-1150°C has a significant effect on microstructure of UNS S32750 welded joints.
The austenite volume fraction in the fusion zone increases after PWHT, the austenite precipitation is quick (about 1 minute), and its volume fraction shows slight variations increasing the holding time; in addition, the austenite quantity tend to decrease with increasing the PWHT temperature.
PWHT tend to restore the elemental partitioning between ferrite and austenite in the fusion zone: after PWHT, ferrite enriches in Chromium and Molybdenum while austenite enriches in Nickel, if compared with the as-welded conditions.
The precipitates detected in the HAZ of the as-welded samples dissolve after PWHT: in fact, chromium nitrides are not stable in the temperature range considered for PWHT.

- The final pitting behavior of a SDSS welded joint isn't directly connected to the austenite volume fraction of the fusion zone after PWHT: while the austenite amount

remains almost constant increasing the PWHT holding time, the pitting behavior of the joint (expressed as weight losses after ASTM G48 test) tends to improve.

In fact, the pitting corrosion of SDSS welded joints depends on the evolution of PREN of ferrite and austenite in the fusion zone: the as-welded ferrite has a low PREN because it is poor in Nitrogen respect to the austenite, and it results deeply attacked during polarization test in 3.5% NaCl at 80°C. After PWHT, ferrite enriches in Chromium and Molybdenum and at the same time increases its PREN, therefore the pitting behavior of the fusion zone improves. Identification of weaker phase in dependence of welding and PWHT processes is useful to determine the final pitting behavior of welded joints made in austenitic/ferritic stainless steels.

The "phase homogenization" diffusional process depends on PWHT temperature and holding time: by choosing carefully these two parameters the optimum pitting behavior can be obtained.

In conclusion, the most important factor to determine the corrosion behavior of UNS S32750 welded joints is the PREN of the weaker phase, as demonstrated by the obtained relationship between pitting potential and PREN. The consequences are important when welded structures made in SDSS and DSS must be applied in corrosive environments.

- The tendency of sigma phase precipitation for Super Duplex UNS S32750 is 2-3 times higher than the Duplex UNS S31803, in relation to isothermal heat treatments in the range 800-900°C. The critical temperature for sigma phase precipitation regarding the Super Duplex grade is slightly higher than the Duplex one. Concerning continuos cooling treatments, which can simulate a cooling resulting from welding operations, it has been found that UNS S32750 is characterized by a critical cooling rate for sigma phase precipitation equal to 0.5°C/s, while the corresponding value for UNS S31803 is 0.3°C/s. These values results to be useful to avoid the presence of undesired phases in welded components made in DSS or SDSS.

Numerical models developed in SYSWELD 11.0® could a helpful tool to predict the final microstructure, in terms of secondary phases precipitation, of DSS and SDSS subjected to welding processes or heat treatments.

ACKNOWLEDGEMENTS

PAPERS

ARTICLE I

METALLURGICAL AND MECHANICAL CHARACTERIZATION OF UNS S32750 WELDED JOINTS WITH INNOVATIVE FILLER WIRE

F. Bonollo, P. Ferro, R. Cervo*

B. Vianello**

M. Durante***

*   *University of Padova, Department of Management and Engineering, Stradella San Nicola 3 - 36100 Vicenza (Italy)*

** *TFA Filinox, S.Vendemiano - Treviso (Italy)*

***   *E.Zanon S.p.A., Schio - Vicenza (Italy)*

ABSTRACT

The excellent combination of mechanical and corrosion properties of superduplex stainless steels is due to the strict control of chemical composition and microstructure balance.

However, a welding operation affects the final properties of the welded joints, in particular by altering the corrosion and mechanical behavior of the material. In particular, the high cooling rates involved in welding, modify the microstructure balance of the material, and the ferrite volume fraction in the weld metal could be higher than the equilibrium value. To avoid this drawback and to obtain a more balanced microstructure, filler wire with enhanced austenite-stabilizers content are used. In this work, the effect of two different filler metals (one is traditional and one is innovative) on a 5 mm thick UNS S32750 superduplex GTA welded joint, is analyzed.

Analysis with LOM (light optical microscopy), SEM (scanning electron microscopy), EDS (energy dispersive spectroscopy), microhardness profiles, tensile test on as-welded specimen and corrosion test using ASTM G48 standard are carried out.

The innovative filler metal, characterized by a higher nickel equivalent content, ensure a more austenite-rich welded joint. Instead, mechanical properties and corrosion resistance of the as-welded joints are not sensitively affected by the different chemical composition of the two filler metals.

KEY WORDS

1. INTRODUCTION

Superduplex stainless steels, characterized by a balanced microstructure characterized of austenite and ferrite, combine the excellent properties of austenitic and ferritic stainless steels: mechanical strength, pitting corrosion and stress corrosion cracking resistance, especially in aggressive environments (containing chlorides or other halides).

In many industrial applications, the major issue when austeno-ferritic stainless steels are worked on, is to maintain their balanced microstructure during the various processes involved in the manufacturing of components.

One of the most critical and widely used process is welding, during which the material is subjected to severe thermal cycles.

Examining diagram in figure 1, where the most common DSS and SDSS are indicated, it can be noted that some steels completely solidify in a ferritic structure (δ ferrite). During the cooling subsequent to solidification, below the δ-solvus temperature (that is between 1200°C and 1300°C in relation to the alloy composition), the solid-state transformation of ferrite to austenite takes place, with the consequent achievement of the dual-phase microstructure.

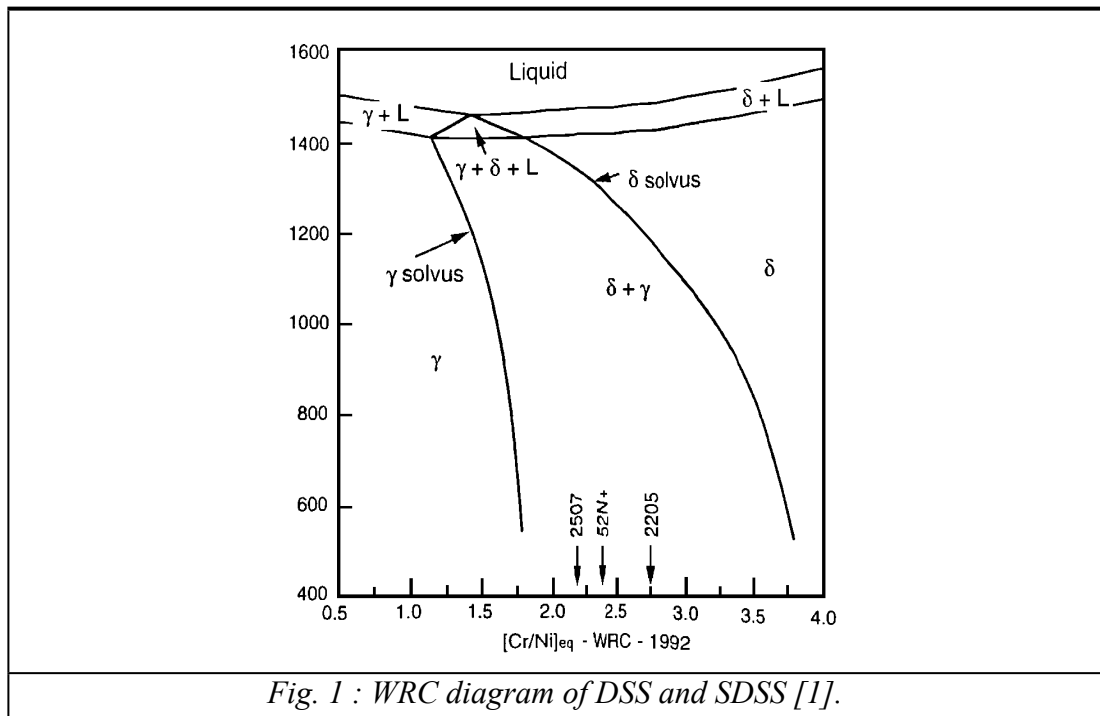*Fig. 1 : WRC diagram of DSS and SDSS [1].*

The reaction's kinetic of this transformation is extensively studied in the literature. Southwick e Honeycombe [2] have carried out a study in isothermal conditions of a 26%Cr-5%Ni steel, identifying an Avrami-type reaction for the growth of austenite in ferrite:

$$T = T_0 + \frac{k_1}{\tau} \exp\left(-\frac{k_2}{(T_{max} - T_0)\tau} \right)^{\frac{1}{j}}$$

(1)

where V_γ = volume fraction of austenite formed at time t;
        V_m = equilibrium austenite volume fraction;
        T   = temperature;
        b,n   = experimental parameters.

Recently, Atamert e King [3] introduced the relation:

$$V_\gamma = C1 + C2 \cdot (Cr_{eq} - Ni_{eq}) + C3 \cdot \Delta t_{1250-800} \tag{2}$$

where, in addition to the already defined symbols:
        $\Delta t_{1250-800}$ = time elapsed, during cooling, to shift from 1250°C to 800°C
        C1, C2 and C3 = constants

A similar formulation has been proposed by Lindblom e Hannerz [4]:

$$V_\gamma = K(\Delta t_{12-8})^m \tag{3}$$

where, in addition to the already defined factors, Δt_{12-8} is the time elapsed, during cooling, to shift from 1200°C to 800°C and m is a parameter depending on composition.

Therefore, the austenite fraction which growth from ferrite is in inverse proportion to the cooling rate in the temperature interval between 1200°C (temperature at which the reaction δ ferrite→ austenite begins to be thermodynamically possible) and 800°C (temperature below which the austenite/ferrite ratio doesn't change significantly – see the diagram in figure 1) and diffusion processes that allow the reaction are importantly decelerated.

The ferrite and austenite compositions are different: austenite is enriched in nickel, nitrogen, manganese, copper and carbon, while ferrite is rich in chromium, molybdenum, silicon and niobium. It is useful to define, for each alloy element, the partitioning coefficient, given by the mass fraction of element in ferrite to mass fraction of element in austenite ratio. It must be specified that partitioning coefficients are narrowly dependent on cooling rate, because partitioning of elements is a diffusion process. A slow cooling allows an efficient partitioning of elements between the two phases, on the basis of their thermodynamics characteristics. Nevertheless, a rapid cooling, inhibiting the diffusion process, tends to homogeneize the composition of ferrite and austenite, and consequent partitioning ratios are close to 1.

Therefore, the final ferrite and austenite volume fractions depends on heat input of welding, that controls the cooling rate and so the ferrite-austenite transformation. If high heat inputs were used, and as a consequence low cooling rates, the austenite transformation is promoted [5], allowing a more balanced joint. On the other hand, these conditions tend to promote a coarse ferrite grain, wide heat affected zones and the possible precipitation of secondary phases, like sigma phase [6], which drastically reduce the mechanical properties and the corrosion resistance [7].

In addition to the cooling rate, which depends on welding parameters and on the welding technology, the final ferrite and austenite volume fraction depends on the chemical composition of the filler metal.

Regarding the heterogeneous welding of DSS or SDSS, like GTAW (Gas Tungsten Arc Welding), weld filler materials are usually overalloyed with 2-4% more Ni than in the base material.

Muthupandi et al. [8] demonstrated that the chemical composition, in particular the nickel content of the filler metal, is very effective in controlling the ferrite/austenite ratio than the cooling rate of the welding process.

The same group of researchers established that by adding low fractions of nitrogen as shielding gas in a GTA welding, the austenite formation is promoted [9].

In addition to the final microstructure, mechanical properties and corrosion behaviour of the welded joint are very relevant. It has been reported [10] that the presence of austenite stabilizer elements in the filler metal, like nickel or nitrogen, mainly affects the toughness, instead the hardness, because of a better phase balance.

A further microstructural evolution is obviously possible by the effect of an annealing treatment. If a dual phase stainless steel is heated up above 1100-1150°C, austenite starts to dissolve, and its volume fraction decrease with increasing the temperature, in relation to the chemical composition of the alloy (fig. 1). When the steel undergoes a rapid cooling from high temperatures, the ferrite-austenite transformation is partially suppressed.

In the present work, the effect of filler metals on a superduplex stainless steel 2507 GTA welded joints is carried out. In particular, two filler wires (one is traditional and one is innovative) with different chemical compositions are compared, maintaining the welding parameters constant. The influence of these different filler on final microstructure, mechanical properties and corrosion resistance of the joint is analysed, both on the as-welded specimens and the solution treated ones.

2. EXPERIMENTAL

The present investigation deals with superduplex stainless steels UNS S32750 welded joints.

The sheets, 5 mm thick and V-edge prepared, were butt-welded keeping the welding parameters constant, varying only the filler wire composition. Table 1 shows the nominal composition (wt %) of the base material and of the two fillers (1.6 mm diameter rods). The filler identified with the letter "A" is the innovative filler wire.

	C	Cr	Cu	Mn	Mo	N	Ni	Si	P	Co	V	Ti	Nb	W	S
Base Material	0.016	25.75	0.28	0.51	3.33	0.27	6.83	0.32	0.022	-	-	-	-	-	<0.0003
Filler "A"	0.020	25.240	0.030	0.370	3.990	0.266	9.930	0.440	0.018	-	-	-	-	0.010	0.001
Filler "B"	0.014	25.12	0.096	0.45	3.91	0.238	9.39	0.39	0.016	0.085	0.050	<0.005	0.01	<0.01	0.0006

Tab. 1 : Compositions of base and filler materials, wt %

It can be noted from table 1, that the innovative filler wire (A) is characterized by a higher nickel content than the traditional filler (B), and also it doesn't contain micro-alloying elements, like cobalt, vanadium, titanium, niobium and tungsten, instead they are revealed in wire B.

The chromium and nickel equivalent were evaluated using formulas reported by Datta et al. [11] (equations (4) and (5)), and table 2 gives the respective values for the materials considered:

$$Cr_{eq} = (Cr) + 2(Si) + 1.5(Mo) + 5(V) + 5.5(Al) + 1.75(Nb) + 1.5(Ti) + 0.75(W) \quad (4)$$

$$Ni_{eq} = (Ni) + (Co) + 0.5(Mn) + 0.3(Cu) + 25(N) + 30(C) \quad (5)$$

	Cr_{eq}	Ni_{eq}
Base Material	31.385	14.399
Filler A	32.1125	17.374
Filler B	32.0475	16.0988

Tab. 2 : Calculated chromium and nickel equivalent for the considered materials

Examining table 2, filler A has a higher nickel equivalent content, and it's 1.5 point per cent greater than the filler B, so it is more austenite stabilizer.
The welding was carried out using manual GTAW (Gas Tungsten Arc Welding)), and two passes were employed, one on each side, to ensure the complete penetration. Welding parameters are listed in table 3 (99.9% argon was used as shielding gas):

Run	Process type	Current		Voltage range [V]	Travel speed [mm/s]	Heat input [kJ/mm]
		Polarization	Intensity range [A]			
1	GTAW	DC-SP	80-90	11.5-12	1	0.4
2	GTAW	DC-SP	130-140	13.5-14	2.33	0.32

Tab. 3 : Welding parameters

The heat input of the welding is calculated using equation (6) [12]:

$$HI[kJ/mm] = \eta \frac{V[V]I[A]}{vel[mm/s] \times 1000} \quad (6)$$

where η is the process efficiency (for a GTAW its value is 0.4 [13]), V is the voltage in Volt, I is the current intensity in Ampere, vel the travel speed in mm/s and 1000 is a conversion factor.

2.1 Macrographs of the joints

First of all, an assessment of the dilution ratio of the welding process was carried out on analysing a transverse section of the welded joint (fig. 2).

| | *Total weld metal area = 47.1 mm^2* |
| | *Melted base metal area = 35.3 mm^2* |

Fig. 2 : Macrography of a transverse section of the welded joint
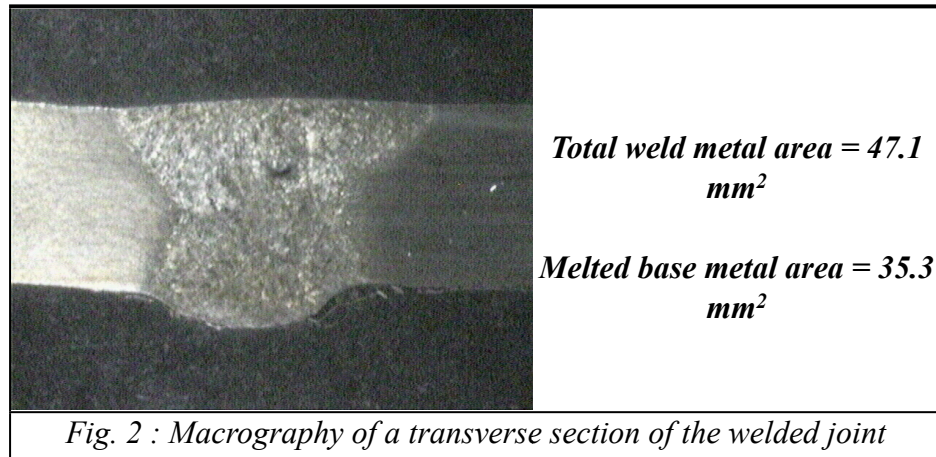
The total weld metal area was estimated using a software for image analysis, and the amount of the base metal melted was calculated as difference between the total weld metal area and the welding gap area.

$$R_d = \frac{melted\,base\,metal\,area}{total\,weld\,metal\,area} = 28.6\% \qquad (7)$$

The dilution ratio experimental value is 28.6%, and it is included in the range of a TIG welding (20-40%).

2.2 Metallographic analysis

Samples for metallographic investigation were obtained form transverse and longitudinal sections of the welded joints; they were ground using silicon carbide paper (180-500-1200-2400 grit) and polished with d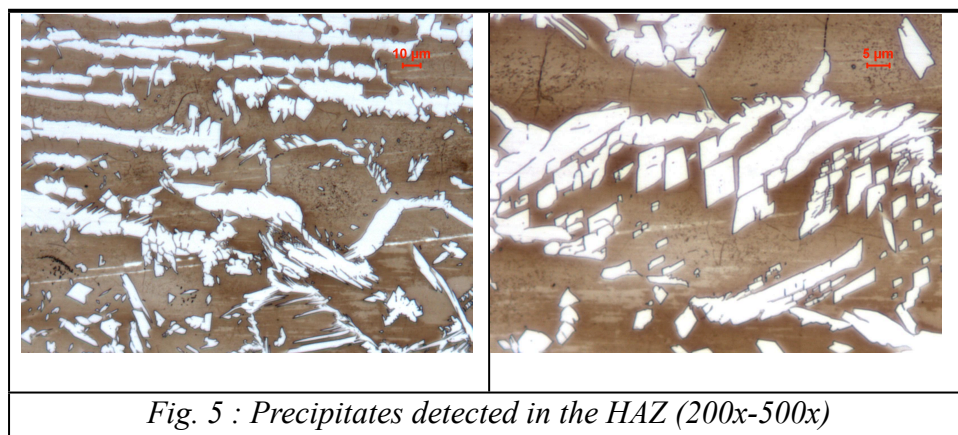iamond paste of 6 and 3 μm. Beraha's tint etch (80 ml H_2O, 30 ml HCl and 1 g $K_2S_2O_5$) was used to reveal the microstructure.

Figures 3 and 4 presents the microstructures of the welded zone and the heat affected zone respectively for to the two fillers (austenite is white, while ferrite is the dark phase). As a first evaluation, it can be noted that filler "A" assures a higher austenite volume fraction in the welded zone than the filler "B"; moreover, the austenite formed using filler "A" is coarser and rounder than austenite formed using filler "B", which is more needle-shaped.

Regarding the heat affected zones, no pronounced differences (in terms of austenite volume fraction austenite morphology or ferrite grain dimensions) are detected between the two fillers, because the effect of the filler metal in these zones is not considerable. Some precipitates were detected inside the ferrite grains of the heat affected zones (fig. 5), that probably are chromium nitrides or secondary austenite; further analysis to confirm the composition of these precipitates are in progress.

Filler A	Filler B

Fig. 3 : LOM micrographs of the welded zones (100x)

Filler A	Filler B

Fig. 4 : LOM micrographs of the heat affected zones (100x)

Fig. 5 : Precipitates detected in the HAZ (200x-500x)
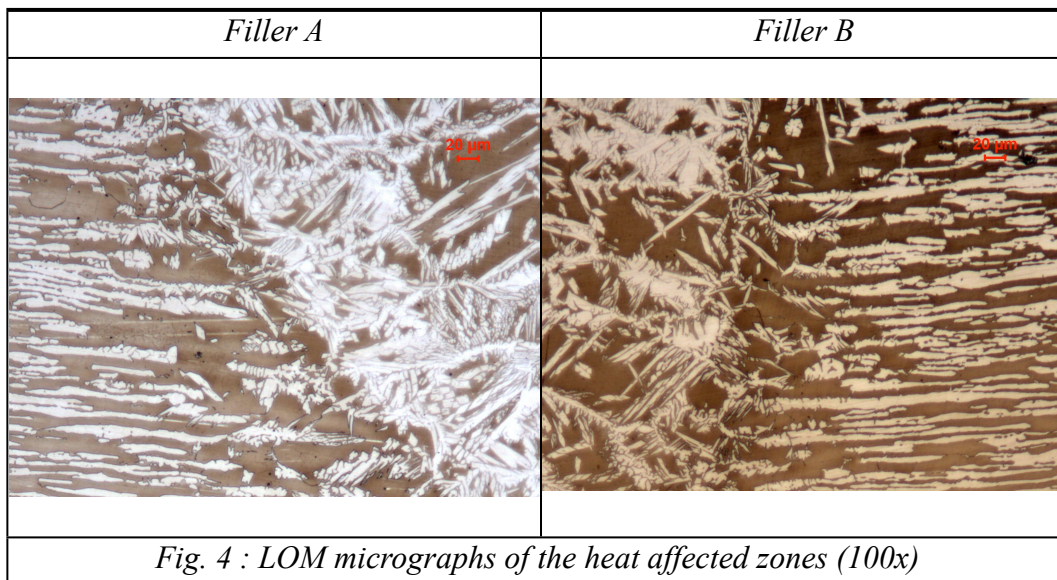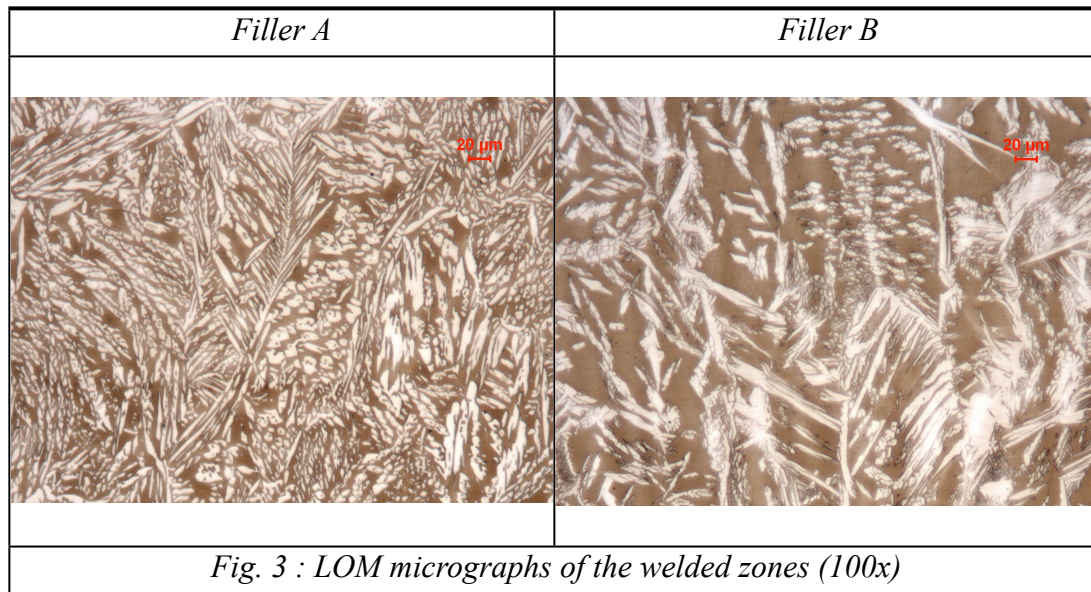
A software for image analysis (LEICA QWIN), was used to determine the phase distribution of the welded joints, considering one transverse section and one longitudinal section close to the welded zone axis (fig. 5), for every filler metal type.

Regarding the transverse sections, 5 areas were examined: welded zone and heat affected zone of the first run, welded zone and heat affected zone of the second run, and base material.

Regarding the longitudinal sections, 7 areas at the same distance of 3 mm each other were analysed, to create a distribution profile.

For the every area, an average of 8 measurement of the phase volume fraction were considered.
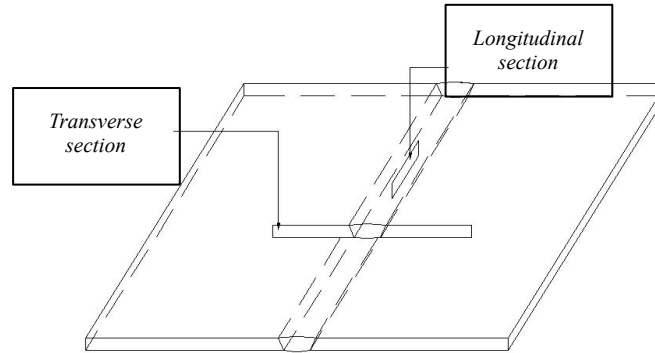
Fig. 6 : Scheme of the sections taken from the welded joints

Phase distribution results are given in fig. 7.

Fig. 7 : Phase distribution of the considered sections
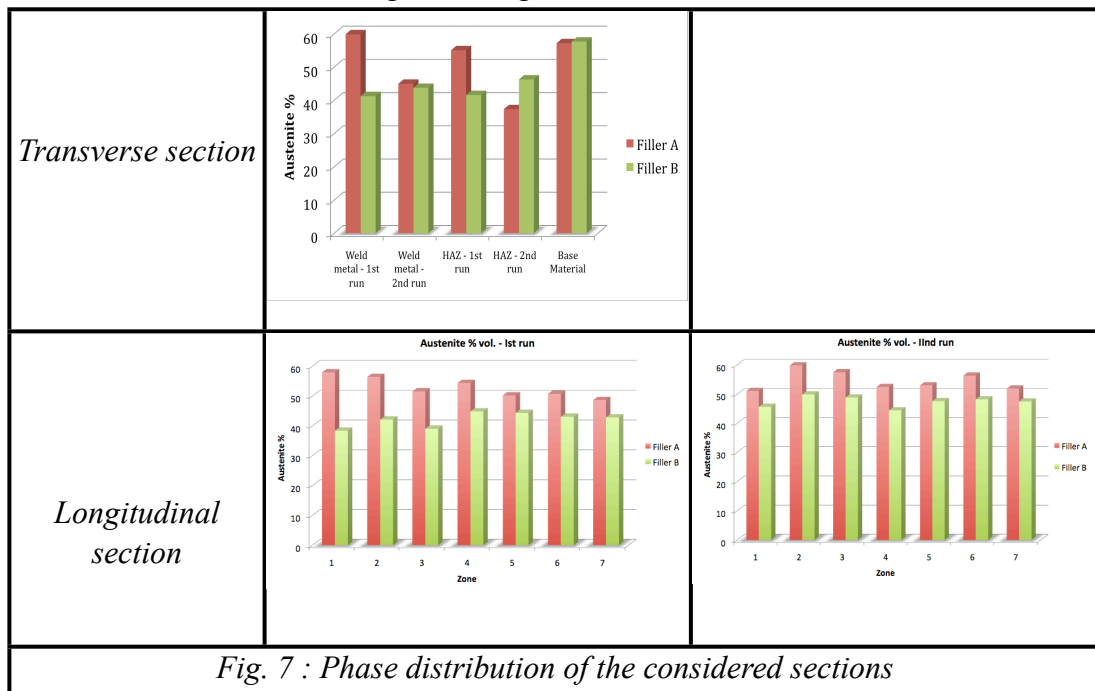
Examining the histograms in figure 7, it can be noted that, like reported before, filler A assures a higher austenite volume fraction in the welded zone, for every section.

Therefore, maintaining constants the welding parameters and welding technology, the innovative filler wire guarantees on average a higher austenite volume fraction both in the transverse section and in the longitudinal section, reducing the typical unbalanced microstructure that results from a DSS welding process.

2.3 SEM/EDS analysis

Scanning Electron Microscopy and Energy Dispersive Spectroscopy was used to analyze the specimens, to evaluate the difference in terms of chemical compositions of the welded zone made with the two fillers.
Figure 8 reports two SEM images of the welded zone at 1000x, for the filler A and B, respectively.
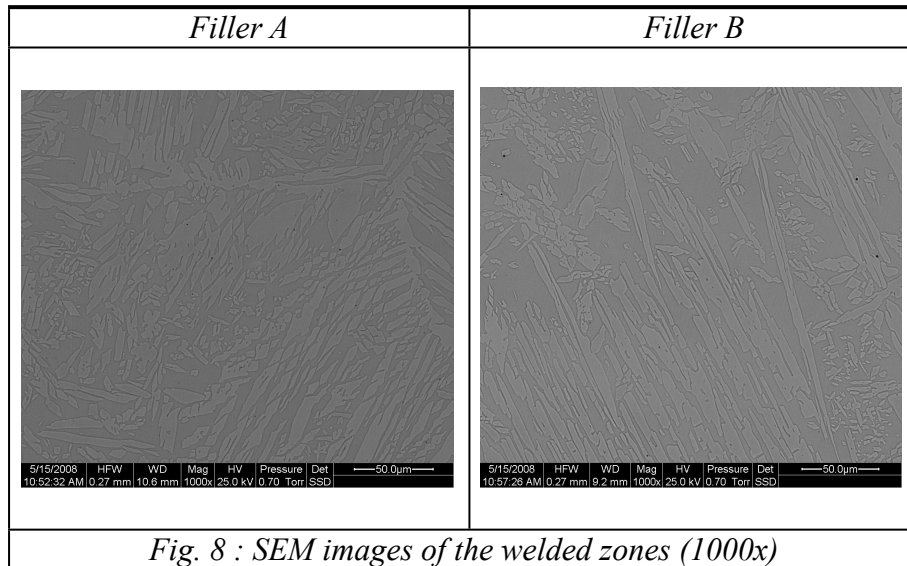
Filler A	*Filler B*

Fig. 8 : SEM images of the welded zones (1000x)

EDS results are summarized in figure 9, which illustrates the distribution of the major alloying elements in austenite and in ferrite for filler A and B.
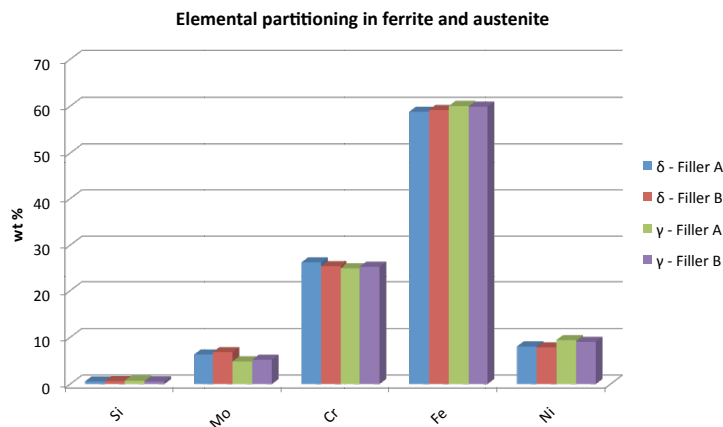
Element	δ - Filler A	δ - Filler B	γ - Filler A	γ - Filler B	Partitioning Ratio - Filler A	Partitioning Ratio - Filler B
Si	0.28	0.41	0.52	0.31	0.54	1.32
Mo	4.18	4.08	3.46	3.29	1.21	1.24
Cr	25.94	25.87	24.89	24.54	1.04	1.05
Fe	61.09	61.34	61.62	62.72	0.99	0.98
Ni	8.51	8.30	9.51	9.14	0.89	0.91

Fig. 9 : Elemental partitioning in austenite and ferrite of the weld metal zones

EDS analysis show that ferrite and austenite phases haven't significant differences, in terms of chemical composition. The experimental partitioning ratios of Mo, Cr and Ni result to be close to 1.

2.4 Mechanical properties

Tensile tests and micro hardness measurements (using a 100 g load) were performed to characterize the mechanical properties of the welded joints
Regarding micro hardness measurements, two profiles were considered: one corresponds to the top pass and the other one corresponds to the bottom pass, each one positioned 1 mm from the respective edge (see fig. 10).

Fig. 10 : Micro hardness profiles of the welded joints analysed
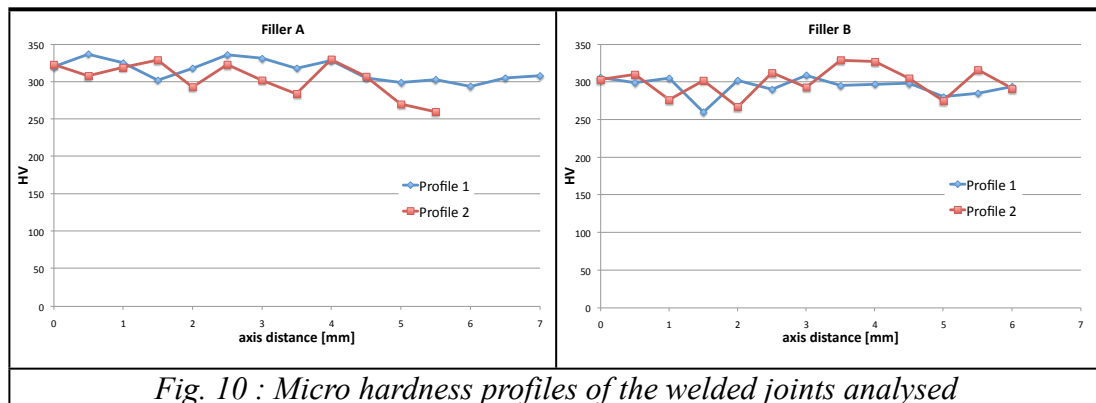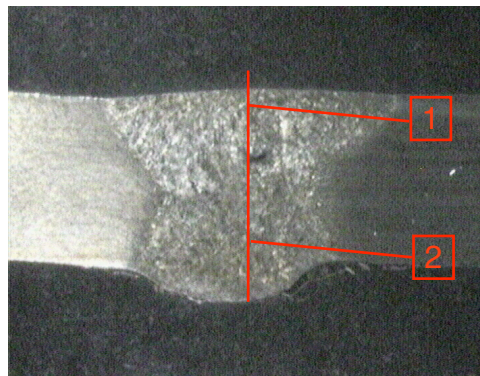
It can be seen that micro hardness profiles are almost constant for both the samples and the average values of hardness is around 300 HV, which is the standard hardness value for a UNS S32750.
Tensile tests are also carried out on three specimens taken from the welded joints for each filler type, using standard UNI EN 895.
All the specimens show fracture in the base material (fig. 11); the average values for yield stress, ultimate strength and Young modulus are respectively: 685 MPa, 885 MPa e 205 GPa. The engineering stress-strain curve is reported in figure 12.

Fig. 11 : Photograph of the specimen before and after the tensile test	*Fig. 12 : Engineering σ-ε curve from tensile tests*
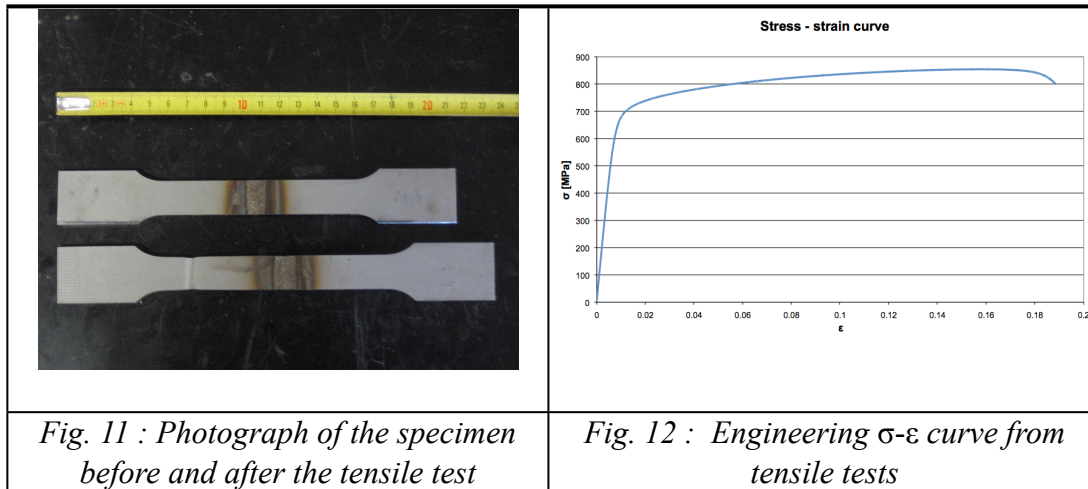
2.5 Corrosion test

The pitting corrosion resistance of the two welded joints was evaluated by gravimetric tests according to ASTM G48 standard - method A [14].

The testing samples (25 x 50 x 5 mm) were removed from butt welding joints. The specimens were pickled for 5 minutes using a solution containing 5% HF, 20% HNO_3 at 60°C, then rinsed in water and dried in air. The solution test consisted of a ferric chloride reagent (100 g $FeCl_3 \cdot 6H_2O$ in 900 ml H_2O), the test temperature was 50 ± 2°C and the test duration was 24h. Before the experiment, the sample area was measured and weighed on a balance with a precision of 1 mg. Upon completion of the experiment, the sample was extracted, ultrasonic-cleaned with acetone, dried in air and then weighed again.

The weigh losses for the as-welded specimens regarding each filler wire were comparable and have an average value of 150 g/m^2.

Some American and European standards (e.g. ASTM A 928/A928M, NORSOK MDS D42) suggest a post-welding heat treatment to homogenize and balance the microstructure of duplex and super duplex stainless steels.

Since the resulting weigh losses of the as-welded specimens are much higher than the standard threshold value for acceptance (which is 4 g/m^2), some specimen were submitted to post welding heat treatment to analyze the possible improvement in the pitting corrosion behavior, like illustrated in other works ([15],[16]).

The post-welding treatments were characterized by several times and temperatures of solubilization.

The average weigh losses of the specimen after corrosion test, in function of heat treatment, are shown in table 4:

HEAT TREATMENT		weigh losses [g/m^2]	
T [°C]	t [min]	FILLER A	FILLER B
1050	4	152.50	80.78
1050	11	69.12	151.41
1050	18	7.50	47.70
1100	4	6.07	4.63
1100	11	0.00	4.37
1100	18	0.00	4.47

Tab. 4 : Weigh losses after ASTM G48 corrosion test of the heat treated samples

Analyzing table 4 it can be noted that weigh losses decrease with increasing the solubilization temperature and time. In addition, filler A is characterized by lower weigh losses if compared with filler B. This fact can be justified by the presence of micro-alloying elements in filler B, which influence the coarsening and coalescing kinetic of secondary austenite, that precipitate after heat treatment [16].

A significant observation is related to the fact that some specimens (in particular the specimens annealed at 1100°C) show weigh losses lower than the threshold value of 4 mg/m^2, and then they pass the corrosion test using ASTM G48 standard.

3. CONCLUSIONS

In the present work, a GTAW process on a UNS S32750 super duplex stainless steel has been considered; in particular, the influence of the filler metal has been evaluated, comparing two different types of filler.

On the base of the experimental analysis the following conclusions can be drawn:

- the innovative filler wire, characterized by a higher Ni content, assures a higher austenite volume fraction in the as-welded joint;

- a significant difference in the phase distribution between the two welded joints, doesn't imply an appreciable variance in terms of mechanical properties (microhardness profiles and tensile properties, in fact the fracture affects the base material);

- the corrosion resistance of the as-welded joints is comparable for each filler metal; instead, after post-welding heat treatment, the pitting corrosion resistance of filler A results to be better than the resistance of filler B.

REFERENCES

[1]   J.-O. NILSSON, Mat. Sc. And Tech. 8 (1992), p. 685.

[2]   P.D.SOUTHWICK, R.W.K. HONEYCOMBE, "Decomposition of ferrite to austenite in 26%-5%Ni stainless steel", *Met. Sci.,* 14, 1980, 253.

[3]   S. ATAMERT, J.E. KING, Mat. Sci. Tech. 1992, 8, 896-911.

[4]   B.E.S. LINDBLOM, N. HANNERZ, Proc. 3rd World Conf. Duplex Stainless Steels '91, Beaune (1991), Les Editions de Phisique, Courtaboeuf (1991), p 951

[5]   H.SIEURIN, R. SANDSTROM, Materials Science and Engineering A418 (2006), p. 250.

[6]   G. MELOTTI, R. BERTELLI, M. ZANESCO, I. CALLIARI, E. RAMOUS, La Metallurgia Italiana 4 (2005), p. 39.

[7]   M.POHL, O.STORZ, T.GLOGOWSKI, Materials Characterization 58 (2007), p. 65.

[8]   V.MUTHUPANDI, P.BALA SRINIVASAN, S.K.SESHANDRI, S.SUNDARESAN, Materials Science and Engineering A358 (2003), p. 9.

[9]   V.MUTHUPANDI, P.BALA SRINIVASAN, S.K.SESHADRI, S.SUNDARESAN, Science and Technology of Welding and Joining Vol. 9 No. 1 (2004), p. 47.

[10] V.MUTHUPANDI, P.BALA SRINIVASAN, V.SHANKAR, S.K.SESHANDRI, S.SUNDARESAN, Materials Letters 59 (2005), p. 2305.

[11] P.DATTA, G.S. UPADHYAYA, Materials Chemistry and Physics 67 (2001), p. 234.

[12] J.NOWACKI, P.RYBICKI, Journal of Mat. Proc. Tech. 164-165 (2005), p. 1082.

[13] Ø. GRONG, Metallurgical Modelling of Welding, The Institute of Materials, 1997.

[14] ANNUAL BOOK OF ASTM STANDARDS, ASTM G48-03, 2003, ASTM.

[15] P. FERRO, A. TIZIANI, F. BONOLLO, Welding Journal, 87 (2008), p. 298.

[16] P. FERRO, A. TIZIANI, R. CERVO, Proceedings of the 32°Convegno Nazionale AIM, Ferrara (2008), paper 80

[17] F. BONOLLO, A. TIZIANI, P. FERRO, La Metallurgia Italiana 2 (2005), p. 27.

[18] F. BONOLLO, A. GREGORI, A. TIZIANI, J-O. NILSSON, Proceedings of the 11th Congress of the International Federation for Heat Treatment and Surface Engineering and the 4th ASM Heat Treatment and Surface Engineering Conference in Europe, Florence - Italy (1998), p. 291.

[19] H. M. EZUBERA, A. EL-HOUDB, F. EL-SHAWESHB, Desalination 207 (2007), p. 268.

[20] N.LOPEZ, M. CID, M. PUIGGALI, Corrosion Science 41 (1999), p. 1615.

[21] H.Y. LIOU, R.I. HSIEH , W.T. TSAI, Materials Chemistry and Physics 74 (2002), p. 33.

[22] J. NOWACKI, A. LUKOJC, Materials Characterization 56 (2006), p. 436.

[23] J. NOWACKI, A. LUKOJC, Journal of Materials Processing Technology 164–165 (2005), p. 1074.

[24] J.D. KORDATOS, G. FOURLARIS AND G. PAPADIMITRIOU, Scripta

mater. 44 (2001), p. 401.

[25] T.H. CHEN, K.L. WENG, J.R. YANG, Materials Science and Engineering A338 (2002), p. 259.

[26] E. ANGELINI, B. DE BENEDETTI, F. ROSALBINO, Corrosion Science 46 (2004), p. 1351.

[27] A.J. RAMIREZ, J.C. LIPPOLD, S.D. BRANDI, Met. and Mec. Trans. A 34A (2003), p. 1575.

ARTICLE II

INFLUENCE OF FILLER METAL CHEMICAL COMPOSITION ON THE PRECIPITATION MECHANISM OF SECONDARY AUSTENITE ON UNS S32750 SOLUTION TREATED WELDED JOINTS

STUDIO DELLA PRECIPITAZIONE DELL'AUSTENITE SECONDARIA E DELLA RESISTENZA A CORROSIONE IN CORDONI DI SALDATURA UNS S32750 TRATTATI TERMICAMENTE: INFLUENZA DELLA COMPOSIZIONE CHIMICA DEL MATERIALE D'APPORTO

A. Tiziani, P. Ferro, R. Cervo*

M. Bulla **

*   *University of Padova, Department of Management and Engineering, Stradella San Nicola 3 - 36100 Vicenza (Italy)*

** *Rivit S.p.A., Caltrano - Vicenza (Italy)*

ABSTRACT

The favorable microstructure of austenitic/ferritic stainless steels is generally upset during the welding operation and their optimum corrosion and mechanical properties could be compromised. In certain situations it could be necessary to subject the component to a post-welding heat treatment (e.g. ASTM A928) to dissolve intermetallic phases formed during welding and to restore the ferrite/austenite balance; this treatment consists in a heating up to a temperature around 1050-1100°C, with the consequent secondary austenite precipitation.

The present work analyzes the secondary austenite precipitation in super duplex UNS S32750 welded joints, subjected to post-welding heat treatment. In particular, two different filler metals has been considered, and the effect of the filler chemical composition both on the precipitation kinetic of secondary austenite during post welding annealing, and on the pitting corrosion behavior of the solution treated welded joints has been evaluated. The presence of micro-alloying elements has been connected with the two factors listed before.

KEY WORDS

1. INTRODUCTION

It is well known that welding procedures on austenitic/ferritic stainless steels (super duplex-SDSS or duplex-DSS) may compromise their optimal microstructure, by changing the ferrite/austenite balance, promoting the precipitation of undesired phases in the heat affected zones (HAZ) and in reheating passes. The local decay of mechanical and corrosion properties is a detrimental effect of this operation.

In SDSS and DSS welding, the filler metal is over-alloyed with 2-4% nickel more than the base material, to obtain a more balanced microstructure. Nevertheless, some American and European standards (ASTM A 928/A928M, NORSOK MDS D42), plan a post welding annealing treatment to dissolve the possible intermetallic phases formed during welding and to raise the austenite volume fraction to equilibrium values.

Young et al. [1] studied the effect of post-welding heat treatment at 1050°C on a UNS S31803 duplex stainless steel, obtaining an acceptable phase balance already after 15 minutes, but achieving excellent results after 30 minutes of solubilization. Moreover, Melotti et al. [2] analyzed the annealing treatment on several types of duplex stainless steels, founding that the minimum annealing temperature (1050°C) is chosen to assure a complete dissolution of detrimental secondary phases, whereas the maximum temperature (1100°C) is chosen to maintain a correct δ/γ ratio; the temperature interval could slightly change between SDSS and DSS due to the effect of alloying elements on the state-diagram [3].

Some researchers [4,5,6], showed that the corrosion resistance of DSS and SDSS is affected by the secondary austenite (γ_2) precipitation. This phase may form as a result of a solid-state transformation, following three main mechanisms: the sigma phase eutectoid reaction $\delta \rightarrow \sigma + \gamma_2$ (in the temperature range 700-900°C), a diffusive transformation at a temperature above 650°C resulting in a Widmanstätten structure, and a non-diffusive isothermal transformation at a temperature lower than 650°C, analogous to a martensitic transformation.

The secondary austenite nucleation takes place mainly at the ferrite/austenite grain boundaries (intergranular γ_2) and at the internal of the ferrite grains (intragranular γ_2). Nilsson et al. [5] demonstrated that the intragranular secondary austenite contains less chromium, molybdenum and nitrogen than the primary one, that are all elements that influence the *pitting resistance equivalent number* (PREN = % Cr + 3.3 % Mo + 16 % N), and which make the secondary austenite less resistant than the primary. Garzón et al. [6], studied how the post welding annealing temperature influence the chemical composition of secondary austenite. Considering the heat treatments at 1100°C, the resulting γ_2 has an external layer rich in chromium and nitrogen (near the γ-δ interface), and a inner core impoverished of this elements; instead, regarding the annealing treatments at 1000°C the resulting γ_2 is more homogeneous.

Because of the important and controversial effect of secondary austenite on mechanical and corrosion properties of SDSS and DSS welded joints, a deep comprehension of the precipitation mechanism, to optimize all the materials and procedures involved into the welding process.

The welded zone is a highly meta stable area: the post welding heat treatment affect considerably the microstrucure of the joint, inducing the precipitation of secondary austenite and modifying the elemental partitioning between the phases.

Aim of this work is to analyze the precipitation of secondary austenite in UNS S32750 super duplex welded joints, induced by annealing treatments. In particular, considering two different filler metals, the influence of filler chemical composition on the nucleation and growth of γ_2 in relation to the heat treatment, and on the resulting pitting corrosion properties has been evaluated.

Particular attention has been paid to the influence of chemical elements on the precipitation kinetic of secondary austenite; Nilsson et al. [7], comparing few SDSS welding performed using different filler metals, have demonstrated that some elements (e.g. tungsten and copper) that promote the γ_2 precipitation.

2. EXPERIMENTAL ANALYSIS

2.1. Materials and methods

Overlays of the 6 mm thick super duplex stainless steel UNS S32750 plates were produced by automatic gas tungsten arc welding using a three-layer procedure. Two different filler metals were used and the edge were V-prepared with an angle of 75°. Tables 1 and 2 show the chemical composition of base, filler metals and the welding parameters used, respectively.

	C	Cr	Cu	Mn	Mo	N	Ni	Si	P	Co	V	Ti	Nb	W	S
Base Material	0.016	24.9	0.13	0.81	3.8	0.28	6.9	0.22	0.021	-	-	-	-	-	0.001
Filler A	0.016	25.06	0.159	0.605	3.88	0.239	9.21	0.436	0.017	-	-	-	-	0.1	0.001
Filler B	0.012	24.98	0.1	0.44	4.04	0.255	9.56	0.38	0.017	0.034	0.042	0.005	0.01	0.01	0.0005

Tab. 1: Chemical composition of the materials considered (weight %)

Run	Process type	Filler metal Ø [mm]	Current Polarization type	Current Intensity range [A]	Voltage range [V]	Travel speed [mm/s]	Heat input [kJ/mm]
1st	GTAW	1.2	DC-SP	185 ± 5	13.5 ± 0.5	4.7	0.21
2nd	GTAW	1.2	DC-SP	205 ± 5	17.7 ± 0.5	2.5	0.58
3rd	GTAW	1.2	DC-SP	200 ± 5	15.4 ± 0.5	4.2	0.29

Tab. 2 : Welding parameters

The two fillers metal's composition is similar, except regarding the presence of micro-alloying elements like Co, V, Ti, Nb, W in the filler indicated as B.

The welding heat input reported in table 2 has been calculated using eq. (1) [8]:

$$HI[kJ/mm] = \eta \frac{V[V]I[A]}{vel[mm/s] \times 1000}$$ (1)

where η is the process efficiency (which value for a GTAW is about 0.4 [9]), V is the average voltage in Volt, I is the average current intensity in Ampere, vel is the average travel speed in mm/s and 1000 is a conversion factor.

The specimens obtained from the welded joints has been subjected to various heat treatments on a laboratory furnace, using different temperatures and holding times, like reported in table 3:

T [°C]	1050					1075					1100				
t [min]	1	4	11	18	27	1	4	11	18	27	1	4	11	18	27

Tab. 3 : Heat treatment performed on the welded joints

2.2 Metallographic analysis and corrosion tests

Transversal sections of the welded joints have been prepared for metallographic analysis by silicon carbide paper grinding (P180, P500, P1200 e P2400) and following polishing using diamond paste until surface finishing of 3 μm. Specimens have then been etched using Beraha's (70 ml H_2O, 30 ml HCl and 1 g $K_2S_2O_5$) to reveal the microstructure.

Metallographic analysis has been carried out by means of Light Optical Microscopy (L.O.M.) and phase quantification has been performed using a software for image analysis LEICA QWIN, analyzing 20 fields (dimension 321 x 241 μm) for each measurement.

To quantify the secondary austenite volume fraction in relation to the heat treatment, the following relation has been used:

$$\% \gamma_2 = \% \gamma_{tt} - \% \gamma_{aw}$$ (2)

where γ_2 is the secondary austenite volume fraction precipitated during heat treatment, γ_{tt} is the total austenite volume fraction after heat treatment, and γ_{aw} is the austenite volume fraction of the as-welded specimen.

Through metallographic analysis, the fractions γ_{tt} and γ_{aw} have been calculated, and then the γ_2 fraction formed during solid-state transformation has been obtained.

For the study of the precipitation kinetic of secondary austenite during isothermal heat treatment, an Avrami-type relationship has been used [10,11,12]:

$$V = V_m \left(1 - e^{-b(T)t^{n(T)}}\right)$$ (3)

where V_m is the equilibrium phase fraction, depending on temperature, t is the time in second, b(T) and n(T) are temperature-dependent parameters.

Corrosion tests using ASTM G48 standards – method A ("Standard Test Methods for Pitting and Crevice Corrosion Resistance of Stainless Steels and Related Alloys by Use of Ferric Chloride Solution") [13], are performed on all the heat-treated specimens (excepting the specimens heat treated for 1 minute of holding time).

The specimens' dimensions (15 x 50 x 6 mm) have been reduced respect to the standard's dimension. After pickling with an aqueous solution of 20 % HNO_3 and 5 % HF at 60°C, the specimens have been immersed in a solution containing $FeCl_3 \cdot 6H_2O$ at 50 ± 2°C for 24 h, and at the end of the test, the weight losses have been calculated.

3. RESULTS AND DISCUSSION

It must be noted that all the analysis and considerations made in this study are referred to the fusion zone, because it is the only characterized by different chemical composition of the metal, keeping the base material and welding parameters constant.

3.1 Metallographic analysis

In the as-welded specimen, in correspondence of the fusion zone, the three welding runs (fig. 1) are characterized by different microstructures.
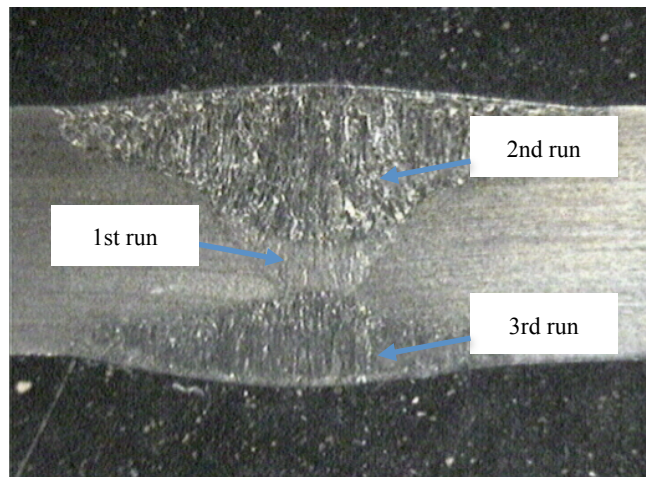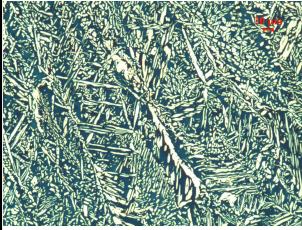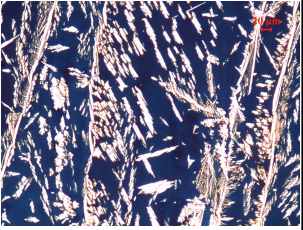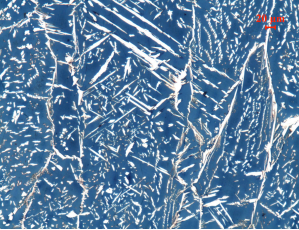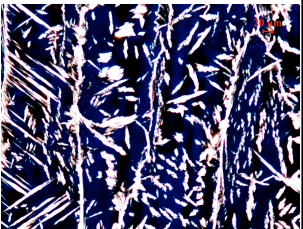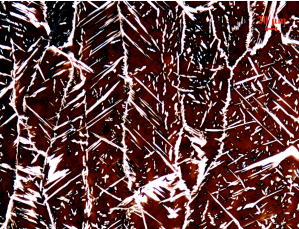
Fig. 1: Transverse section of the welded joint showing the different welding runs

For both the fillers type, the second and third runs have similar microstructures, constituted by ferrite and primary austenite precipitated during solidification, instead the first pass (in the centre of the section) is characterized by ferrite, primary austenite, and some secondary austenite precipitated during the reheating induced by the others subsequent passes. The presence of other intermetallic phases has not been detected in the fusion zone.

As a consequence, only the second and the third pass will be considered for the study of secondary austenite precipitation, because eq. (2) could be applied only on these runs, which are characterized by an initial γ_2 volume fraction equal to zero.

Figure 2 reports the micrographs of the fusion zone of the considered specimens:

	I Pass	*II Pass*	*III Pass*
Filler A			
Filler B			
Fig. 2 : Micrographs of the various passes of fusion zone (100x) – dark phase: ferrite (δ), white phase : austenite (γ)			
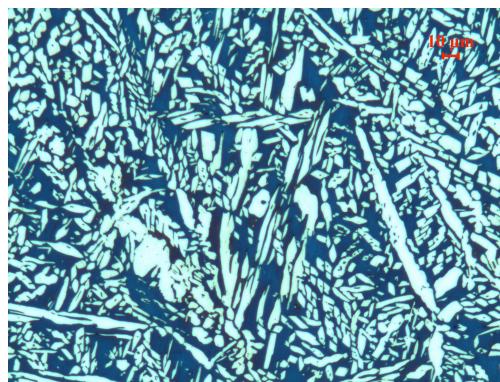
Fig. 3 : Secondary austenite detected in the first welding run (200x)

The austenite volume fraction of the fusion zone of the as-welded specimens results to be, for both the filler metals: 27% in the second and third pass and 44% in the first pass.

After annealing treatment, the microstructure of the fusion zone results to be constituted by ferrite, primary austenite and secondary austenite. Like the as-welded specimen, the second and third runs have similar microstructure regarding the same specimen. The secondary austenite, in form of Widmanstätten plates, assumes the typical needles morphology for short holding times, while increasing the holding time, it tends to grow and become coarser (fig. 4).

1 min	27 min
Fig. 4 : Growth of secondary austenite in the specimens treated at 1100°C (100x)	
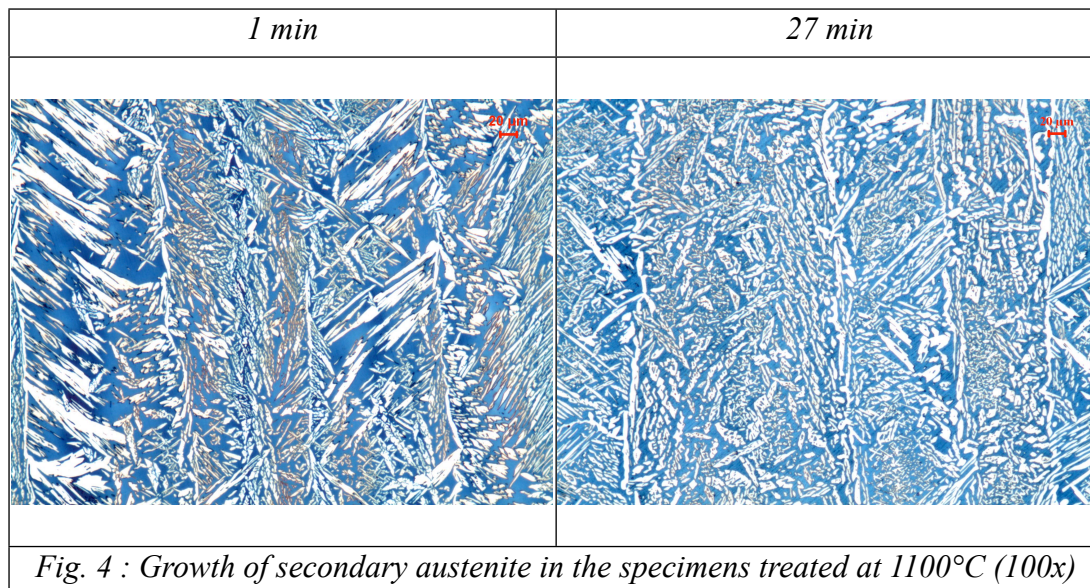
Regarding the microstructure of the annealed specimens at 1050°C and 1075°C, it could be noted that increasing the holding time, the metal welded with filler B is characterized by a secondary austenite less coarse than the filler B (fig. 5-6).

T = 1050°C	*1 min*	*27 min*
Filler A		
Filler B		
Fig. 5 : Microstructure of the weld metal of the annealed specimens at 1050°C (500x)		

T = 1075°C	1 min	27 min
Filler A		
Filler B		

Fig. 6 : Microstructure of the weld metal of the annealed specimens at 1075°C (500x)
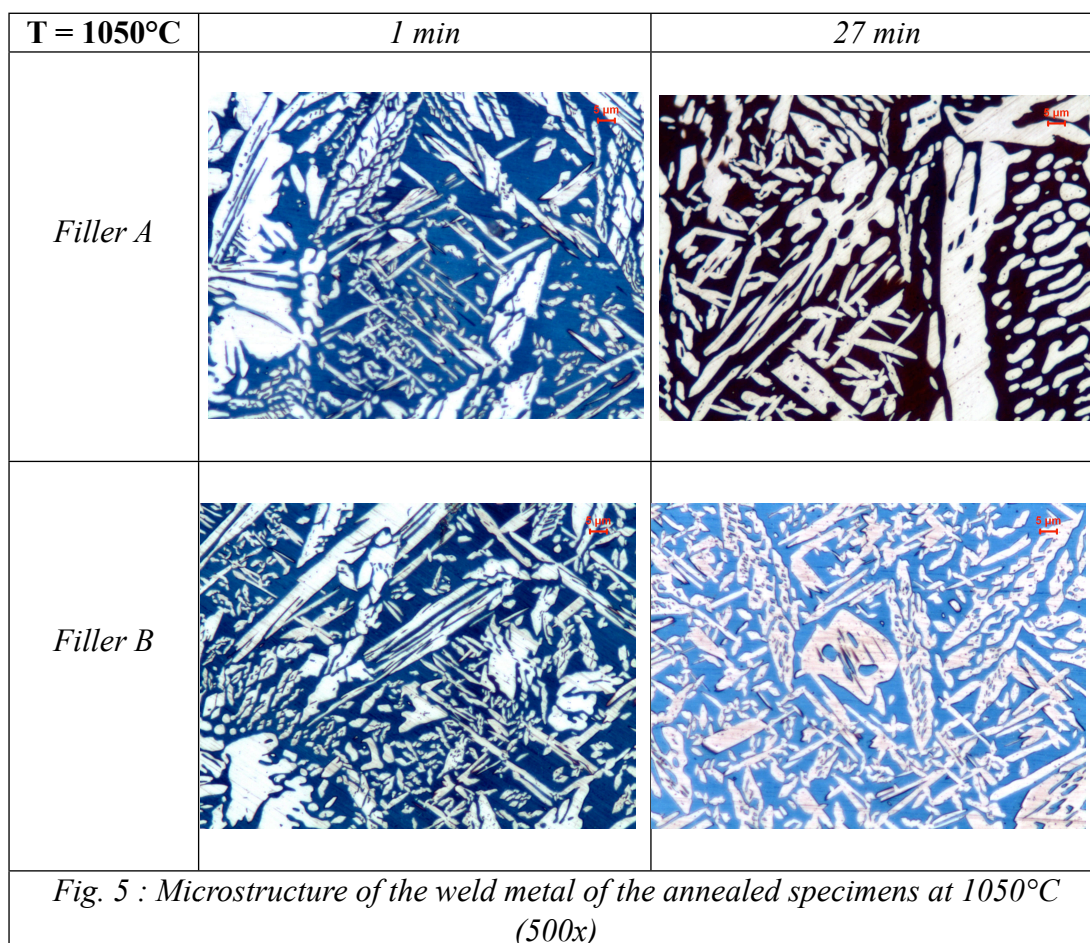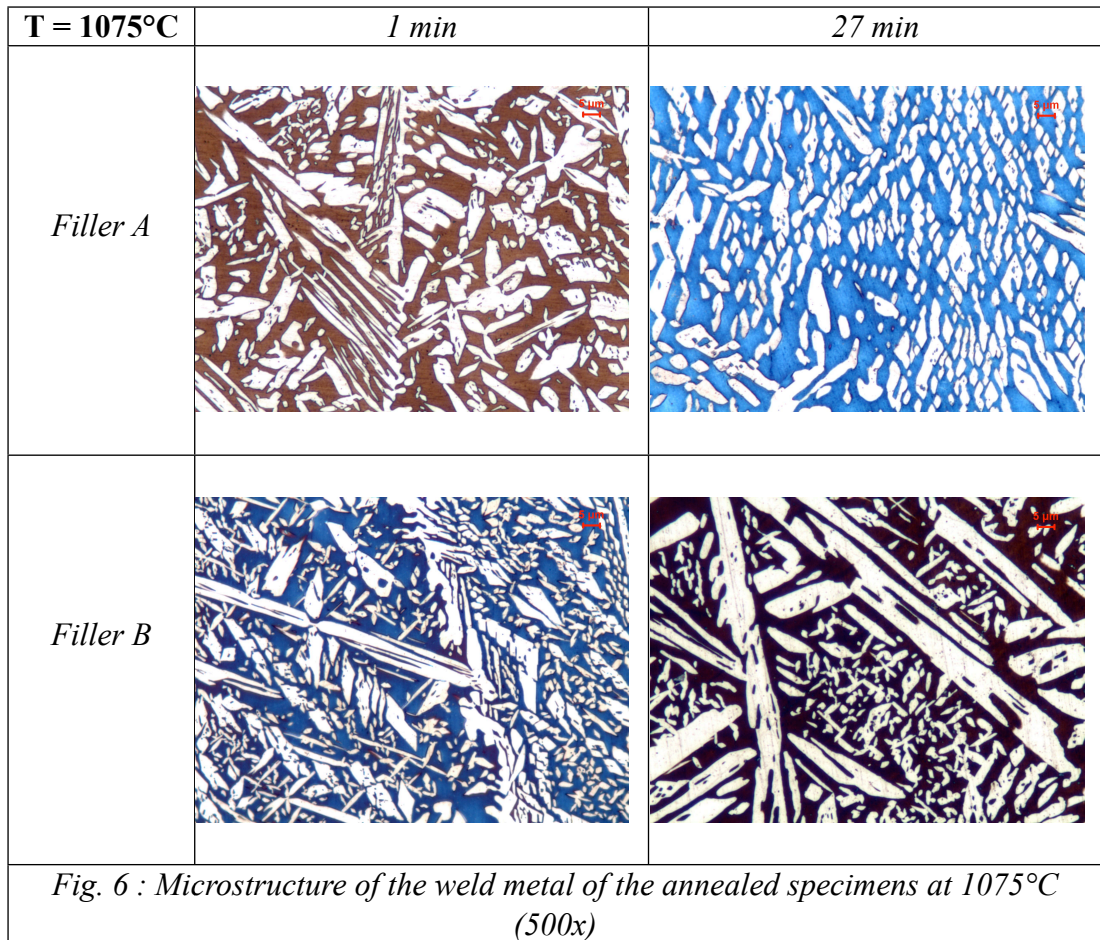
Table 4 summarizes the average secondary austenite volume fraction (calculated using eq. (2)) of the weld metal, regarding the 2nd and the 3rd runs, of the heat-treated specimens:

FILLER A			FILLER B		
T [°C]	t [min]	% γ_2	T [°C]	t [min]	% γ_2
1050	1	17.1	1050	1	15.0
	4	13.9		4	11.9
	11	16.6		11	14.5
	18	17.7		18	17.1
	27	16.9		27	20.4
1075	1	14.4	1075	1	13.1
	4	15.1		4	15.7
	11	15.1		11	14.6
	18	17.5		18	16.5
	27	16.8		27	17.2
1100	1	15.8	1100	1	15.5
	4	16.1		4	17.7
	11	17.5		11	17.9
	18	19.2		18	18.0
	27	16.8		27	17.6

Tab. 4 : Average secondary austenite volume fraction calculated using eq. (2)

The experimental data collected in table 4. has been interpolated using an Avrami-type relationship (eq. (3)), varying the V_m, b and n parameters, for the three temperatures analyzed.

Figure 7 reports the graphics that show the secondary austenite volume fraction in function of holding time, with the respective values of V_m, b and n:

	T = 1050°C	T = 1075°C	T = 1100°C
Filler A			
	$b = 0.0085$ $n = 1.4$ $V_m = 16.8$	$b = 0.002$ $n = 1.75$ $V_m = 15.2$	$b = 0.00065$ $n = 2$ $V_m = 17.2$
Filler B			
	$b = 0.007$ $n = 1.4$ $V_m = 15.2$	$b = 0.0015$ $n = 1.75$ $V_m = 15.5$	$b = 0.00055$ $n = 2$ $V_m = 17.8$
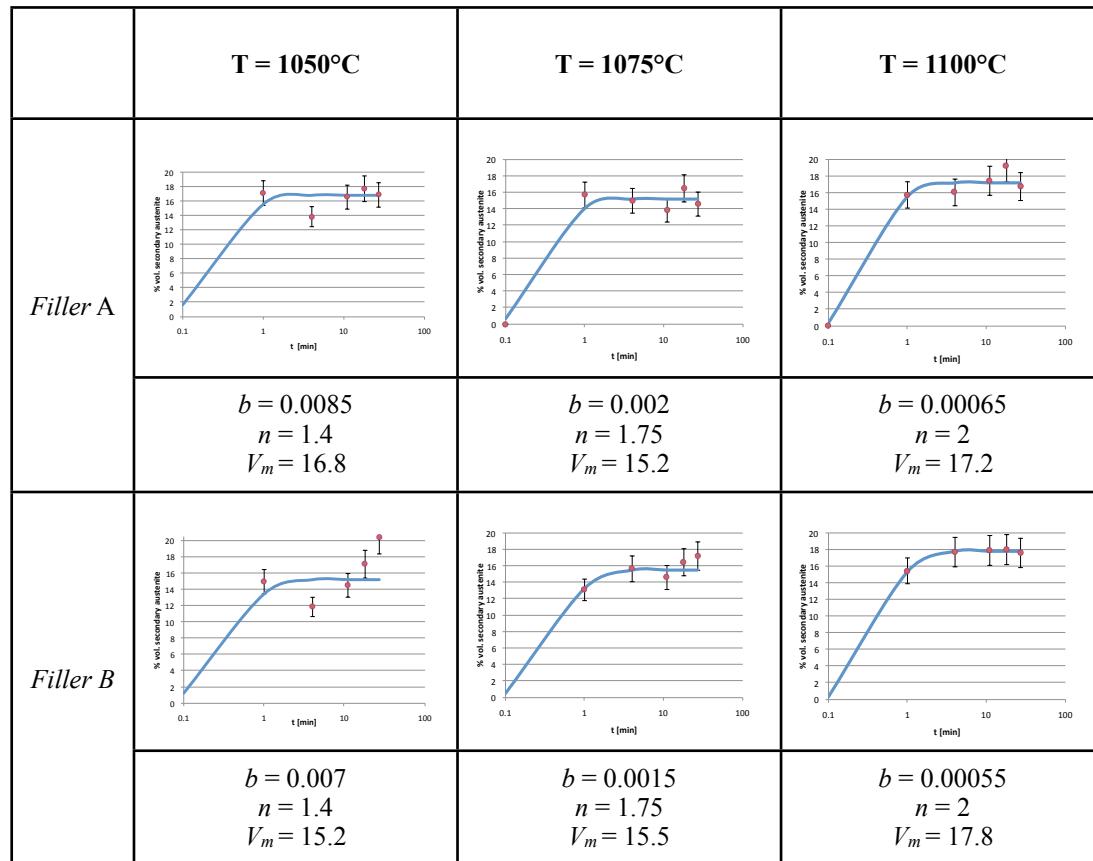
Fig. 7 : Interpolation using an Avrami-type relationship of the precipitation of secondary austenite

Figure 8 summarizes the secondary austenite volume fraction of the respective fusion zones. keeping constant the temperature:
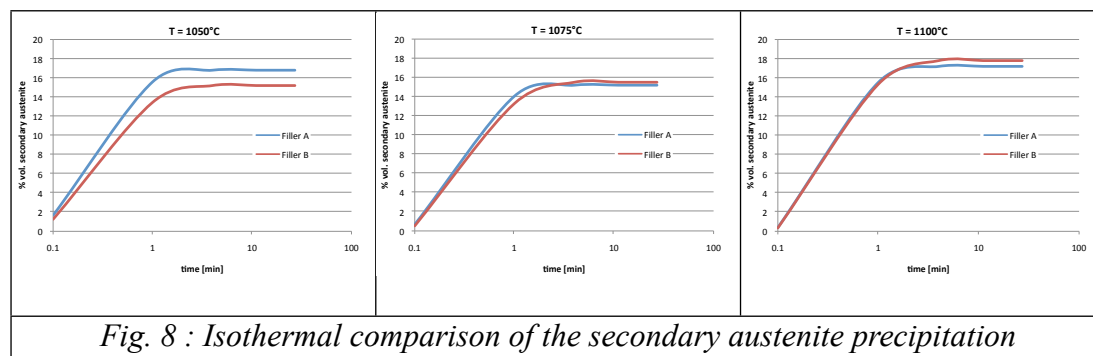
Fig. 8 : Isothermal comparison of the secondary austenite precipitation

Examining fig. 7 and 8, it can be noted immediately the high precipitation rate of secondary austenite in the fusion zone: already after one minute of holding time, the

precipitated austenite volume fraction is about 13-17%, reaching the values of 17-20% after 27 minutes of solubilization treatment.

Then, it is easy to assume that the total austenite volume fraction doesn't undergo significant changes with increasing the holding time.

On the basis of the fig. 7, 8 and the table 4, the precipitation kinetic is similar for the two filler, excepting the temperature of 1050°C, characterized by a γ_2 precipitation rate slightly lower for the filler B if compared with the filler A.

Referring to the micrographs reported in fig. 6, a smaller degree of coarsening of secondary austenite relatively to the fusion zone B, considering high holding times. This difference could be attributed to the presence of some ferrite-stabilizer elements (W, V, Ti, Ni) in the filler B, which could retard the secondary austenite nucleation and growth. In addition, filler B has a higher nitrogen content, in fact this element tends to slow down the precipitation of γ_2, like demonstrated by Gregori and Nilsson [14].

3.2 Corrosion tests

Figure 9 reports the results of corrosion tests on heat-treated specimens. The points indicated in the diagrams are an average of three measurements.

Fig. 9 : Average weight losses after ASTM G48 corrosion test
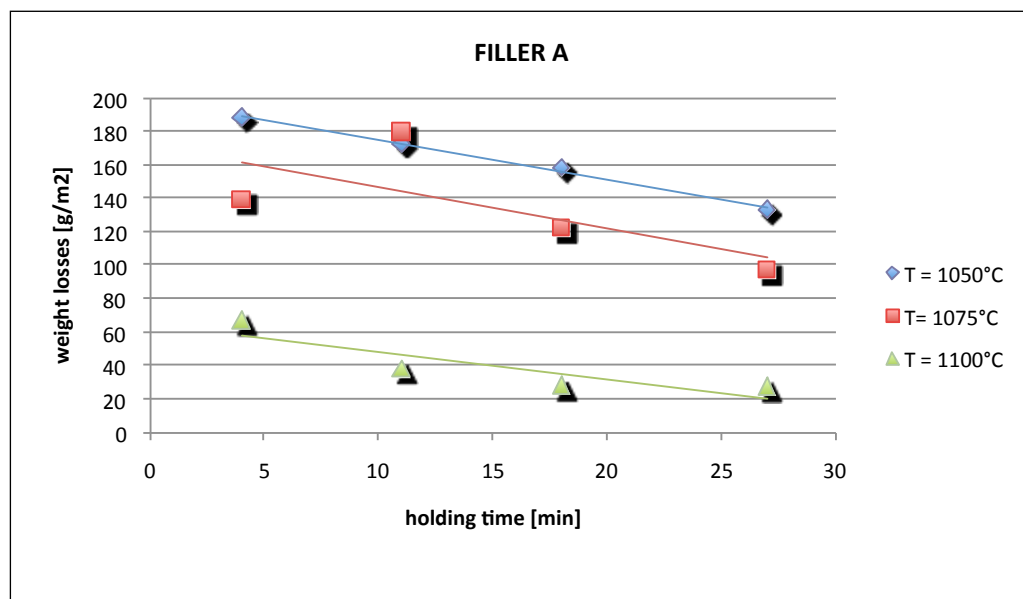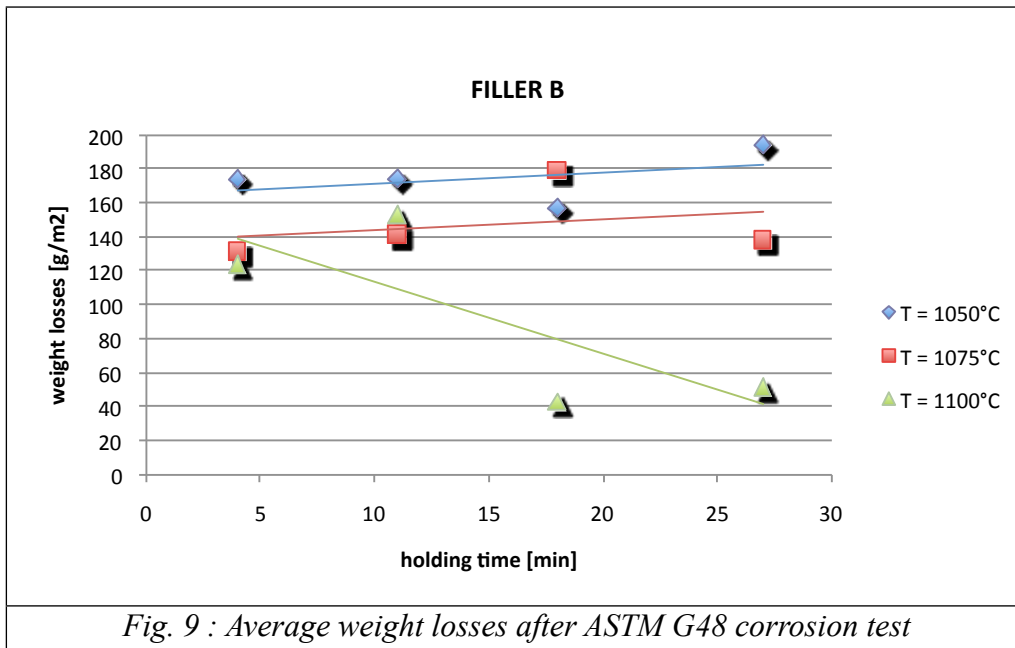
Weight losses of as-welded specimens (which aren't reported in the previous diagrams) results to be 170 g/m^2 for the filler A, and 145 g/m^2 for the filler B. Therefore, comparing the graphics in figure 9 with these values, it can be noted that the corrosion resistance (expressed by weight losses) of the specimens analyzed improves for given treatments. For example, the filler A improves its corrosion behavior for all the solubilization treatments at 1075°C and 1100°C for holding times higher than 15 minutes, and the weight losses for these mentioned treatments are smaller than the as-welded condition; instead, regarding the filler B, only the solubilization treatments at 1100°C for holding times higher than 15 minutes guarantee smaller weight losses than the as-welded condition.

In addition, it could be observed that the weight losses decrease with increasing both the annealing temperature and the holding time (the described trend is more evident for the material welded with filler A).

These evaluations are in agreement with that reported by previous works of Nowacki et al. [4], Garzón et al. [15], Ferro et al. [16] for Duplex Stainless Steels. This behavior could be explained considering the evolution of the morphology of secondary austenite during heat treatment: more needle-sharp for smaller holding times and annealing temperatures, coarser and rounder for higher holding times. Moreover, increasing the holding times, the initial meta-stable microstructure of the fusion zone, becomes more homogeneous considering the chemical composition (in fact, Garzón et al. [6] have demonstrated that the nitrogen content tends to be equal between γ and intragranular γ$_2$ increasing the holding times at 1200°C).

Analyzing in depth the pitting corrosion behavior of the two filler metals is possible to draw some important considerations: on average, the corrosion behavior of the joint obtained using filler A is better than that obtained using filler B after solubilization treatment, even if the behavior of the as-welded specimens is opposite. In addition, the filler metal of type B requires a higher solubilization temperature to obtain a pitting corrosion resistance comparable to filler A (weight losses for annealing treatment at 1050°C and 1075°C remain constant varying the holding time,

only at 1100°C the weight losses start to decrease increasing the time). Given that the corrosion attack arises at $\gamma_2/\ \delta$ interface, this smaller sensitivity to the annealing treatment for filler B could be connected with the lower tendency to growth of secondary austenite during heat treatment.

Like already observed and on the base of the results obtained, when Super Duplex Stainless Steels are solubilized, the annealing temperatures should be slightly higher than those considered for DSS (1070-1120°C in place of 1050-1100°C).

Finally, the presence of some points external to the interpolating line (e.g. 1075°C – 14 min for the filler A, 1050°C - 21 min and 1075°C - 14 min for the filler B) could be noticed; however, given the randomness of the phenomenon, further data will be necessary to clarify the character of these curves.

4. CONCLUSIONS

On the basis of the analysis carried out on the joints it is possible to draw some general conclusions:
-   The post welding treatment on SDSS, if performed with the correct way (in terms of temperature and holding time), improves the corrosion resistance compared to the as-welded joint;
-   The corrosion resistance of annealed specimens increases with the annealing temperature (in the considered interval 1050°C-1100°C) and the holding time, like already demonstrated for DSS;
-   The corrosion resistance isn't directly connected to the austenite volume fraction, in fact, even if the total austenite volume fraction remains constant between certain limits increasing the holding time, the corrosion resistance increases. Other factors act on corrosion behavior of the joint, like the morphology of γ_2 and the homogeneity of microstructure;

The comparative analysis between the two filler metals, underlined that:
-   The filler metal of type B requires a higher solubilization temperature compared with the filler A, which shows smaller weight losses, keeping constant the annealing temperature;
-   The filler B is characterized by a secondary austenite with a slower nucleation and a lower growth rate during the post welding heat treatment if compared with the filler A (especially at lower annealing temperatures); this behavior could be attributed to the different chemical composition of the filler, in particular to the presence of micro alloying elements that act on the precipitation of γ_2;
-   Keeping constant the process parameters (in terms of welding and solubilization treatment), the joint performed with the filler A has a better corrosion behavior if compared with the joint with filler B; this aspect could be related to the smaller surface of contact between γ_2 and δ induced by the higher coarsening of the secondary austenite during the annealing treatment.

To confirm the results obtained in this work, further analysis are in progress to evaluate the evolution of chemical composition of the phases during the heat treatments, and further annealing treatments at temperatures higher than 1100°C to

determine the weight losses after corrosion tests (the ASTM G48 acceptance threshold is 4 g/m^2, which is a result never obtained in the present study).

Acknowledgements

REFERENCES

[1]   M.C. YOUNG, L.W. TSAY, C.-S. SHIN, S.L.I. CHAN, International Journal of Fatigue. 29 (2007) p. 2115.

[2]   G. MELOTTI, R. BERTELLI, M. ZANESCO, I. CALLIARI, E. RAMOUS, La Metallurgia Italiana. 4 (2005), p. 39.

[3]   F. BONOLLO, A. TIZIANI, P. FERRO, La Metallurgia Italiana 2 (2005), p. 27.

[4]   J. NOWACKI, A. LUKOJC, Journal of Materials Processing Technology 164-165 (2005), p. 1074.

[5]   J.O. NILSSON, L. KARLSSON, J.-O. ANDERSSON, Mater. Sci. Tech. 11 (1995), p. 276.

[6]   C.M. GARZÓN, A.J. RAMIREZ, Acta Materialia. 54 (2006), p. 3321.

[7]   J.-O. NILSSON, T. HUHTALA, P. JONSSON, L. KARLSSON, A. WILSON, Metall. Mater. Trans. A 27A (1996), p. 2196.

[8]   J.NOWACKI, P.RYBICKI, Journal of Mat. Proc. Tech. 164-165 (2005), p. 1082.

[9]   Ø. GRONG, Metallurgical Modelling of Welding, The Institute of Materials, 1997.

[10]   M. AVRAMI, J. Chem. Phys. 7 (1939), p. 1103.

[11]   M. AVRAMI, J. Chem. Phys. 8 (1940), p. 212.

[12]   M. AVRAMI, J. Chem. Phys. 9 (1941), p. 177.

[13]   ANNUAL BOOK OF ASTM STANDARDS, ASTM A928, 2003, ASTM.

[14]   A. GREGORI, J.-O. NILSSON, Met. Mat. Trans. A 33A (2002), p. 1009.

[15]   C.M. GARZON, C. A. SERNA, S. D. BRANDI, A. J. RAMIREZ, J. Mater. Sci. 42 (2007), p. 9021.

[16]   P. FERRO, A. TIZIANI, F. BONOLLO, Proceedings of International conference Duplex 2007, Grado, Italy.

[17]   S. HERTZMAN, P. J. FERREIRA, B. BROLUND, Metall. Mater. Trans. A 28A (1997), p. 277.

[18]   J. NOWAKI, A. LUKOJC, Materials Characterization 56 (2006), p. 436.

[19]   J.-O. NILSSON, A. WILSON, Mat. Sc. And Tech., 9 (1993), p. 545.

[20]   A.J. RAMIREZ, J.C. LIPPOLD, S.D. BRANDI, Metall. Mater. Trans. A 34A (2003), p. 1575.

[21]   S. HERTZMAN, ISIJ International, 41 (2001), p.580.

[22]   S. HERTZMAN, R. PETTERSSON, K.FRISK, T. JERWIN, Proceedings of the Duplex Stainless Steel 2000, Venice, Italy (2000), p.347.

[23]   J.O. NILSSON, Mat. Sc. And Tech. 8 (1992), p. 685.

[24]   V.MUTHUPANDI, P.BALA SRINIVASAN, S. K.SESHADRI, S.SUNDARESAN, Science and Technology of Welding and Joining Vol. 9 No. 1 (2004), p. 47.

[25]   L. WEBER, P.J. UGGOWITZER, Materials Science and Engineering A242 (1998), p. 222.

ARTICLE III

ANNEALING TEMPERATURE EFFECTS ON SUPER DUPLEX STAINLESS STEEL UNS S32750 WELDED JOINTS. I: MICROSTRUCTURE AND PARTITIONING OF ELEMENTS

R. Cervo, P. Ferro, A. Tiziani

University of Padova, Department of Management and Engineering,
Stradella San Nicola 3 - 36100 Vicenza (Italy)

ABSTRACT

Welding of austeno-ferritic stainless steels is a crucial operation and all the materials and parameters used in this process must be optimized in order to obtain the suitable corrosion and mechanical properties. Since a great part of super duplex stainless steels is used in very aggressive environment, their corrosion resistance, referred in particular to pitting and crevice corrosion, is an all-important facet in production and processing of this type of steels.

Pitting corrosion resistance of super duplex stainless steels welded joints depends on several aspects: microstructure of the bead, elemental partitioning between ferrite and austenite, and the possible presence of secondary phases. For these reasons, a post-weld annealing is generally performed to homogenize the microstructure. The annealing temperature is the most important parameter to be optimized in this heat treatment.

In the present work, a comparison between the as-welded and solution treated joints is carried out. An effort has been made to correlate the main factors that affect pitting corrosion of the welded joints (microstructure, secondary phases, chemical composition of single phases) with the experimental data obtained from corrosion tests. In this first part of the work the results regarding microstructure and partitioning of elements are presented.

The phase balance and the austenite morphology are locally upset during submerged arc welding of UNS S32750. In the fused zone, the two phases (ferrite and austenite) result to have approximately the same composition regarding Cr, Mo and Ni content, while nitrogen is heavily concentrated in austenite. After annealing treatment, the austenite volume fraction increases and the partitioning ratios of elements reach the equilibrium values.

The base material results to be less sensitive to annealing treatment than the fused zone, and the partitioning of elements in the base material is in agreement with previous works reported in the literature.

KEY WORDS

Superduplex Stainless Steels, welding, pitting corrosion resistance, elemental partitioning, microstructure.

1. INTRODUCTION

Super Duplex Stainless Steels (SDSS) are corrosion resistant alloys being widely used in the chemical and petrochemicals industries, construction of oil platforms, pulp and paper industries [1]. Since they work in very aggressive environments containing chlorides or other halides, their performance, particularly in term of localized corrosion resistance (pitting and crevice), is a very important subject for researchers and material scientists [2,3,4].

It is well known that pitting corrosion resistance of SDSS strongly depends on the microstructure characteristics, such as the ferrite/austenite proportion, the presence of intermetallic phases, and elemental partitioning between the austenite and ferrite phases. Such features are all affected by the thermal cycles induced by the welding operation.

In particular, the fusion zone (FZ) and the heat affected zone (HAZ) are generally characterized by an unbalanced ratio between ferrite and austenite because of the high temperatures reached and the high cooling rates which characterize the welding process. Since the peak temperature in HAZ is much higher than the upper limit of phase balance between δ-ferrite and austenite (figure 1), most of the γ islands in prior duplex structure dissolve into the δ-ferrite matrix during the heating period. During cooling, in the temperature range between 1300°C and 800°C, the austenite starts to precipitate, both in FZ and HAZ, at the ferrite grain boundaries due to higher free energy of these locations [5]. Because of the high cooling rate of the weld metal, the ferrite-austenite transformation is inhibited and less austenite will be formed if compared with base material.

Therefore, to achieve the desired microstructure, the heat input must be well controlled during welding of duplex and super duplex stainless steel [5]. Nowacki and Rybicki [6] found in particular that the increase of welding heat input reduces the occurrence of inadmissible welding imperfections in joints, which reduces the costs of testing and repairs. Very low heat inputs lead to high ferrite contents and intense chromium nitride precipitation. On the other hand, high heat inputs and long exposure to temperatures in the 1000–600°C range may cause precipitation of brittle intermetallic phases such as σ or χ (figure 2).

Another important feature to be considered when corrosion and mechanical properties have to be evaluated in SDSS joints, is the filler metal chemical composition, which influences the FZ microstructure. Usually, filler metals are over alloyed, with 2–4% Ni greater than in the base metal (BM) content, to assure a more acceptable austenite content in FZ. In their work, Muthupandi et al. [5] found that nickel enrichment in chemical composition of FZ has a greater influence on the ferrite-austenite ratio than the cooling rate. Tavares et al. [7] studied the corrosion resistance and toughness of a multipass weld joint of superduplex stainless steel UNS S32750. The microstructure and chemical composition were determined and correlated to the corrosion and mechanical properties. The root pass was welded with low nickel filler metal and, as a consequence, presented low austenite content and significant precipitation. This precipitation was reflected in the corrosion and mechanical properties. They found that, despite its lower austenite volume fraction (34.2%), the root pass presented a higher Charpy toughness then the filler passes at

room temperature; this was attributed to the finer microstructure of the root pass and high oxygen content of the filler passes. Cyclic polarization tests showed that the base metal, root pass and filler passes present about the same pitting potential (~ 1.0 V_{sce}) and similar PRE (Pitting Resistance Equivalent) indexes. However, the root pass, which contained an excess of ferrite phase and chromium nitride precipitates, was more intensively corroded during the cyclic test. In that work no effort was made in order to study the heat treatment necessary to improve the chemical and mechanical characteristic of the as-welded joints.

Finally, also the partitioning of elements has to be considered in the pitting corrosion behavior of such materials. Austenitic/ferritic stainless steels are characterized by two phases with different chemical compositions and the alloy elements are partitioned in different ways between them. Thus, the Pitting Resistance Equivalent Number (PREN)

$$PREN = \%Cr + 3,3 \cdot \%Mo + k \cdot \%N \qquad (1)$$

with k = 16 ÷ 30, could be evaluated and analyzed for each phase. Since the rapid thermal cycles involved in the welding process, the partitioning of elements in ferrite and austenite is inhibited, and consequently, the pitting corrosion properties of the welded material may be compromised. Perren et al. [3] used a new microelectrochemical method to investigate the individual corrosion behavior of both single phases in super duplex stainless steels. The results showed a good correlation with the empirical PREN of the corresponding single phases. In particular, both the pitting potentials, evaluated by means of macroelectrochemical experiments in pH-neutral lithium chloride electrolyte, and the critical crevice corrosion temperatures showed a good correlation with the PREN of the weaker phase. Even if the annealing temperature in that work was correlated with the PREN of single phases, tests were performed only on the base material so that these kind of data related to welded joints are still lacking.

In conclusion, welding of DSS and SDSS is often a critical operation [7,8,9]. The main difficulty is to obtain austenite amounts close to 50% and to avoid the precipitation of deleterious phases [10]. Therefore, it is generally necessary to perform a solution heat treatment on welded joints in order to homogenize the post-welding metastable microstructure. This annealing treatment consists in a heating up to a temperature between 1050°C and 1150°C for 30 minutes or 1 hour, followed by a rapid cooling in order to prevent the precipitation of intermediate-phases such as σ, χ and carbides [11]. The temperature of this solution heat treatment seems to be a key parameter to determine the final corrosion properties of the welded joint. The main issue is to obtain the best corrosion properties both on the weld metal and on the base material, which are different in terms of chemical composition. To the authors' best knowledge, a satisfactory comprehension of the correlation between post-welding heat treatment (PWHT) process parameter and corrosion properties of SDSS is still no reached. An effort was made in this field by Ferro et al. [11] who studied the effect of PWHT on corrosion properties of the DSS SAF 2205. They found a good correlation between the corrosion properties and the secondary austenite morphology which in turn depended on the PWHT parameters.

Aim of this study is to determine the PWHT conditions to obtain the most favorable pitting resistance corrosion properties of the final SDSS welded joints. Special attention is paid to the comparison between the as-welded and the annealed microstructure, the evolution of phase balance and the partitioning of elements for different solution temperatures.

In part I of this work, all the aspects which regard the evolution of the microstructure on UNS S32750 submerged-arc welded joints in relation to the annealing temperature are taken into account to define the appropriate conditions for the PWHT.

In part II the predicted pitting corrosion resistance (in the as-welded and in heat-treated joints) obtained by PREN evaluations, is compared with the actual pitting corrosion behavior, measured through anodic polarization curves and ASTM G48 standard.
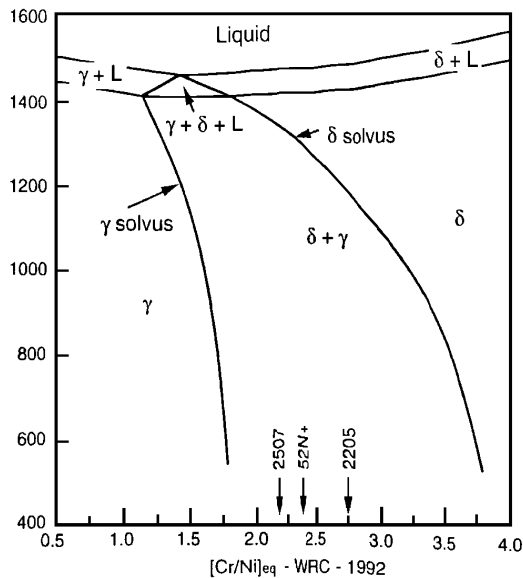
Fig. 1 : The constant (70% wt. Fe) vertical section of the Fe-Cr-Ni system [1]
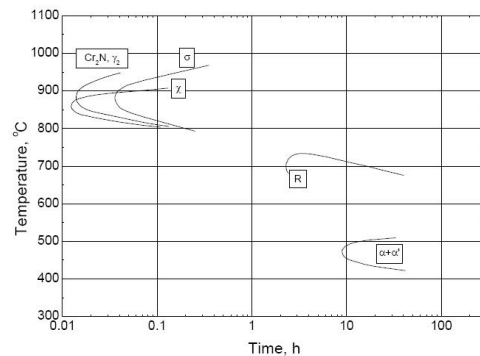
Fig. 2 : TTT diagram for UNS 32750. Curves indicates 1% volume fraction of precipitates [1]

2. EXPERIMENTAL PROCEDURE

2.1 Materials, welding process and post-welding heat treatment

Two 15 mm thick plates of UNS S32750 stainless steel (previously solubilized at 1070°C, then water quenched) were butt welded, with the groove schematically represented in fig. 3. The nominal compositions of the base and filler metal are shown in table 1.

	C	Cr	Cu	Mn	Mo	N	Ni	Si	P	Co	V	Ti	Nb	W	S
Base Metal - UNS S32750	0.018	24.8	0.32	0.79	3.85	0.27	6.92	0.22	0.025	-	-	-	-	-	0.001
Filler Metal - 25 9 4 NL	0.014	25.12	0.096	0.45	4.04	0.228	9.6	0.39	0.014	0.085	0.047	0.005	0.01	0.01	0.0005

Table 1 : Chemical composition (wt%) of the materials used in the study

It can be noted from table 1 that the filler metal is enriched in nickel if compared to the base material in order to ensure the correct austenite/ferrite ratio in the FZ.
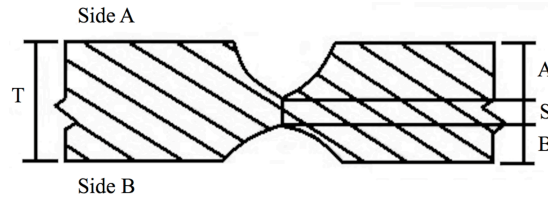
Fig. 3 : Schematic representation of the adopted groove (T = 15 mm, A = 4 mm, S = 5 mm, B = 6 mm)

Welding was carried out by means of three runs, using Submerged Arc Welding (SAW) process. The process parameters are listed in table 2; the heat input was calculated by using Eq. 2 [6]:

Weld layer	Side	Filler metal		Current			Volt range [V]		Travel speed range [cm/min]		Average heat input [kJ/mm]
		Class	Diameter [mm]	Type polarity	Ampere range [A]						
1	A	25 9 4 NL	2.4	DC-EP	340	360	29	31	54	56	1.09
2	A	25 9 4 NL	2.4	DC-EP	390	410	32	34	46	48	1.60
3	B	25 9 4 NL	2.4	DC-EP	540	560	39	40	36	38	3.35

Table 2: Welding parameters

$$HI[kJ/mm] = \eta \frac{V[V] \cdot I[A]}{vel[mm/s] \times 1000}$$

(2)

where V is the voltage, I is the amperage, vel is the travel speed and η is a coefficient approximately equal to 0.95 for submerged arc welding [12].
After welding, the solution annealing were performed in laboratory furnaces at 1050, 1100 and 1150°C for a holding time of 1h, followed by water quenching. These heat

treatments were performed in the "precipitation-free" temperature range as can be observed in fig. 2.

2.2 Metallographic examinations and chemical analysis

Preparation of metallographic sections transverse to the weld bead consisted of silicon carbide paper grinding followed by diamond paste polishing. Beraha's tint etch (80 ml H_2O, 30 ml HCl and 1g $K_2S_2O_5$) was used to reveal the microstructure while oxalic etchant (100 ml H_2O, 10 g oxalic acid, electrolytic 6V) was used to identify the possible presence of precipitates.

Microstructural investigations were carried out by means of Light Optical Microscopy (LEICA) and Environmental Scanning Electron Microscopy (FEI QUANTA 400). The volume fraction of ferrite and austenite was evaluated carefully by means of LOM interfaced with an image analyzer (LEICA QWIN); the final value is the average of at least 12 measurements, each at different zones of the samples.

Chemical analysis of the joints was performed by using an optical spectrometer for chromium, molybdenum and nickel content; nitrogen content was determined using a LECO oxygen nitrogen analyzer. EDAX GENESIS Energy Dispersive Spectroscopy (EDS) interfaced with ESEM was used to measure the content of substitutional alloying elements in austenite and ferrite (using 25 kV of accelerating voltage). Each value is an average of more than 10 EDS measurements normalized with respect to the chemical composition using the following equations:

$$c_{El}^{\gamma} = \frac{c_{El}^{tot}}{V^{\gamma}(1 - P_{El}^{\gamma}) + P_{El}^{\gamma}} \quad (3)$$

$$c_{El}^{\alpha} = \frac{c_{El}^{tot} P_{El}^{\gamma}}{V^{\gamma}(1 - P_{El}^{\gamma}) + P_{El}^{\gamma}} \quad (4)$$

where c^{tot}_{El} is the total content of the analyzed element (El) obtained from chemical analysis in the case of chromium, molybdenum and nickel, and from LECO in the case of nitrogen; V^{γ} is the volume fraction of austenite and P^{γ}_{El} is the partitioning ratio of the element calculated from experimental data and given by the ratio between the mass fraction of the element in ferrite and the mass fraction of the element in austenite. Such temperature dependent value, was estimated, for nitrogen, on the basis of previous work of Atamert and King [13]. A good agreement between the calculated nitrogen content in single phases and the measurements with different techniques (Wavelength Dispersive X-ray Spectroscopy, WDX and X-ray diffraction) was verified [14].

3. RESULTS AND DISCUSSION

3.1 Chemical analysis

Fig. 4 shows the macrostructural appearance of a cross section of the joint.
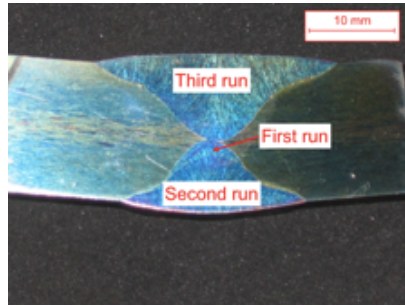
Fig. 4 : Macrography of the analyzed multipass welded joint

It can be noted that the first pass is characterized by a very small area, thus, hereafter only the second and the third runs will be considered for investigations. They will be identified as bottom and top pass, respectively. The dilution ratio was calculated both for the total joint (54%) and for each pass (61% and 43% for top pass (TP) and bottom pass (BP) respectively). It can be observed that the dilution ratio of the top pass is higher than the dilution ratio of the bottom pass because of the different thermal inputs used in such zones (table 2).

Chemical investigations on top pass, bottom pass and base metal were performed with an optical spectrometer in order to verify the actual chemical composition of the FZ and BM. Table 3 shows the results obtained and the calculated values of $PREN_{20}$ and $PREN_{30}$ (Eq. (1), with k = 20 and 30, respectively):

Sample	Cr*	Mo*	Ni*	N**	$PREN_{20}$	$PREN_{30}$
TOP PASS	23.91	3.63	7.93	0.23	40.5	42.8
BOTTOM PASS	23.36	3.58	9.28	0.23	39.8	42.1
BASE METAL	24.32	3.70	6.62	0.27	41.9	44.6

* derived from optical spectrometer analysis   ** derived from LECO analysis

Table 3 : Chemical analysis (wt%) and calculated PREN of base and weld metal

The results collected in table 3 show that chromium, molybdenum and nitrogen contents don't change considerably from top to bottom pass; while TP is poorer in nickel than BT. This fact is due to the lower dilution ratio of this last zone compared to upper zone of the bead, thus the effect of the filler metal, in terms of nickel content, is less evident. The values of pitting resistance equivalent number calculated in the as-welded condition is similar for the two passes considered. Chromium, molybdenum and nitrogen contents in base material are higher than in FZ, and consequently the calculated PREN for the base metal is higher than the one calculated for the bead.

Hereafter, the chemical composition obtained from chemical analysis, that is an "average" value referring to welded zone, was supposed to be constant with the solution temperature; while the "local" chemical composition, referred to austenite and ferrite phases, was supposed to change in relation to the annealing temperature.

3.2 Microstructure evolution

The microstructure of the base material in the as-received conditions (austenite volume fraction. 53 ± 1.94 %) is shown in figure 5.
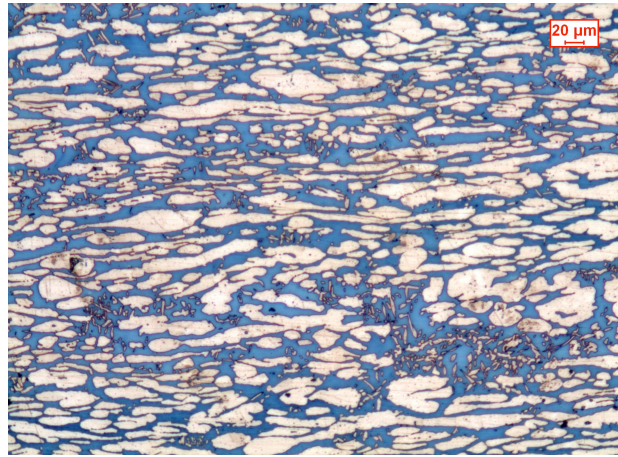
Fig. 5 : LOM micrograph of the as-received material; blue phase: ferrite; white phase: austenite.

The microstructure of the as-welded specimen in the FZ was modified as a consequence of the rapid cooling involved in SAW process. The microstructures of top and bottom pass are very similar and consist of primary ferrite grain decorated with grain boundary austenite and side-plates austenite (Widmanstätten-type) nucleated from grain boundary austenite (fig. 6). The austenite volume fractions were 48.1 ± 1.9% and 48.3 ± 3% in the top and bottom pass respectively.
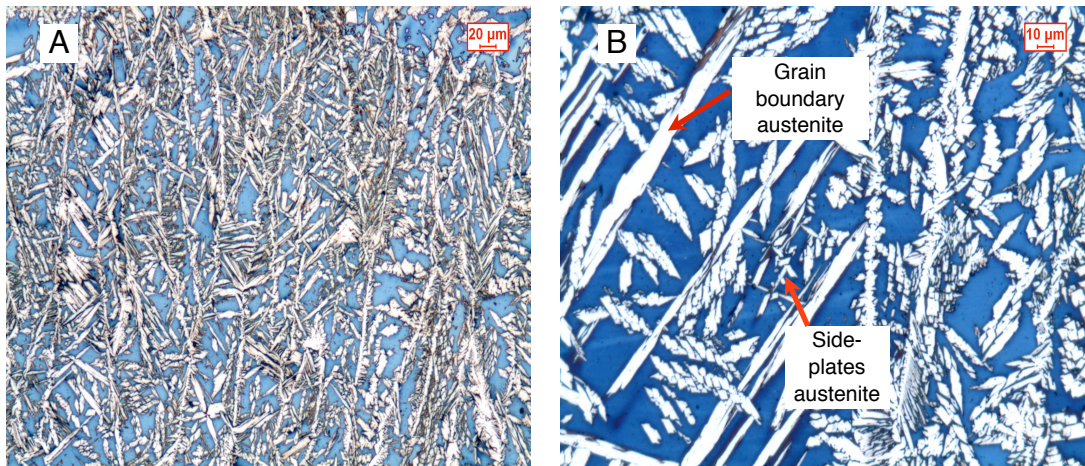
Fig. 6 : LOM micrographs of the FZ of the as-welded specimen; blue phase: ferrite; white phase: austenite.

Oxalic acid etchant was used to reveal the presence of secondary phases. The possibility of chromium nitride precipitation in HAZ during welding of DSS was indicated in several studies [15,16]. It is more likely to occur in ferrite phase because the solubility of nitrogen in ferrite drops rapidly with a decrease in temperature. In this case, some chromium-rich and nickel-poor precipitates were observed in HAZ

(which had a very limited extension, approximately 100 μm). These precipitates were mainly detected in the bottom pass which is characterized by a lower heat input and thus a higher cooling rate (fig. 7). They are observable inside the ferrite grain, at the ferrite/austenite grain boundaries, and at the ferrite sub-grains boundaries (fig. 8). It was reported that these secondary phases can have a detrimental effect on corrosion properties [6,17,18,19]. Finally, no other kind of precipitate were observed.

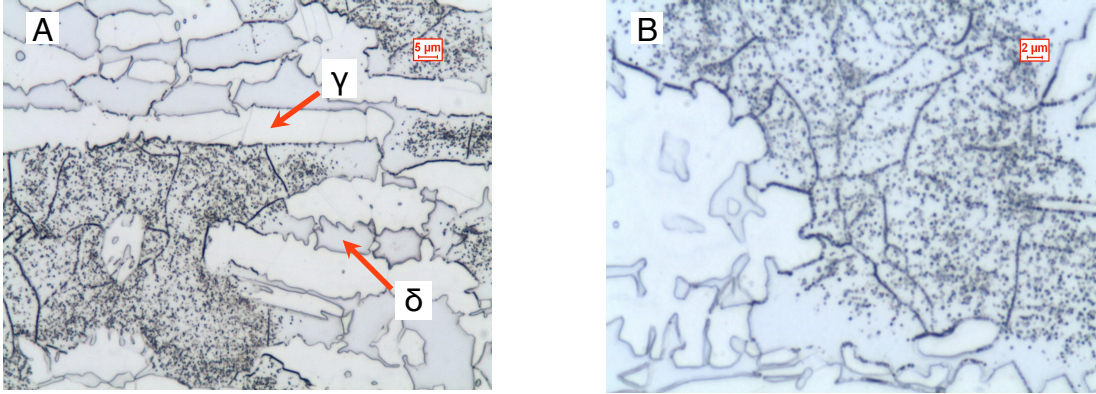*Fig. 7 : LOM micrograph of the HAZ of the as-welded specimen.*
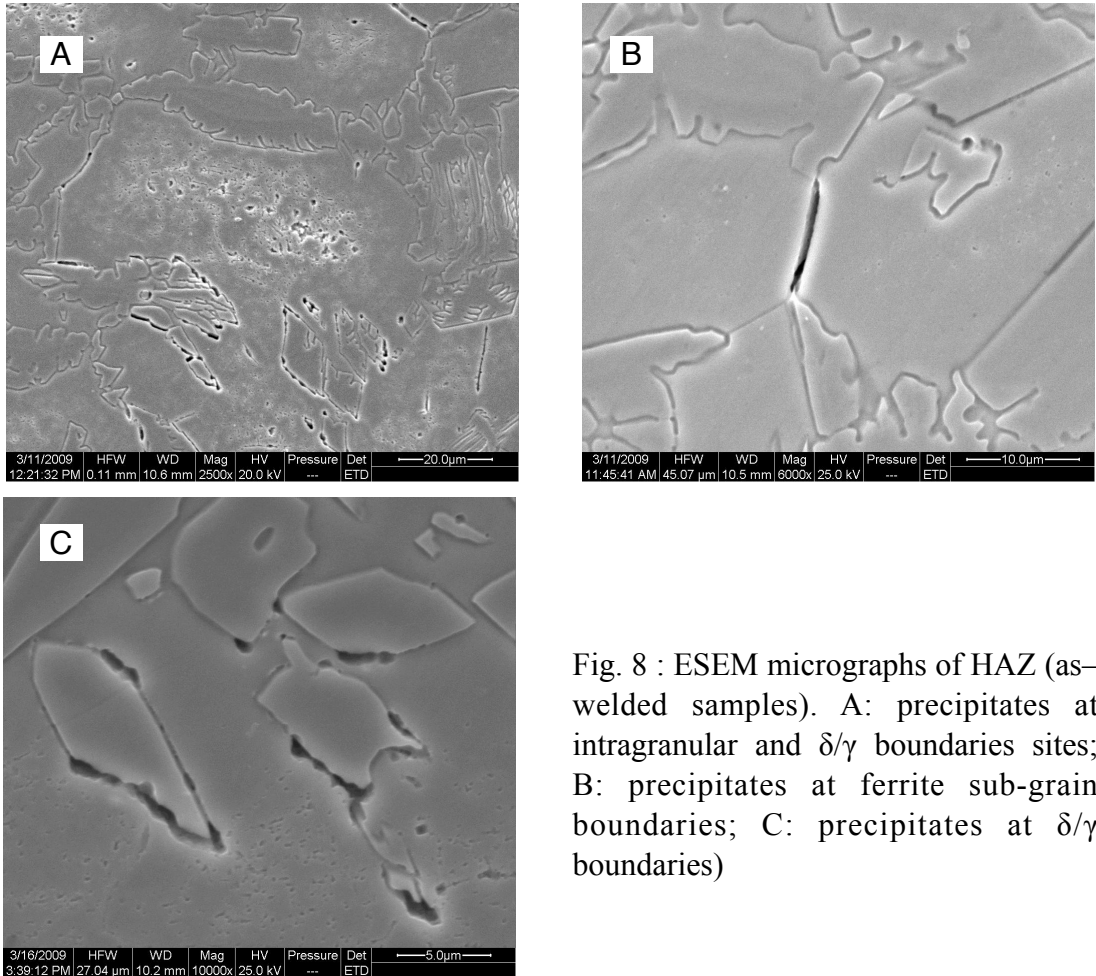

Fig. 8 : ESEM micrographs of HAZ (as–welded samples). A: precipitates at intragranular and δ/γ boundaries sites; B: precipitates at ferrite sub-grain boundaries; C: precipitates at δ/γ boundaries)

Some FZ micrographs of the solution-treated specimens are reported in figure 9. Compared to the as-welded conditions, both intragranular austenite, precipitated on

ferrite grains, and Widmanstätten-type austenite, nucleated at grain boundaries and grown inside the ferrite, was observed [13] (Fig. 9B); as a consequence, the total austenite volume fraction in the welded zone increased after solution annealing. Results from image analysis are summarized in table 4.
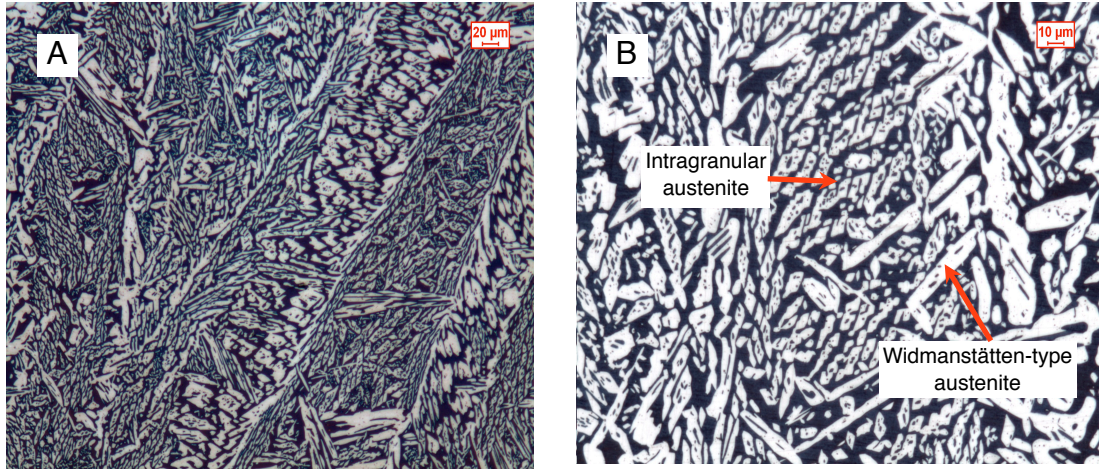
Fig. 9 : LOM micrographs of the welded zone of the solution treated samples (A: 1050°, B: 1100°C); (dark phase: ferrite; white phase: austenite)

SAMPLE	FUSED ZONE - TOP PASS	FUSED ZONE - BOTTOM PASS	BASE MATERIAL
AS-WELDED	48.1 ± 1.9	48.3 ± 3	53 ± 3.3
ST 1050°C	64.9 ± 3.7	65.8 ± 1.6	55.6 ± 1.2
ST 1100°C	58.8 ± 3.7	62.3 ± 3	49.3 ± 2
ST 1150°C	48.6 ± 0.7	51.8 ± 2	47.8 ± 2.3

Table 4 : Experimental austenite volume fractions at different zones of FZ and BM as a function of the annealing temperature

The obtained results have shown that FZ is more sensitive than the base material, in terms of austenite volume fractions variations as a function of the solution temperature. Moreover, it can be seen that for the weld metal, the austenite volume fraction increases after solution treatment, if compared with the as-welded specimen. This phenomenon occurs at all the annealing temperatures up to 1150°C. The higher the solution treatment temperature, the lower is the final austenite volume fractions, as justified by the equilibrium diagram reported in fig. 1. Both the top and the bottom part of the FZ showed a similar phase balance after the heat treatment. Nevertheless, the austenite volume fraction in BM decreases after solution treatment if compared with the as-received conditions. One has to remember that the base material was previously solubilized at 1070°C, thus, the heat treated and the as received materials shown the same austenite fraction value at about 1050-1060°C). In particular, it was found that annealing temperatures at around 1150°C are much higher for the BM solution treatment.

Regarding the heat affected zones, the precipitates observed in the as-welded joints are not detected in the solution treated specimens. This fact is in agreement with the TTT diagram shown in fig. 2 in which it can be seen that for temperatures higher than 950°C the precipitates are not stable and thus dissolve into the matrix during the heat treatment. Moreover, the growth of austenite particles takes place inside the ferrite grains and starting from grain boundaries-austenite, where the precipitates were observed before the solution treatment (fig. 10); since Ramirez et al. [20] have found a direct relation between the secondary austenite nucleation and chromium nitrides dissolution in HAZ, it can be hypnotized that the observed precipitates in the specimens analyzed in this work are the same.
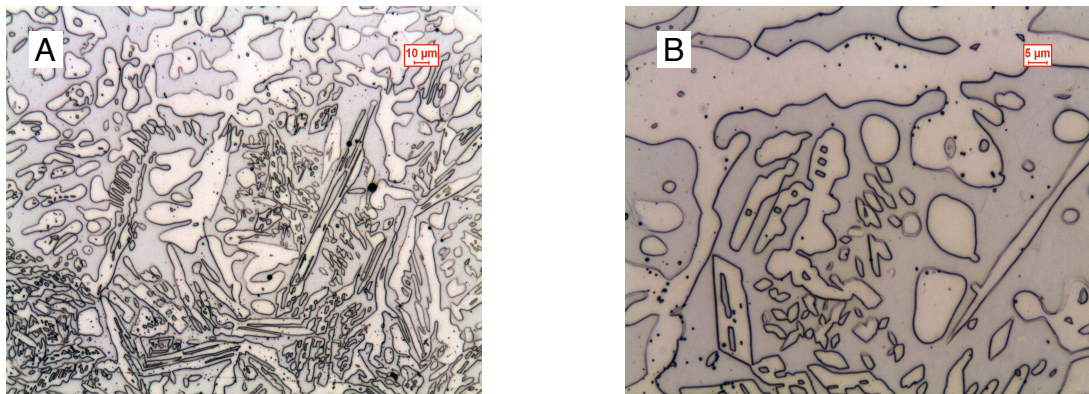
Fig. 10 : HAZ micrographs of the solution treated specimen at 1100°C.

3.3 EDS analysis

Table 5 collects the normalized chromium, nickel and molybdenum contents as a function of phase (ferrite, austenite), solution temperature and position (FZ, BM).

SAMPLE	ZONE	AUSTENITE			FERRITE		
		Cr	Ni	Mo	Cr	Ni	Mo
AS - WELDED	FZ	23.59±0.16	8.81±0.49	3.47±0.11	23.67±0.12	8.41±0.48	3.73±0.61
	BM	23.24±0.10	7.87±0.24	2.93±0.17	25.61±0.23	5.12±0.22	4.62±0.20
ST 1050°C	FZ	22.70±0.52	9.76±0.40	2.81±0.15	25.40±0.71	6.41±0.58	5.11±0.41
	BM	23.12±0.19	8.02±0.27	2.88±0.35	25.79±0.18	4.90±0.21	4.70±0.24
ST 1100°C	FZ	22.69±0.51	9.87±0.60	2.72±0.26	25.09±0.65	6.65±0.44	4.97±0.61
	BM	22.97±0.15	7.91±0.33	3.09±0.20	25.84±0.20	5.17±0.13	4.39±0.07
ST 1150°C	FZ	22.46±0.12	10.09±0.38	2.69±0.19	25.01±0.47	6.84±0.23	4.68±0.18
	BM	23.39±0.25	7.90±0.23	2.98±0.12	25.32±0.14	5.24±0.11	4.48±0.18

Table 5 : Cr, Mo and Ni contents (wt%) of the specimens analyzed (ST = Solution Treated)

The data collected in table 5 show that ferrite (both in FZ and BM) becomes richer in chromium and molybdenum and poorer in nickel content as the annealing temperature increases. These results are in agreement with the observations made by Badji et al. [21] and by Tan et al. in a similar material [22]. However, when the solution temperature increases, the increasing in the ferrite volume fraction induces a short of dilution effect and this phase becomes poorer and poorer in ferrite-stabilizer elements.

It can be observed that nickel content is higher in the FZ than in the BM because of the filler metal influence. Finally, EDS analysis shows that chemical composition of austenite and BM is more stable than ferrite and welded metal respectively. In fact, the bead is a metastable zone if compared with the base material, and it is easy to suppose that the major changing, in terms of phase chemical composition, affects above all the welded joint.

3.4 Partitioning of substitutional elements

3.4.1- Weld metal

Table 6 summarizes the experimentally calculated partitioning ratios (P^{γ}_{EI}) of molybdenum, chromium and nickel in the FZ of as-welded and annealed specimens.

SAMPLE	Cr	Ni	Mo
AS - WELDED	1.00	0.96	1.08
ST 1050°C	1.12	0.66	1.82
ST 1100°C	1.11	0.67	1.83
ST 1150°C	1.11	0.68	1.74

Table 6 : Experimental partitioning ratios calculated in FZ (ST = Solution Treated)

It can be noted that P^{γ}_{EI} values for Mo, Cr and Ni in the as-welded condition are close to 1, as reported in literature [9]. This is in agreement with the fact that in the FZ the cooling rate is high enough to inhibit the partitioning of elements between austenite and ferrite. After solution treatments, partitioning ratios of Cr and Mo reach the equilibrium values; ferrite enriches in chromium and molybdenum, and becomes poorer in Ni. It can be noted that, molybdenum is characterized by a higher partitioning ratios than chromium, thus it can be considered a stronger ferrite stabilizer than chromium, as found by Weber et al. for the same material [23].

3.4.2 Base material

Table 7 collects the experimentally calculated partitioning ratios for chromium, nickel and molybdenum in the BM, both for as-welded and solution-treated samples, and the values derived from the experimental measurements carried out by Tan et al. [12] and Charles [24] for the same material.

	EXPERIMENTAL		
SAMPLE	Cr	Ni	Mo
AS - WELDED	1.10	0.65	1.58
ST 1050°C	1.12	0.61	1.63
ST 1100°C	1.12	0.65	1.42
ST 1150°C	1.08	0.66	1.50
	LITERATURE		
ST 1030°C*	1.17	0.62	1.81
ST 1050°C*	1.17	0.64	1.72
ST 1080°C*	1.16	0.66	1.56
ST 1100°C*	1.15	0.67	1.50
ST 1150°C*	1.13	0.70	1.49
ST 1180°C*	1.13	0.72	1.50
ST 1200°C*	1.12	0.73	1.41
ST 1080°C**	1.15	0.65	1.60

* values reported by Tan et al. [12]
** values reported by Charles [24]

Table 7 : Experimental partitioning ratios in BM (ST = Solution Treated)

A comparison between partitioning ratios as a function of annealing temperature reported by Tan et al. [12] and the values found in this study is shown in figure 11.
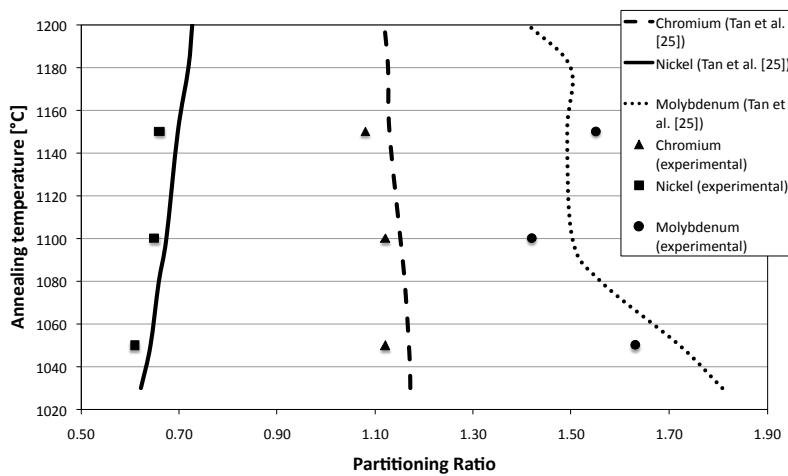

Fig. 11 : Comparison between the partitioning ratios calculated in this work and the values derived from literature versus annealing temperature in BM

A sufficient agreement was found between the experimental data and the values reported in literature for all the annealing temperatures.

3.5 Nitrogen content calculation

Nitrogen weight fraction and its partitioning between ferrite and austenite is fundamental for determining the pitting corrosion behavior of super duplex stainless steels.

Concerning the as-welded conditions of austenitic/ferritic stainless steels, it has been shown by Liljas [25] that at high cooling rates, the interstitial elements controlling the reaction (e.g. nitrogen) are heavily concentrated to the austenite. In particular, a nitrogen P^{γ}_{EI} value of about 1/10 has been measured [25] and used in this study for estimating the nitrogen content in the as-welded conditions. Instead, regarding the annealed specimens, the nitrogen P^{γ}_{EI} value was assumed to follow the ratio given by Atamert and King [13]: the nitrogen mass fraction in the γ-phase being about seven and eight times higher than in the δ-phase at 1050 °C and 1250 °C respectively. For the intermediate annealing temperatures considered in the present study, the value was, in first approximation, linearly interpolated.

Table 8 shows the calculated nitrogen contents for austenite and ferrite at different annealing temperatures, both for BM and FZ (the base metal was previously solubilized at 1070°C):

SAMPLE	ZONE	AUSTENITE	FERRITE	
AS - WELDED	FZ	0.42	0.05	*Nitrogen - FZ*
	BM	0.46	0.06	
ST 1050°C	FZ	0.33	0.05	
	BM	0.45	0.06	*Nitrogen - BM*
ST 1100°C	EZ	0.35	0.05	
	BM	0.47	0.06	
ST 1150°C	FZ	0.38	0.05	
	BM	0.49	0.06	

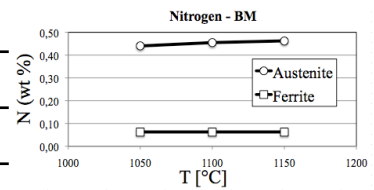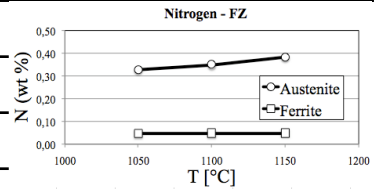*Table 8 : Calculated nitrogen content (wt%) for ferrite and austenite at different solution temperatures*

It can be observed that austenite becomes more reach in nitrogen as the solution temperature increases, while the nitrogen content in ferrite does not substantially change. Moreover, the austenite in the bead seems to be more sensitive to annealing treatments, in term of nitrogen content.

CONCLUSIONS

Chemical composition, microstructure and partitioning of elements were evaluated on UNS S32750 submerged arc welded joints in the as-welded and annealed conditions.

The following specific conclusions can be drawn for the as-welded and annealed specimens:

As-welded specimens

• Even if a nickel-reach filler metal was used, the phase balance of UNS S32750 was upset during welding as a consequence of the rapid cooling involved in SAW; the austenite amount decreases if compared with BM and its morphology changes to grain boundary austenite and side plates Widmanstätten austenite.

• Some chromium-rich precipitates were detected in the HAZ, which might affect the corrosion properties of the welded joint.

• The experimental (Cr, Mo, Ni) partitioning ratios of the substitutional elements in the as welded specimen are close to 1, as reported in the literature. Thus, austenite and ferrite have the same chemical composition with the exception of nitrogen content, which is heavily concentrated in austenite.

Annealed specimens

• The austenite volume fraction in the FZ increases for all the annealing temperatures up to 1150°C, if compared with the as-welded samples. However, the austenite volume fractions decreases as the post-welding annealing temperature increases. The more favorable phase balance in the welded zone is reached at annealing temperatures ranging between 1100°C and 1150°C.

• The base material is less sensitive to annealing temperature and the austenite volume fractions generally decrease if compared with the as-welded conditions (except for annealing temperatures around 1060°C). The best phase balance for the base material is achieved at temperatures between 1050°C and 1100°C.

• After solubilization treatment, the precipitates detected in the HAZ dissolve.

• After solution treatment the partitioning ratios in FZ reach the equilibrium values, that is, ferrite enriches in Chromium and Molybdenum while austenite enriches in Nickel and Nitrogen. P^{γ}_{El} values for Chromium and Molybdenum decrease while for Nickel slightly increase with temperature, both for the BM and FZ. However, it was found that FZ is more sensitive to P^{γ}_{El} variations with annealing temperature.

• A high annealing temperature (1150°C) increases the ferrite content, thus the key alloying elements (in particular Chromium and Molybdenum), both for BM and FZ, becomes more diluted in this phase; on the other hand, austenite enriches in nitrogen as the heat treatment temperature increases.

• The partition coefficients of the alloying elements in BM were found in good agreement with those reported in literature.

REFERENCES

[1]   J.O. Nilsson, "Super duplex stainless steels", Materials Science and Technology 8 (1992), pp. 685-700

[2]   D.M. Garcia, Garcia, J. Garcia-Anton, A. Igual-Munoz, E. Blasco-Tamarit, "Effect of cavitation on the corrosion behaviour of welded and non-welded duplex stainless steel in aqueous LiBr solutions", Corrosion Science 48 (2006), pp. 2380-2405

[3]   R.A. Perren, T.A. Suter, P.J. Uggowitzer, L. Weber, R. Magdowski, H. Bohni, M.O. Speidel, "Corrosion resistance of super duplex stainless steels in chloride ion containing environments: investigations by means of a new microelectrochemical method: I. Precipitation-free states", Corrosion Science 43 (2001), pp. 707-726

[4]   R.A. Perren , T. Suter, C. Solenthaler, G. Gullo, P.J. Uggowitzer , H. Bohni, M.O. Speidel, "Corrosion resistance of super duplex stainless steels in chloride ion containing environments: investigations by means of a new microelectrochemical method: II. Influence of precipitates", Corrosion Science 43 (2001), pp. 727-745

[5]   V. Muthupandi, P. Bala Srinivasan, S.K. Seshadri, S. Sundaresan, "Effect of weld metal chemistry and heat input on the structure and properties of duplex stainless steel welds", Materials Science and Engineering A358 (2003), pp. 9-16

[6]   Jerzy Nowacki, Pawel Rybicki, "The influence of welding heat input on submerged arc welded duplex steel joints imperfections", Journal of Materials Processing Technology, 164–165 (2005), pp. 1082–1088

[7]   S.S.M. Tavares, J.M. Pardal, L.D. Lima, I.N. Bastos, A.M. Nascimento, J.A. de Souza, "Characterization of microstructure, chemical composition, corrosion resistance and toughness of a multipass weld joint of superduplex stainless steel UNS S32750", Materials Characterization 58 (2007), pp. 610-616

[8]   S. Atamert, J.E. King "Superduplex stainless steels Part 1. Heat affected zone microstructures", Mat. Science and Technology 8 (1992), p. 896-911

[9]   F. Bonollo, A. Tiziani, P. Ferro, "Advances in Duplex Stainless Steels" - Chapter 4, ISTE LTD. London, In press.

[10]   J.O. Nilsson, L. Karlsson, J.O. Anderson, "Secondary austenite formation and its relation to pitting corrosion in duplex stainless steel weld metal", Materials Science and Technology 11 (1995), pp. 276-283

[11]   P. Ferro, A. Tiziani, F. Bonollo, "Influence of induction and furnace post welding heat treatment on corrosion properties of SAF 2205 (UNS 31803)", Welding Journal. 87 (2008), pp. 298–306

[12]   Ø. Grong, Metallurgical Modelling of Welding, The Institute of Materials, 1997

[13]   S. Atamert, J.E. King, "Elemental partitioning and microstructural development in duplex stainless steel weld metal", Acta Metall. Mater. 39 (1991), pp. 273-285

[14] L. Weber, P.J. Uggowitzer, Proc. Int. Symp. High Perfor. Steels Struct. Appl., ASM, Cleveland, 1995, pp. 291-298

[15] T. Ogawa, T. Koseki, Welding Journal 68 (1989), pp. 181-191

[16] F. Bonollo, A. Gregori, A. Tiziani, J.-O. Nilsson, "A study on microstructural evolution of superduplex steels (SAF 2507) induced by isothermal heat treatment" Proc. 11th Congress of The International Federation for Heat Treatment and Surface Engineering, Firenze (19-21 ottobre 1998), 3, 291-300; Associazione Italiana di Metallurgia - Milano

[17] H.-Y. Liou, R.-I. Hsieh, W.-T. Tsai, "Microstructure and pitting corrosion in simulated heat-affected zones of duplex stainless steels", Materials Chemistry and Physics 74 (2002), pp. 33-42

[18] J.O. Nilsson, A. Wilson, "Influence of isothermal phase transformation on toughness and pitting corrosion of super duplex stainless steel SAF 2507", Material Science and Technology 9 (1993), pp. 545-554.

[19] HeonYoung Ha, HyukSang Kwon, "Effects of Cr_2N on the pitting corrosion of high nitrogen stainless steels" Electrochimica Acta 52 (2007), pp. 2175–2180

[20] A.J. Ramirez, J.C. Lippold, S.D. Brandi, "The Relationship between Chromium Nitride and Secondary Austenite Precipitation in Duplex Stainless Steels" Metallurgical and Materials Transactions 34A (2003), pp. 1575-1597

[21] R.Badji, M. Bouadballah, B.Bacroix, C.Kahloun, K.Bettahar, N.Kherrouba, "Effect of solution treatment temperature on the precipitation kinetic of sigma phase in 2205 duplex stainless steel welds", Materials Science and Technology A496 (2008), pp. 447-454

[22] Hua Tan, Yiming Jiang, Bo Deng, Tao Sun, Juliang Xu, Jin Li, "Effect of annealing temperature on the pitting corrosion resistance of super duplex stainless steel UNS S32750", Materials Characterization (2009), doi 10.106/j.matchar.2009.04.009

[23] L. Weber, P.J. Uggowitzer, "Partitioning of chromium and molybdenum in super duplex stainless steels with respect to nitrogen and nickel content", Materials Science and Engineering A 242 (1998), pp. 222-229

[24] J. Charles, Proc. Duplex Stainless Steels 91, Ed. Physique 1 (1991), pp. 3-41

[25] M. Liljas, "The welding metallurgy of duplex stainless steels", Proc. Duplex Stainless Steels 94, 1994, Glasgow, Scotland.

ARTICLE IV

ANNEALING TEMPERATURE EFFECTS ON SUPER DUPLEX STAINLESS STEEL UNS S32750 WELDED JOINTS. II: PITTING CORROSION RESISTANCE EVALUATION

R. Cervo*, P. Ferro*, A. Tiziani*

F. Zucchi**

University of Padova, Department of Management and Engineering, Stradella San Nicola 3 – I-36100 Vicenza

**University of Ferrara, Corrosion Study Centre A. Daccò, Via G. Saragat, 4A, I-44100 Ferrara*

ABSTRACT

This work deals with the effect of the annealing temperature on the pitting corrosion resistance of UNS S32750 submerged arc-welded joints.

In a companion paper (Part I), the influence of post-weld annealing temperature on microstructure evolution and chemical composition of austenite and ferrite was analyzed; this work can thus be considered directly connected with the previous one. The pitting corrosion resistance of the heat-treated welded joints were evaluated by using both electrochemical measurements and ASTM G48 standard gravimetric tests; examinations of initiation sites of pitting attack were carried out in order to correlate the experimental data obtained in this work with the predicted pitting corrosion behavior obtained by using the results described in Part I.

Generally, the post-weld annealing treatment enhances the pitting corrosion resistance of the analyzed joints; in particular, the most favorable annealing temperature for the analyzed alloy was founded to be 1100°C.

KEYWORDS

1. INTRODUCTION

It is well known that ferrite/austenite balance and phases chemical composition of superduplex stainless steels (SDSS) is generally altered by welding operations [1,2,3,4], and the precipitation of detrimental phases in the reheated weld beads and heat affected zone (HAZ) could take place [5,6,7,8]. Consequently, the excellent corrosion properties of such alloys, especially in terms of pitting corrosion resistance, could be compromised [9,10,11,12]. The diagram of fig. 1 shows the effect of ferrite content on pitting rate, indicating the importance of phases balance control in order to obtain suitable corrosion properties [13].
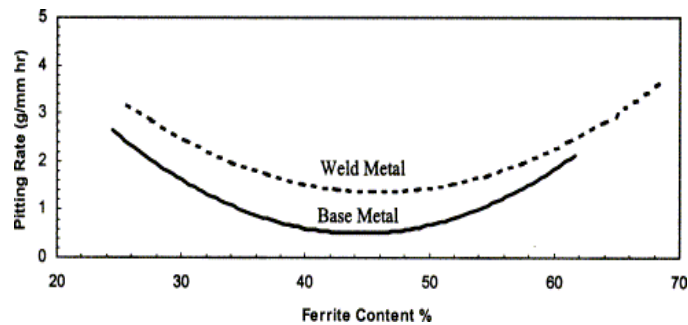
Fig. 1: Effect of ferrite content on pitting rate of SAF 2205 welded joint [12]

In order to assure a more balanced microstructure, appropriate filler metals enriched in austenite-stabilizer elements are used during welding of DSS and SDSS [14]. However, a post-weld solution heat treatment could be required in order to restore the optimal pitting corrosion resistance of such joints [15].

The pitting corrosion of stainless steels is generally associated to a local breakdown of the protective passive layer and their susceptibility to a such damage can be evaluated by using different methods: critical pitting temperature measurements, gravimetric tests after immersion in high-aggressive solutions, and electrochemical measurements. It is generally accepted that pitting initiates when the pitting potential reaches a critical value (E_p), which depends on the chemical composition of the alloy and on the environment (temperature and chloride concentration). E_p is often measured by potentiodynamic anodic polarization tests. In these measurements the onset of pitting corrosion is observed as an irreversible increase in current density (Fig. 2). The higher the E_p value, the more resistant is the alloy to pitting corrosion in the environment considered [16].
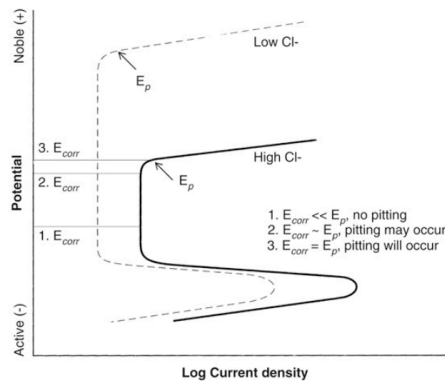
Fig. 2: Schematic representation of a polarization curve, determining the pitting corrosion risk [16]

Compared to the one phase stainless steels, a complication arises when the pitting corrosion resistance of DSS and SDSS has to be evaluated because of the presence of two phases with different composition and elemental partitioning.

The Pitting Resistance Equivalent Number (PREN = %Cr + 3.3 %Mo + (16÷30) %N) is the first parameter that can be considered when selecting the pitting corrosion resistance of austeno/ferritic stainless steels. The literature offers a variety of standard formulas for PREN [1,17,18,19], which are considered in detail in the experimental part of this work.

In the case of SDSS, since the corrosion resistance is controlled by the weaker phase, the PREN value of both the ferrite and austenite should be calculated [20,21]. Moreover, the best corrosion resistance of the alloy is found when the two phases has the same PREN value. The partitioning behavior of chromium and molybdenum as well as the volume fraction of ferrite and austenite has a strong influence on the chemical composition of the two phases and then on each PREN value.

Since the ferrite volume fraction increases with increasing temperature, chromium and molybdenum become more diluted in this phase and thus the $PREN_{ferrite}$ decreases. On the other hand, a smaller austenite volume fraction leads to a higher concentration of nitrogen in γ phase, i.e. $PREN_{austenite}$ increases. To summarize, as the annealing temperature increases, PREN of austenite increases and PREN of ferrite decreases.

Consequently, Bernhardsson [22] and other authors such as Tuck et *al*. [23] and Tal et *al*. [24], suggested that the optimum annealing temperature can be reached when the two PREN-Temperature curves cross each other. In this condition the PREN reaches the maximum value for both the phases and the alloy reaches the best pitting corrosion resistance.

Because of the strict relationship between pitting corrosion behavior and the annealing temperature, the latter results to be a key parameter in order to determine the final corrosion properties of SDSS welded joints. Moreover, since the use of filler metal implies the presence of two different materials in terms of chemical composition (the base material (BM) and the fusion zone (FZ)), the welded joint is

generally characterized by two different solubilization temperatures. Two annealing temperatures can be obtained and thus, when the optimum post welding annealing temperature has to be chosen, a "trade-off" is required.

In the present part II, the pitting corrosion resistance of UNS S32750 welded joints (in the as-welded and annealed conditions) was experimentally evaluated by electrochemical measurements and ASTM G48 gravimetric tests. An effort has been made in order to correlate the main factors that affect pitting corrosion resistance of the SDSS welded joints (phase balance, intermetallic phases, partitioning of elements in ferrite and austenite, PREN), with the experimental data obtained from corrosion tests. Aim of the work is to determine the solution treatments conditions to obtain the best corrosion properties of the welded component. To author's best knowledge, this topic, already treated in literature [22] for the base material, is still lacking in the case of welded joints.

2. EXPERIMENTAL PROCEDURE

2.1 Materials and solubilization heat treatments
The present study deals with UNS S32750 submerged-arc welded joints both in the as-welded and in the annealed conditions, as described in Part I.

To summarize, three post-weld solubilization treatment temperatures were considered: 1050°C, 1100°C and 1150°C. All the experimental results described in Part I were used in the present work, especially in terms of chemical composition obtained by optical spectrometer, microstructural features and phase distribution obtained by metallographic analysis with a combination of LOM and SEM examinations, and finally chemical composition of the single phases achieved by EDS analysis.

2.2 PREN calculations
The pitting corrosion behavior was estimated on the basis of PREN calculations and microstructural analysis. A comparison with the experimental data obtained from corrosion tests was also carried out. The literature offers different formulas for PREN calculation [16,17, 24]:

$$PREN_{16} = \%Cr + 3.3\%Mo + 16\%N \tag{1}$$

$$PREN_{20} = \%Cr + 3.3\%Mo + 20\%N \tag{2}$$

$$PREN_{30} = \%Cr + 3.3\%Mo + 30\%N \tag{3}$$

For stainless steels, the results included in references [23, 25-27] show that $PREN_{16}$ gives a good correlation between corrosion resistance and chemical composition of DSS. Nevertheless, some authors [18,24] suggest the use of the coefficient 20 or 30

for the nitrogen in order to emphasize the importance of this element in the behavior of the alloy, especially for SDSS.

Concerning the present work, PREN was calculated, both for BM and FZ, by using Eqs. (2) and (3).

2.3 Pitting corrosion evaluation

The pitting corrosion resistance of the welded joints in the as-welded and in the annealed conditions, was evaluated both by anodic polarization measurements and by gravimetric tests according to ASTM G48 standard - method A [28]. Even if gravimetric tests provide general information about the pitting corrosion resistance of welded joints, they are unable to differentiate the different zones of the joint. Therefore, in order to study the corrosion performance of base and weld metal separately, anodic polarization measurements were also performed.

2.3.1 ASTM G48 gravimetric tests

Pitting corrosion resistance was also evaluated according to the Standard ASTM G48 - method A, which is often applied in welding procedure qualifications. The specimens (15 x 15 x 50 mm) after being pickled for 5 minutes (10% HF, 20% HNO_3 at 60°C), were passivated in pure nitric acid for 15 min at room temperature. Finally, they were dipped for 24 h in ferric chloride reagent (100g $FeCl_3 \cdot 6H_2O$ in 900 ml H_2O); exposure was performed at 50 ± 2°C.

The corrosion rate was then calculated starting from the weight losses per unit of surface area according to the following equation:

$$Corrosion\ Rate = \frac{Wt_i - Wt_f}{A} \tag{4}$$

where Wt_i and Wt_f are the weights of the sample measured before and after the test, respectively, and A is the exposed surface area. Weight losses were measured by means of a balance with a tolerance of 1 mg and ultrasonic post-cleaning (5 min. in acetone) was applied to the specimens.

2.3.2 Anodic polarization measurements

The anodic behavior of each specimen was analyzed. Since the HAZ was very narrow (about 100 μm), only the behaviors of BM and FZ (bottom pass) were differentiated.

Specimens preparation for the electrochemical tests was the same as described in the previous work (Part I) for the metallographic analysis. In particular, the final surface finishing was 6 μm. In order to prevent crevice corrosion the samples were passivated (15 min. in pure nitric acid, room temperature) and a resin for edge retention was used.

The working electrode was built up using the samples embedded in epoxy resin, with a copper wire providing electrical contact.

The tests were carried out in a 3.5% NaCl open to air solution at 80°C (which is approximately the critical pitting temperature of UNS S32750 [29]) by using a potentiostat-galvanostat (Princeton Applied Research Mod. 263A). The

electrochemical cell was suspended in a water bath to control the solution temperature. An Ag/AgCl 3M KCl electrode was used as the reference electrode and the auxiliary electrode was a platinum sheet. The specimens were cleaned, degreased and dried before starting the polarization tests. All data were recorded after an initial delay of 60 min for the specimen to stabilize at free corrosion potential; then the potential was increased from the free corrosion potential in the anodic direction at a scan rate of 1 mV/s until a current density of 1 mA/cm^2 was reached. The curves obtained are an average of three replicate tests of the same specimen. Finally, the corrosion behavior was evaluated by the absolute value of the pitting potential (E_p).

After polarization tests, each specimen was ultrasonic-cleaned with acetone, chemically etched with Beraha's etchant (80 ml H_2O, 30 ml HCl, 1 g $K_2S_2O_5$) and examined at SEM to observe the pit morphology and the sites of pit nucleation, with a particular attention to the specific phase where the corrosion attack started.

3. RESULTS AND DISCUSSION

3.1 PREN analysis

It is known that the pitting resistance equivalent number could be used to quickly estimate the pitting corrosion resistance of super duplex stainless steels under sound plate or joint conditions (i.e.: absence of deleterious precipitates, secondary phases, etc.) [19, 21-27].

In this study, such index has been calculated for both the whole alloy and the single phases by using the data reported in the previous work (Part I). In particular values for both BM and FZ were obtained and the results were summarized in table (1).

	Sample	Phase	PREN$_{20}$ (alloy)*	PREN$_{30}$ (alloy)*	PREN$_{20}$ (phase composition)**	PREN$_{30}$ (phase composition)**
FZ	As - Welded	Ferrite	40.2	42.5	37.0	37.5
		Austenite			43.4	47.6
	S.T. 1050°C	Ferrite			43.3	43.8
		Austenite			38.6	41.9
	S.T. 1100°C	Ferrite			42.5	43.0
		Austenite			38.7	42.2
	S.T. 1150°C	Ferrite			41.5	42.0
		Austenite			38.9	42.7
BM	As - Welded	Ferrite	41.9	44.6	42.1	42.7
		Austenite			42.1	46.7
	S.T. 1050°C	Ferrite			42.5	43.1
		Austenite			41.6	46.1
	S.T. 1100°C	Ferrite			41.5	42.1
		Austenite			42.6	47.3
	S.T. 1150°C	Ferrite			41.3	41.9
		Austenite			43.0	47.9

* calculated by using the chemical compositions obtained by optical spectrometer
** calculated by using compositions obtained by EDS analysis

Tab. 1 : PREN values calculated for base and weld metal (S.T. = Solution Treated)

It can be noted that in the as-welded conditions, very different values of $PREN_{austenite}$ and $PREN_{ferrite}$ were found in the FZ. On the other hand, the PREN values for the BM of the as-welded samples are similar to those of the annealed ones at a temperature of 1050 °C. This is in agreement with the fact that the BM in the as-received conditions was previously solubilized at 1070°C.

Figure 3 shows the calculated values of $PREN_{30}$, both in BM and FZ, as a function of annealing temperature and phases.
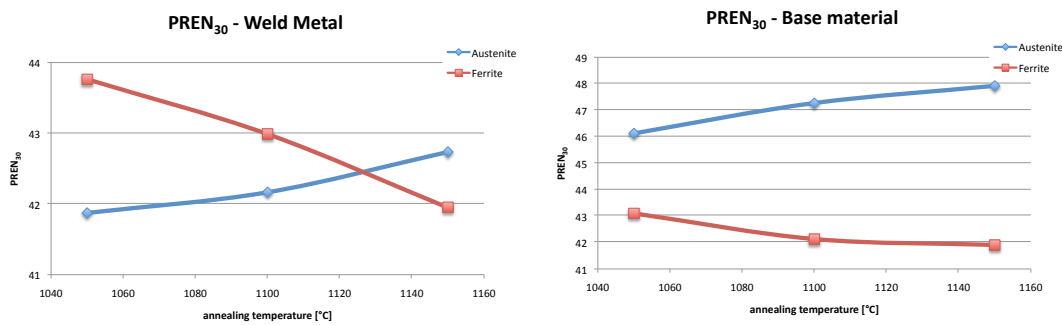

Fig. 3 : Calculated values of $PREN_{30}$, both in BM and FZ, as a function of annealing temperature and phases

Like expected, the solution treated specimens show an increase in $PREN_{austenite}$ value with the increase of the annealing temperature; an inverse behavior was found for $PREN_{ferrite}$. As described in the introduction section, the ferrite proportion increases with the annealing temperature so that its key elements such as chromium and molybdenum became more diluted. On the other hand, the decrease in austenite fraction results in a more concentrate content of nitrogen in it.

One can observe that the two $PREN_{30}$ curves, calculated in the FZ, cross each other at the annealing temperature of about 1125 °C. At this temperature the two phases reach the same $PREN_{30}$ value (42.5) so that it can be considered as the optimum value for the heat treatment of such a zone. This phenomenon is not capture for the BM if $PREN_{30}$ is used. However, by using the $PREN_{20}$ values, again the two curves cross each other (Fig. 4) and the same considerations made for the FZ can be transferred to the BM.
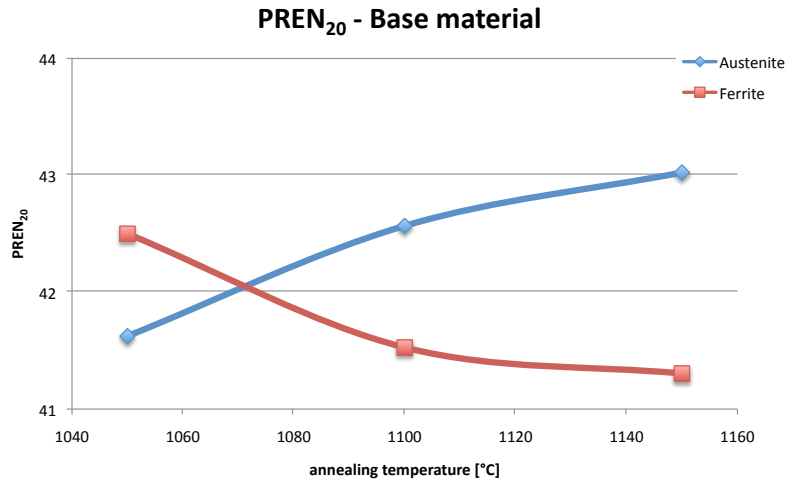
Fig. 4 : Calculated PREN$_{20}$ for austenite and ferrite as function of annealing temperature - base material

In this case, the optimum annealing temperature value was found to be 1070 °C (PREN$_{20}$ = 42). It can be noted that for the BM UNS S32750 and by using the PREN$_{20}$ definition, Tan et *al*. found a value of 1080 °C [24]. When PREN is used as a criterion for estimating the pitting susceptibility of DSS and SDSS to pitting corrosion, it has to be remarked that one should consider the PREN of the weaker phase, which is generally different from the PREN calculated using the alloy composition (Table 1). The histograms of Fig. 5 collect the calculated PREN$_{20}$ and PREN$_{30}$ of the weaker phase for all the samples considered:
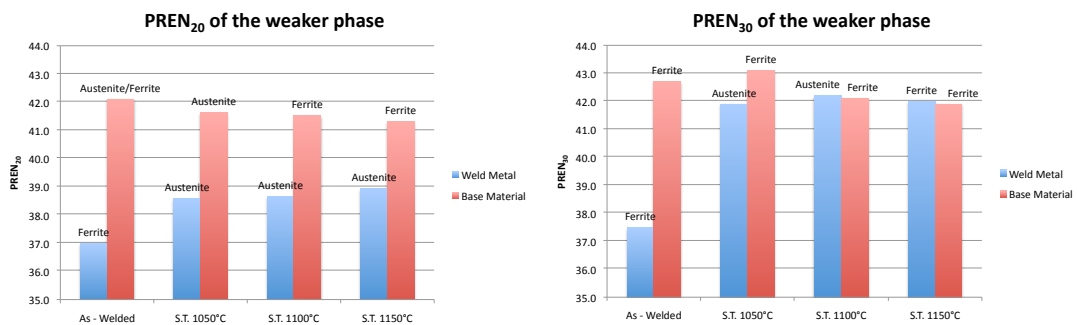
Fig. 5 : Calculated values of PREN of the weaker phase as function of the specimen conditions

Fig. 5 shows that a post-weld annealing treatment induces a remarkable increase of the minimum pitting resistance equivalent number in FZ (an increment of about 1.5 or 4.5 by using PREN$_{20}$ or PREN$_{30}$, respectively). Finally, it can be observed that for the weld metal, the phases that result more susceptible to pitting corrosion (i.e. which have the lower PREN$_{30}$ value) are:

- *ferrite* in the as-welded conditions and in the specimen annealed at 1150°C;

- *austenite* in the specimen annealed at 1050°C and 1100°C;

Concerning the BM, the weaker phase results to be *ferrite* in all the conditions.

3.2 Corrosion tests

3.2.1 ASTM G48 corrosion test results
The corrosion rates, measured according to the ASTM G48 corrosion test, are summarized in the histogram of Figure 6, where the average value together with the standard deviation of three measurements are also reported:
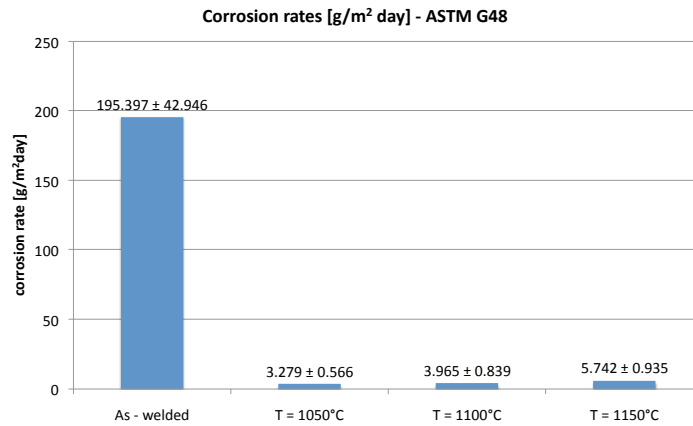
Fig. 6 : Histogram showing the corrosion rates of the specimens after pitting corrosion test in 6 wt% FeCl solution, 24 h

Figure 7 shows the as-welded specimen after the ASTM G48 corrosion test; a deep corrosion attack can be seen in the welded zone.

Fig. 7 : As-welded specimen after the ASTM G48 test, 24 h.

The obtained experimental results confirmed the beneficial effect of a post-weld annealing treatment on the pitting corrosion resistance of UNS S32750 welded joints: a pronounced drop of the corrosion rates was found by comparing the as-welded specimen with the annealed ones. For the samples annealed at 1050°C and 1100°C the average corrosion rates are extremely low (lower than the acceptance threshold value of 4 g/m^2); while, a slightly increase in the corrosion rate is observable in the sample annealed at 1150°C, if compared with the previous ones.

3.2.2 Electrochemical measurements
The potentiodynamic anodic polarization technique was used to investigate the electrochemical behavior of the weld metal and base material separately. The average anodic polarization curves in 3.5% NaCl solution (open to air) at 80°C are shown in figure 8.

Fig. 8 : Anodic polarization curves in 3.5% NaCl solution at 80°C, open to air
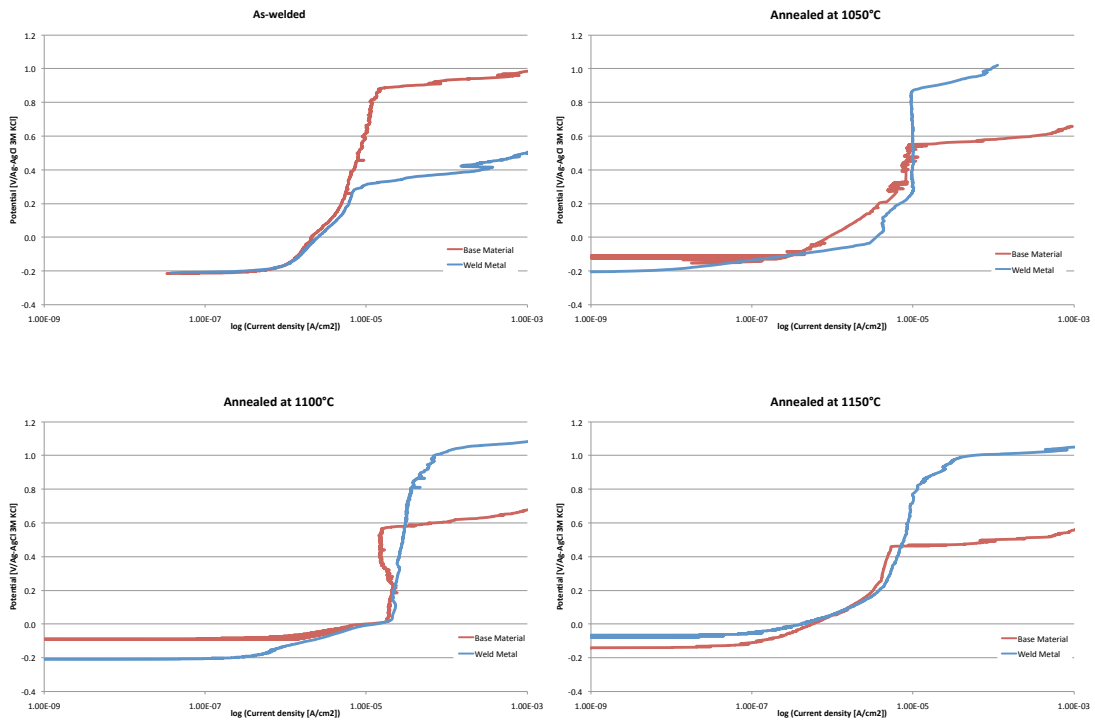
The corrosion parameters, including free corrosion potentials (E_C) and pitting corrosion potentials (E_P) of all the specimens analyzed, are summarized in table 2 (values are an average of at least three measurements).

ZONE	SAMPLE	E_C [mV vs Ag/AgCl 3M KCl]		E_P [mV vs Ag/AgCl 3M KCl]	
		AVG.	STD. DEV.	AVG.	STD. DEV.
	As-welded	-228	25	327	20
	S.T. 1050°C	-177	63	947	74
FZ	S.T. 1100°C	-249	39	1045	100
	S.T. 1150°C	-160	36	978	55
	As-welded	-283	25	734	158
	S.T. 1050°C	-157	12	521	71
BM	S.T. 1100°C	-249	39	510	65
	S.T. 1150°C	-201	64	413	83

Tab. 2 : Experimental values of pitting potential and free corrosion potential (vs Ag/ AgCl 3M KCl) of the specimen analyzed

All the specimens exhibited passivity in 3.5 % NaCl at 80 °C. Concerning the as-welded specimens, it can be seen that the BM shows a higher pitting resistance than the FZ. However, after heat treatment, substantial changes in the average pitting potential of FZ have been detected. In particular, it was found that pitting potential value of the as-welded specimens (327 mV) is much lower than those of the annealed

ones (947, 1045, 978 mV). Thus, a high increase in the pitting potential can be easily noted in FZ after annealing treatment.

However, the data reported in table 2 show that the average free corrosion potentials values of all the specimens are not affected by significant changes (all the values lie in the range 160-280 mV vs Ag/AgCl).

The diagrams of Fig. 9 show all the pitting potentials data obtained by potentiodynamic tests as a function of specimen conditions, both for the base and the weld metal.
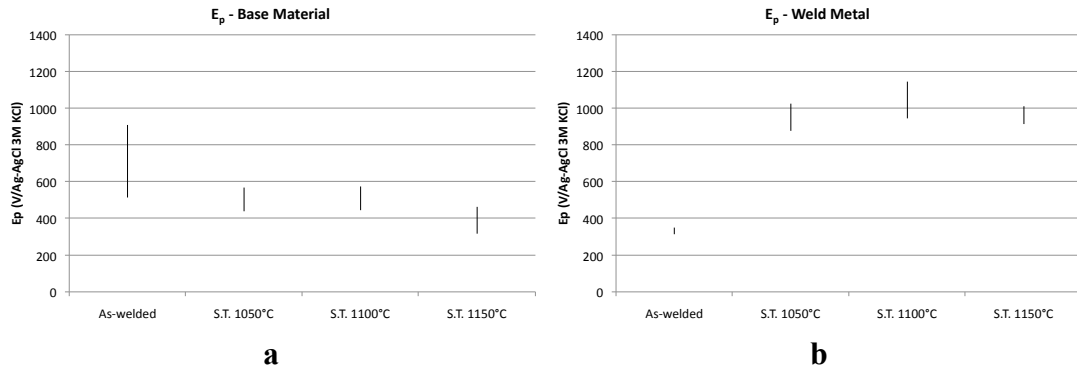

a   **b**

Fig. 9 : Pitting potential values obtained in 3.5% NaCl at 80°C for base (a) and weld (b) metal (S.T. = solution treated)

The data reported in figure 9a, show that the as-welded specimen has the highest pitting potential. In fact, the base material in the as-welded conditions was previously solubilized at 1070°C, which is the optimum annealing temperature as above defined (see fig. 4). Concerning the annealing temperatures of 1050°C and 1100°C, the BM shows similar $PREN_{20}$ and E_p values. At the annealing temperature of 1150°C, the E_p is affected by a slight decrease like the corresponding $PREN_{20}$ value (fig. 4). If the FZ is considered (Fig. 7b), after solution treatment, the pitting potential increases for all the annealing temperatures; in particular the highest value is obtained at a temperature of 1100°C. For annealing temperatures of 1050°C and 1150°C the pitting potential values show a slightly decrease compared to the previous one, like the calculated $PREN_{30}$ (fig. 3).

To summarize, the ranking of the pitting corrosion resistance of the specimens analysed is as follows:

weld metal: A.W. < S.T. 1050-1150°C < S.T. 1100°C

base material: S.T. 1150°C < S.T. 1050-1100°C < A.W. (S.T. 1070°C)

Like reported in literature [30], the following exponential relationship between the calculated $PREN_{30}$ of weaker phase and experimental pitting potential was observed:

$$E_p = A \exp \cdot (B \cdot PREN_{30}) \tag{5}$$

where, for the welded metal, $A = 0.035$ (mV vs Ag/AgCl 3M KCl) and $B = 0.243$. Figure 10 shows the data regarding the weld metal and the interpolation curve (Eq. (5)):

E_{pitt} vs PREN$_{30}$ - Weld Metal
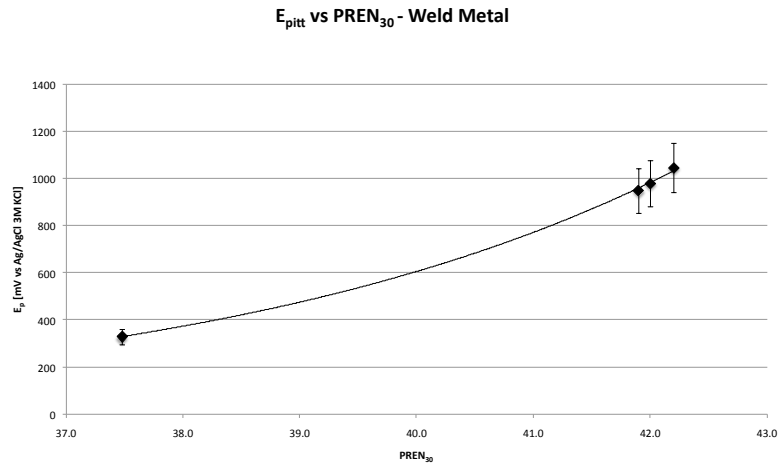
Fig. 10 : Pitting potential vs PREN$_{30}$ of the weaker phase (weld metal)

To summarize, Table 3 collects the main microstructural features that could affect pitting corrosion together with the measured pitting corrosion behavior of the welded joints analyzed in this study.

Sample	Zone	δ/γ ratio	Microstructure		Experimental pitting corrosion behavior	
			Precipitates detected (zone)	Calculated PREN$_{30}$ (weaker phase)	Average E_P [mV vs Ag/AgCl 3M KCl]	Average corrosion rate [g/m^2 day]
As-welded	FZ	1.07	-	37.5 (Ferrite)	327	195.397
	BM	0.89	Cr$_2$N (HAZ)	42.7 (Ferrite)	734	
S.T. 1050°C	FZ	0.53	-	41.9 (Austenite)	947	3.279
	BM	0.80	-	43.1 (Ferrite)	521	
S.T. 1100°C	FZ	0.65	-	42.2 (Austenite)	1045	3.965
	BM	1.03	-	42.1 (Ferrite)	510	
S.T. 1150°C	FZ	0.99	-	42.0 (Ferrite)	978	5.742
	BM	1.09	-	41.9 (Ferrite)	413	

Tab. 3 : Summary of the main microstructural features and experimental pitting corrosion behavior of the welded joints analyzed in the study (FZ = fusion zone, BM = base material)

3.3 Pit morphology

Fig. 11 shows the FZ SEM micrographs of the as-welded specimen after potentiodynamic tests.
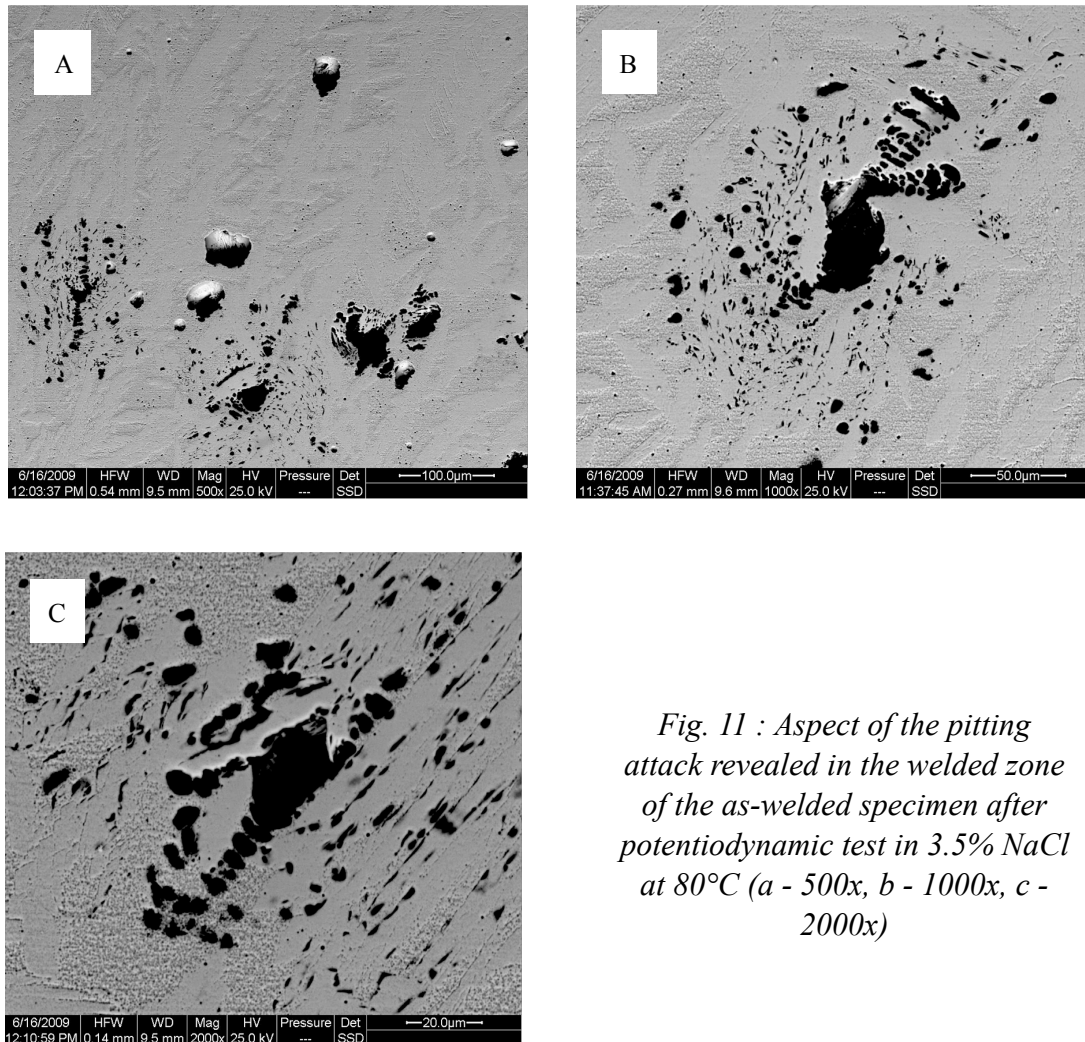
Fig. 11 : Aspect of the pitting attack revealed in the welded zone of the as-welded specimen after potentiodynamic test in 3.5% NaCl at 80°C (a - 500x, b - 1000x, c - 2000x)

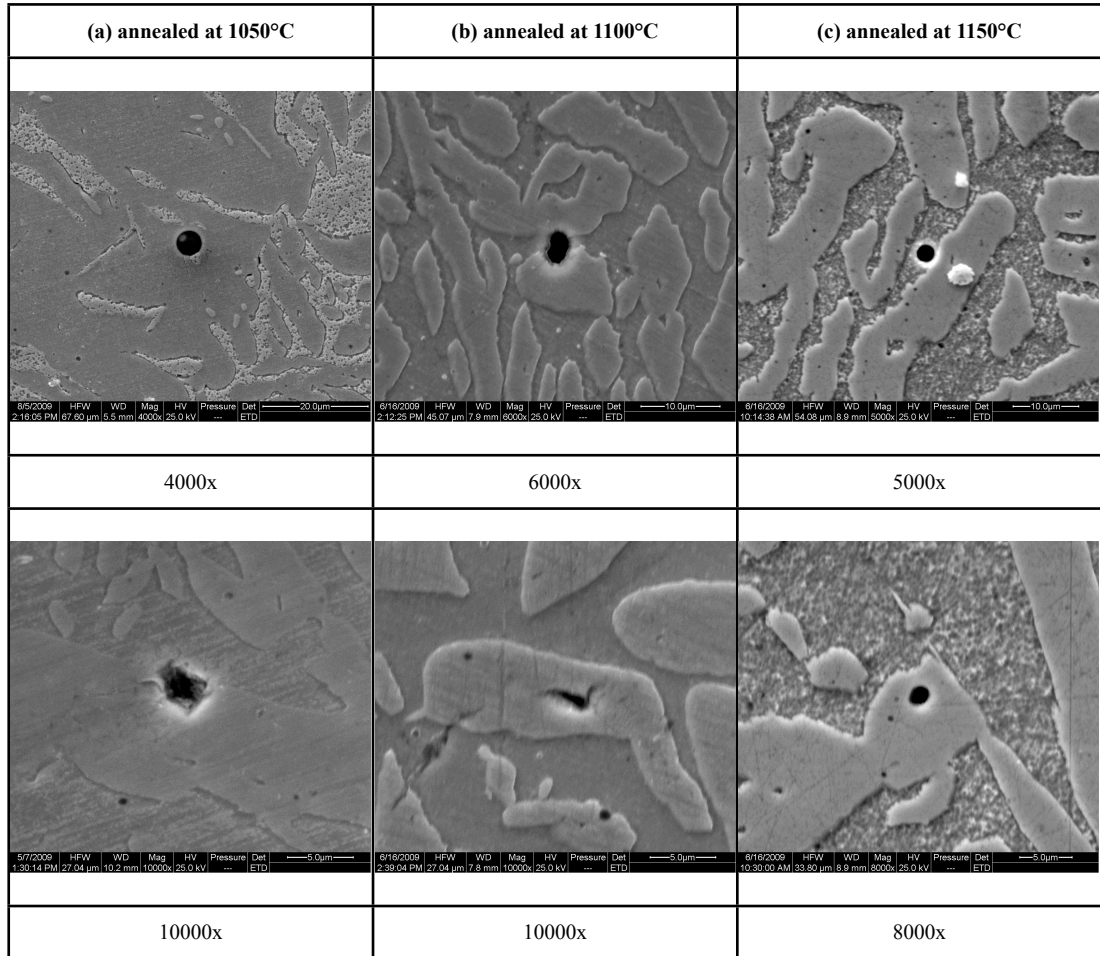Intensive selective pitting corrosion occurred in the ferrite phase of as-welded FZ. The corrosion process started at the ferrite/austenite grain boundaries or inside the ferrite grains. Pitting onset inside the ferrite grains could be attributed to the lower $PREN_{30}$ value of ferrite compared to that of austenite (37.5 against 47.6 of austenite). This is due to the low nitrogen content of the as-welded ferrite. It must be noted that the $PREN_{30}$ calculated by using the weld metal composition (42.5) is quite higher than the correct $PREN_{30}$ value which corresponds to the one of the weaker phase (Table 1). The pitting onset at the ferrite/austenite grain boundaries (Fig. 11c), may be due to the composition gradient inside the ferrite grains. In fact, during the solidification process, the δ-stabilizing elements concentrate more at the core than at the boundary of ferrite grains. As a consequence, the PREN values at the grain core are higher than those close to the grain boundaries. Thus, the grain boundary regions of the ferrite are more susceptible to localized pitting corrosion [31]. Moreover, the grain boundary is a transitional region characterized by a non-uniform and weaker passive film, which constitutes a preferential site for the pitting onset.

The BSE-SEM images collected in figure 12 show the pits detected in the welded metal of the annealed specimens after potentiodynamic tests.

(a) annealed at 1050°C	(b) annealed at 1100°C	(c) annealed at 1150°C
4000x	6000x	5000x
10000x	10000x	8000x

Fig. 12 : BSE-SEM images of the pits revealed in the welded zone of the annealed specimens after potentiodynamic tests in 3.5% NaCl at 80°C

It must be firstly noted that in the annealed specimens the pitting attack is less intense than in the as-welded sample. Secondly, by analyzing the images in figure 12, the phase affected by the pitting attack results to be:

- austenite in the sample annealed at 1050°C (12a) (austenite has a lower calculated $PREN_{30}$ value than ferrite (41.9 against 43.8));
- mainly austenite but also ferrite in the sample annealed at 1100°C (12b) (in fact the calculated $PREN_{30}$ value for both phases are slightly similar (42.2 and 43.0 for austenite and ferrite, respectively));
- both austenite and ferrite in the sample annealed at 1150°C (12c); (the calculated $PREN_{30}$ values in this case are 42.0 and 42.7 for ferrite and austenite, respectively).

The SEM micrographs collected in Fig. 13 show the aspect of the etched surface of BM after potentiodynamic test and at different magnifications.

	as-welded	annealed at 1050°C	annealed at 1100°C	annealed at 1150°C
	2000x	4000x	2000x	5000x
	8000x	9000x	3000x	6000x
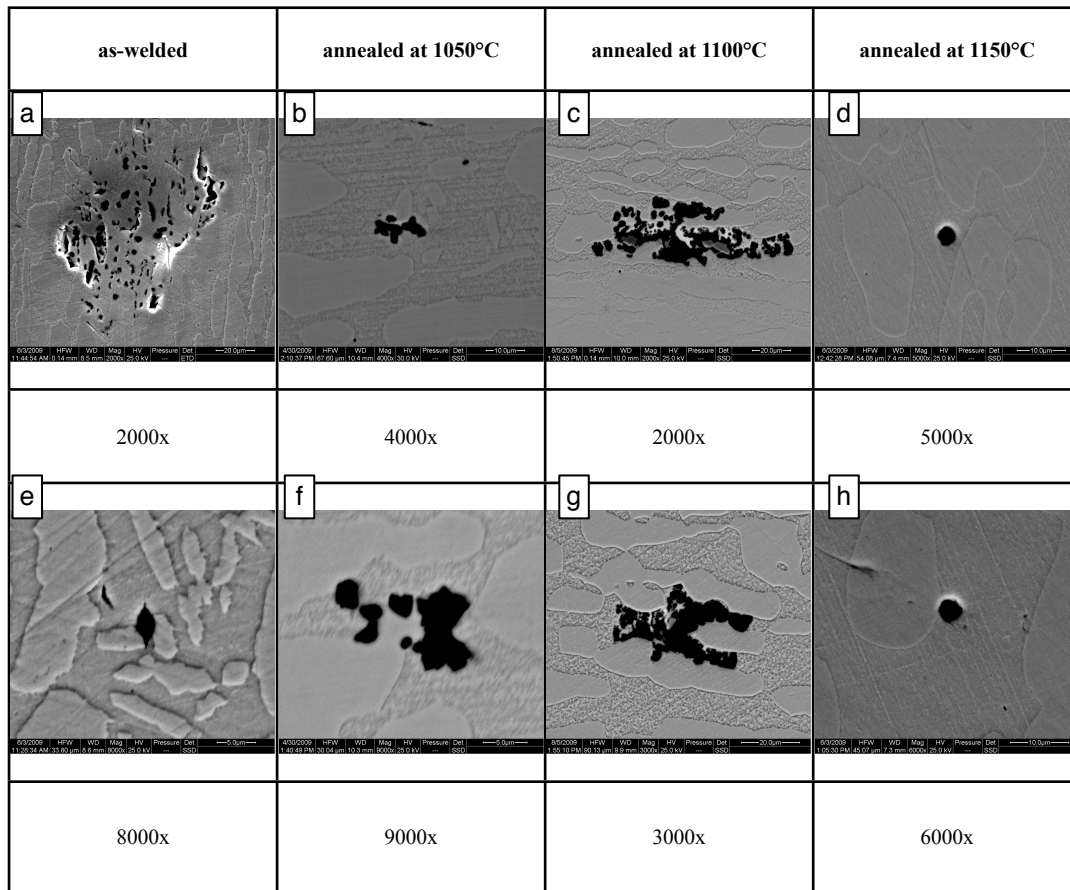
Fig. 13: Pit morphologies found after potentiodynamic test in 3.5% NaCl at 80°C in the base material

Pits were observed preferentially in the ferrite phase of the base material for all the samples conditions. As a matter of fact, the $PREN_{30}$ of ferrite is always lower than that of austenite. The pitting attack starts both on the ferrite/austenite grain boundaries (Figs. 13a, 13b, 13f) and inside the ferrite grains (Figs. 13d, 13h). However, it hast to be noted that in the as-welded and in the solution treated at 1050°C specimens, sometimes pits were observed also in the austenite phase (Figs. 13a, 13b, 13f); this phenomenon can be captured only if $PREN_{20}$ is taken into account. In fact its value is lower (or equal, in the case of the as-welded specimen) in austenite phase than in ferrite.

3.4 Overall discussion on pitting corrosion behavior

As-welded specimen shows the maximum corrosion rate in terms of weight losses per day after ASTM G48 test; the pitting attack is heavily concentrated in the welded zone, which has a lower pitting potential and $PREN_{30}$ compared to the base material. The ferrite and austenite phase of the welded zone have approximately the same chromium and molybdenum content, but austenite is enriched in nitrogen, which raises significantly its PREN. Due to the very low PREN value of ferrite, intense pitting attack takes place in this phase pertaining to the as-welded FZ.

After post-welding solution annealing, a high decrease of the corrosion rates occurred. This phenomenon is mainly due to the concurrent increase of both the pitting potential (from 327 mV to values greater than 950 mV vs Ag/AgCl 3M KCl) and the calculated $PREN_{30}$ of the FZ (from a value of 37.5 to values up to 42). The ferrite phase in FZ, by enriching in chromium and molybdenum, increases its PREN value, whereas the content of these elements in austenite decreases. Moreover, the precipitates detected in the heat-affected zone of the as-welded specimen (described in the previous work and which could be deleterious for pitting corrosion resistance of the joint) tend to dissolve after all the annealing treatment.

Concerning the annealed samples, the best pitting corrosion resistance, in terms of weight losses per day, was reached at annealing temperatures of 1050°C and 1100°C. This can be justified by combining the results obtained from potentiodynamic tests. The highest pitting potential in the weld metal was obtained with the specimen treated at 1100°C, while, regarding the base material, the most favorable pitting behavior was found with the specimens in the as-welded conditions (i.e.: previously solubilized at 1070°C).

However, among the annealed samples, the corrosion rate of the specimen heat treated at 1150°C shows a slightly decrease; as a matter of fact, the E_p and PREN decrease both in the base material and in the FZ. In addition, concerning the weld metal, an exponential relationship between the calculated values of $PREN_{30}$ and experimental values of E_p was found.

A good agreement between the predicted weaker phase (by using PREN values) and experimental observations was found in all the analyzed specimens.

In this study, the calculated optimum annealing temperatures corresponds to 1070°C and 1125 °C for BM and FZ, respectively. As a consequence, an intermediate annealing temperature of 1100°C results to be optimal for the annealing heat treatment of UNS S32750 welded joints.

CONCLUSIONS

In the present work, the pitting corrosion behavior of UNS S32750 submerged-arc welded joints was analyzed. The obtained results are strictly correlated to the microstructure and partitioning of elements treated in the previous work (Part I) for the same sample. Thus, a brief summary of the conclusions described in the companion paper is supplied.

About the microstructure of as-welded joints, it was found an excess of ferrite in FZ and some precipitates were observed in HAZ. While, in the solution treated welded joints, the austenite proportion increased, and the precipitates previously detected in the HAZ dissolved.

In the FZ of as-welded specimens, substitutional elements (such as chromium, molybdenum and nickel) are homogeneously distributed in both phases, while nitrogen is supposed (according to results found in literature) to be heavily concentrated in austenite. Therefore, $PREN_{30}$ of ferrite results lower (37.5) if compared with that of austenite (47.6).

After post welding heat treatment, ferrite enriches in chromium and molybdenum and thus it increases its PREN; on the other hand, PREN of austenite decreases because it becomes depleted in these elements. During the heat treatment the PREN value of the two phases follows the trend found by Bernhardsonn [22]. In particular, the FZ $PREN_{30}$ reaches the maximum value around 1125°C, while the BM $PREN_{20}$ reaches the maximum value at a temperature of 1070°C.

Finally, the following conclusions about the pitting corrosion resistance of the analyzed welded joints can be collected:

1. In the as-welded conditions, the PREN of the welded zone, which corresponds to the PREN of ferrite phase, is lower than the PREN of the base material.
2. Deep pitting corrosion attack takes place in the ferrite pertaining to the FZ of as-welded joints.
3. After post welding heat treatment the different elemental distribution between the two phases increases the pitting corrosion resistance of the FZ.
4. PREN calculated from bulk composition is unlikely to be a good guide to assess pitting resistance of super duplex stainless steels; a better understanding can be achieved through calculating PREN values for the two phases.
5. The most important factor to determine the corrosion behavior of UNS S32750 welded joints is the PREN of the weaker phase.
6. The best pitting resistance was found in samples treated at 1100 °C for the FZ and at 1070 °C for the BM (as-received conditions) which are temperature values very close to those theoretically calculated.
7. In order to obtain the best pitting resistance of the whole joint, an intermediate annealing temperature of 1100°C is proposed for post-weld treatment.
8. Additional microstructural factors, firstly the presence of precipitates, may need to be considered to fully understand the relative pitting resistances of UNS S32750 welded joints.

Acknowledgements

REFERENCES

[1]   J. O. Nilsson (1992) "Overview Super Duplex Stainless Steels", Materials Science and Technology 8:685-700
[2]   S. Atamert, J.E. King (1991) "Elemental partitioning and microstructural development in duplex stainless steel weld metal" Acta Metall. Mater. vol. 39, N°3:273-285
[3]   F. Bonollo, A. Tiziani, P. Ferro (In press) "Advances in Duplex Stainless Steels" - Chapter 4, ISTE LTD. London.

[4] S.S.M. Tavares, J.M. Pardal, L.D. Lima, I.N. Bastos, A.M. Nascimento, J.A. de Souza (2007) "Characterization of microstructure, chemical composition, corrosion resistance and toughness of a multipass weld joint of superduplex stainless   steel UNS S32750", Materials Characterization 58:610-616

[5] T. Ogawa, T. Koseki (1989) Welding Journal 68:181-191

[6] J. Liao (2001)"Nitride Precipitation in Weld HAZs of a Duplex Stainless Steel", ISIJ International, Vol. 41 (2001), No. 5:460–467

[7] H.-Y. Liou, R.-I. Hsieh, W.-T. Tsai (2002) "Microstructure and pitting corrosion in simulated heat-affected zones of duplex stainless steels", Materials Chemistry and Physics 74:33-42

[8] J.O. Nilsson, L. Karlsson, J.O. Anderson (1995) "Secondary austenite formation and its relation to pitting corrosion in duplex stainless steel weld metal", Materials Science and Technology 11:276-283

[9] C.T. Kwok, S.L. Fong, F.T. Cheng, H.C. Man (2006) "Pitting and galvanic corrosion behavior of laser-welded stainless steels", Journal of Materials Processing Technology 176:168-178

[10] J.D. Kordatos, G. Fourlaris and G. Papadimitriou (2001) "The effect of cooling rate on the mechanical and corrosion properties of SAF 2205 (UNS 31803) duplex stainless steel welds", Scripta mater. 44:401– 408

[11] A. Bautista, G. Blanco, F. Velasco, M.A. Martinez (2007) "Corrosion performance of welded stainless steels reinforcements in simulated pore solutions" Construction and Building Materials 21:1267–1276

[12] C.M. Garzon, C. A. Serna, S. D. Brandi, A. J. Ramirez (2007) "The relationship between atomic partitioning and corrosion resistance in the weld-heat affected zone microstructures of UNS S32304 duplex stainless steel", J Mater Sci, 42:9021–9029 DOI 10.1007/s10853-007-1881-6

[13] Z. Sun, M. Kuo, I. Annergren, D. Pan (2003) "Effect of dual torch technique on duplex stainless steel welds", Materials Science and Engineering A356:274-282

[14] V. Muthupandi, P. Bala Srinivasan, S.K. Seshadri, S. Sundaresan (2003) "Effect of weld metal chemistry and heat input on the structure and properties of duplex stainless steel welds", Materials Science and Engineering A358:9-16

[15] P. Ferro, A. Tiziani, F. Bonollo (2008) "Influence of induction and furnace post welding heat treatment on corrosion properties of SAF 2205 (UNS 31803)", Welding Journal. 87:298–306

[16] P. Pohjanne, L. Carpén, T. Hakkarainen, P. Kinnunen (2008) "A method to predict pitting corrosion of stainless steels in evaporative conditions", Journal of Constructional Steel Research 64:1325-1331

[17] G. Herbsleb (1982) Werkst. Korros. 33:334

[18] K. Lorenz, G. Medawar (1969) Thyssen Forschung 1:97

[19] R. Dölling, V.Neubert and P. Knoll (1991) "Corrosion behavior of super duplex steel cast alloys with a PREN>41", Proceedings Duplex Stainless Steels 91, Beaune, France:1341-1351

[20] H. Vannevik, J.O. Nilsson, J. Frodigh, P. Kangas (1996) "Effect of Elemental Partitioning on Pitting Resistance of High Nitrogen Duplex Stainless Steels",ISIJ Int.   36 (7):807-812

[21] L. Weber, P.J. Uggowitzer (1998) "Partitioning of chromium and molybdenum in super duplex stainless steels with respect to nitrogen and nickel content", Mater. Sci. Engineering A 242:222-229

[22] S. Bernhardsonn (1991)"The corrosion resistance of duplex stainless steels", Proceedings of the Duplex Stainless Steels Conference, Beaune, France:185

[23] C.D.S. Tuck, J.M. Sykes, L.F. Garfias-Mesias (1994) "The influence of specific alloying elements in the control of pitting mechanism of 25% duplex steels", 4th Int. Conf. Duplex Stainless Steels, Glasgow, paper 15

[24] T. Hua, J. Yiming, Deng Bo, S. Tao, X. J. Liang, L. Jin (2009) "Effect of annealing temperature on the pitting corrosion resistance of super duplex stainless steel UNS S32750", Materials Characterization doi: 10.1016/ j.matchar. 2009.04.009

[25] A. Van Bennekom, Stainless Steel World, 1998, 54

[26] L.F. Garfias-Mesias, J.M. Sykes, C.D.S. Tuck (1996) Corros. Sci. 38:1319

[27] H. Vannevik, J.O. Nilsson, J. Frodigh, P. Kangas (1996) ISIJ Int. 36:807

[28] ANNUAL BOOK OF ASTM STANDARDS, ASTM G48-03, 2003, ASTM

[29] B. Deng, Y. Jiang, J. Gong, C. Zhong, J. Gao, J. Li (2008) "Critical p i t t i n g and repassivation temperatures for duplex stainless steel in chloride solutions" Electrochimica Acta 53:5220–5225

[30] R. Merello, F.J. Botana, J. Botella, M.V. Matres, M. Marcos (2003) "Influence of chemical composition on the pitting corrosion resistance of non-standard low-Ni high-Mn–N duplex stainless steels", Corrosion Science 45:909–921

[31] S.R.F. Batista, S.E. Kuri (2004) "Aspects of selective and pitting corrosion in cast duplex stainless steels", Anti-Corrosion Methods and Materials 51(3): 205-208.

ARTICLE V

MODELING SIGMA PHASE PRECIPITATION IN UNS S31803 AND UNS S32750 DUPLEX STAINLESS STEELS: EXPERIMENTAL ANALYSIS AND NUMERICAL MODELS

expanded version of the paper:

SET UP AND IMPLEMENTATION OF A NUMERICAL MODEL FOR THE SIMULATION OF HEAT TREATMENT OF DUPLEX STAINLESS STEELS

P. Ferro*, R. Cervo*, F. Bonollo*

R. Bertelli**

*   *DTG University of Padova, Str. S. Nicola, 3 I-36100 Vicenza – Italy*

**   *Acciaierie Valbruna, Vicenza, Italy*

ABSTRACT

Duplex Stainless Steels (DSS) and Super Duplex Stainless Steels (SDSS) represent an important and expanding class of stainless steels with an attractive combination of mechanical properties and corrosion resistance. However, a variety of undesired phases (sigma, chi, chromium nitrides etc.) could precipitate in these alloys at high temperatures.
This paper is aimed at setting up a numerical model describing the precipitation of sigma phase in duplex (UNS S31803) and super duplex (UNS S32750) stainless steels due to isothermal and anisothermal heat treatments, starting from experimental tests carried out on laboratory specimens. The model, based on the Avrami's equation, is also implemented into a commercial simulation code, in order to calculate and visualize the distribution of phases resulting from heat treatments, with reference to industrially significant products.

KEYWORDS

1. INTRODUCTION

Duplex Stainless Steels (DSS) and Super Duplex Stainless Steels (SDSS) are two-phase alloys consisting of approximately equal proportions of ferrite (δ) and austenite (γ) phases. In particular, SDSS are highly alloyed DSS, having increased mechanical and corrosion properties. The balanced microstructure offers a combination of high toughness, good weldability, satisfactory corrosion resistance, and high strength [1,2].

The knowledge of microstructural evolution of DSS and SDSS, as the result of their thermal history, is a fundamental issue to achieve the expected mechanical behavior and corrosion resistance. The time-temperature history, deriving for instance from industrial heat treatments or welding processes, may lead to the precipitation of various compounds, such as chromium nitrides, and some other intermetallic phases, like σ phase. These microstructural features are usually associated to detrimental effects on the mechanical behaviour and corrosion resistance of the steel.

In fact, σ phase precipitation dramatically decreases the toughness of DSS and SDSS [3-11]. Moreover, it can deteriorate the corrosion properties, since Mo and Cr accumulate in this phase [10-13]. Good toughness properties are achieved by applying proper solution temperatures and cooling rates [14-16].

In particular, σ phase is a Cr- and Mo-rich intermetallic phase, which can form after relatively long holding times at temperatures ranging from 650 to 1000°C, or after cooling from high temperatures, like in the heat-affected of welded components.

The precipitation kinetic of sigma phase depends on the chemical composition of the considered alloy; in particular, the content of some elements (which are added to increase the corrosion resistance of the steel) acts on the TTT curves like illustrated in fig. 1, and make the material more prone to the formation of undesired phases.
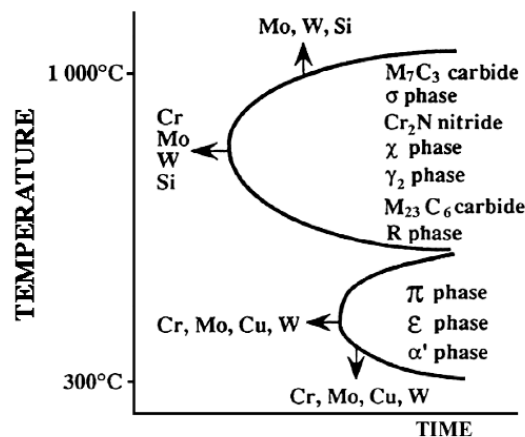

Fig. 1: Secondary phases in DSSs and the effects of alloying elements on the location and shape of the TTT curve for these phases [17]

Cr, Mo and Si are the main elements which increase the susceptibility to σ phase precipitation. The "sigma equivalent" (σ_{eq}) is a parameter proposed by Ramirez-

Londoño [18] to measure the tendency of a DSS or SDSS to σ precipitation:

$$\sigma_{eq} = X_{Cr(\delta)} + 4.5 X_{Mo(\delta)} + 1.5 X_{Si(\delta)} \tag{1}$$

where, $X_{Cr(\delta)}$, $X_{Mo(\delta)}$ and $X_{Si(\delta)}$ are the amounts of Cr, Mo and Si in the ferritic matrix. It has been found that the precipitation rate of σ phase is maximum for isothermal aging carried out at temperature around 865°C for DSS 2205 [19]. The higher the aging temperature, the larger the size of phase precipitates [20].

The precipitation of σ phase is a nucleation and growth process, whose kinetics is controlled by the thermodynamic driving forces and by diffusion. Sieurin et al. [19] model the σ precipitation in DSS 2205 during isothermal heat treatments and continuous cooling from high temperatures. Like other intermetallic compounds, σ phase nucleates predominantly on the ferrite-ferrite and ferrite-austenite grains, and grows into the adjacent ferrite grains [5,9,21-25].

In many studies about the kinetics of reactions occurring in steels, the fraction of transformed phase is measured as a function of time, while temperature is maintained constant. The kinetics of many reactions (including the formation of σ phase) can be described by the Avrami equation [26,27].

The aim of the present study is to set up a numerical model (based on the Avrami's equation) describing the microstructural evolution of duplex and superduplex stainless steels due to isothermal and anisothermal heat treatments, in particular to predict the final distribution of sigma phase at room temperature. This model starts from experimental tests carried out on laboratory specimens, but it can be extended to industrially significant products. SYSWELD 11.0® numerical code was used for the FE analyses of thermal fields induced during treatments and for predicting the final microstructure from the thermal history.

2. EXPERIMENTAL PROCEDURE

The materials analyzed in this study are a UNS S31803 duplex stainless steel and a UNS S32750 super duplex stainless steel, available in the solution and water quenched state.

The chemical compositions of the materials, obtained by chemical analysis with an optical spectrometer, are shown in Table 1.

	C	Mn	Si	P	S	Cr	Ni	Mo	Cu	N	Fe
UNS S31803	0.035	1.6	0.44	0.027	0.001	22.43	4.94	3.00	0.42	0.13	bal.
UNS S32750	0.018	0.79	0.22	0.025	0.002	24.8	6.92	3.85	0.32	0.27	bal.

Table 1: Chemical composition (wt%) of the materials analysed

Specimens of about 6000 mm³ volume, have been used for heat treatment experiments. In order to promote σ phase precipitation, they have been heat-treated in a laboratory furnace under different conditions. In order to control the temperature

during the treatments, a K-type (Chromel - Alumel) thermocouple, connected to a data acquisition and control system, was inserted into the core of the specimens.

Since previous studies have shown that the most critical temperature for σ precipitation in DSS UNS S31803 is about 850°C [4,19,28], temperatures for isothermal heat treatments have been chosen around this value. In particular, treatments at temperatures of 800, 850 and 900 °C, for time intervals of 1, 5, 10, 30, 180 and 420 min, have been performed.

For the UNS S32750 grade, the critical temperature range for σ precipitation is higher [2], because of the greater content of alloying elements (cf. fig. 1); therefore, heat treatments at 950°C has been also performed.

Some anisothermal heat treatments have been also carried out, in order to study the continuous cooling kinetics of σ precipitation. Specimens have been heated up to 1050°C and 1070°C for the UNS S31803 and UNS S32750 respectively, and then cooled at different cooling rates (-0.3, -0.11, -0.0811, -0.033°C/s for the duplex grade, and -0.5, -0.3, -0.12, -0.033°C/s for the superduplex one).

Preparation of metallographic samples for LOM consisted of silicon carbide paper grinding followed by diamond paste polishing (until surface finishing of 3 μm). Beraha's tint etch (80 ml H_2O, 20 ml HCl and 1g $K_2S_2O_5$) was used to reveal the microstructure. The volume fraction of ferrite and austenite was evaluated carefully using a software for image analysis (LEICA QWIN) interfaced with the LOM (Light Optical Microscopy). The average of at least 10 measurements of the phase fractions, each at different sites of the samples, was taken as the phase volume fraction. KOH electrolytic etching (50g KOH, 100 ml H_2O, 2V) was used to determine the amount of σ phase formed after isothermal and anisothermal heat treatments by means of LEICA QWIN Image Analysis code (the value taken as sigma phase volume fraction is an average of at least 16 measurements).

Energy Dispersive Spectroscopy (EDS) was used to measure the content of substitutional alloying elements in austenite and in ferrite. Each value is an average of 10 EDS measurements normalized with respect to the chemical composition reported in table 1, using the following equations:

$$c_{El}^{\gamma} = \frac{c_{El}^{tot}}{V^{\gamma}(1 - P_{El}^{\gamma}) + P_{El}^{\gamma}} \qquad (2)$$

$$c_{El}^{\alpha} = \frac{c_{El}^{tot} P_{El}^{\gamma}}{V^{\gamma}(1 - P_{El}^{\gamma}) + P_{El}^{\gamma}} \qquad (3)$$

where c^{tot}_{El} is the total content of the analyzed element (El) obtained from chemical analysis (cfr. table 1); V^{γ} is the volume fraction of austenite and P^{γ}_{El} is the partitioning ratio of the element calculated from experimental data and given by the ratio between the mass fraction of the element in ferrite and the mass fraction of the element in austenite.

3. EXPERIMENTAL RESULTS AND DISCUSSION

The as-received materials present a good ferrite-austenite balance, and no secondary precipitates have been detected. Fig. 2 shows some micrograph of the base materials, and table 2 collects the results of microstructural analysis.

	UNS S31803	*UNS S32750*
Ferrite (% vol.)	56 ± 1.6	46.1 ± 3.2
Austenite (% vol.)	44 ± 1.6	53.9 ± 3.2

Table 2: Austenite and ferrite amount in the as-received material

UNS S31803	UNS S32750
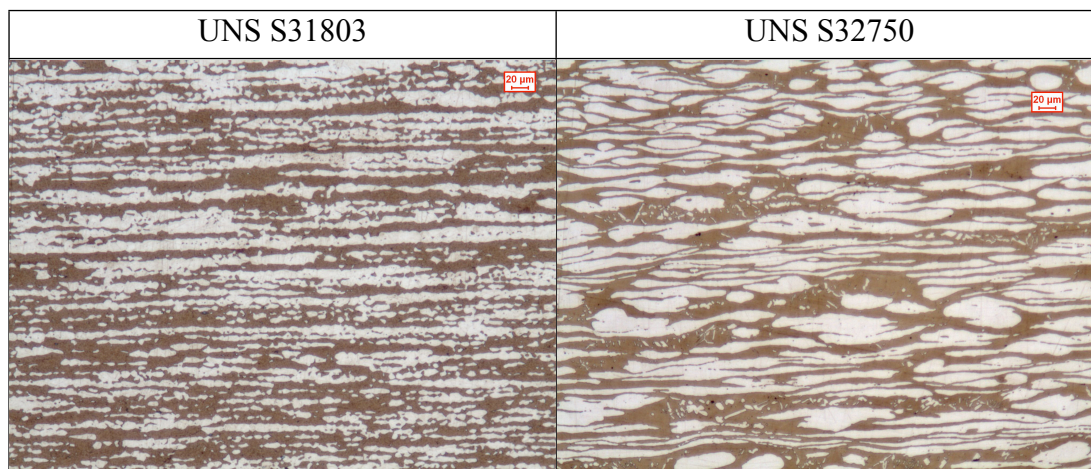
Fig. 2: Optical micrograph of the base materials (100x). Dark phase: ferrite; white phase: austenite.

Results of EDS analysis of ferrite and austenite of the respective base materials are shown in table 3:

		Wt %			
Material	**Phase**	**Cr**	**Mo**	**Ni**	**Si**
UNS S31803	*Ferrite*	23.77 ± 0.18	3.56 ± 0.18	3.90 ± 0.15	0.48 ± 0.09
	Austenite	20.72 ± 0.21	2.28 ± 0.29	6.26 ± 0.20	0.38 ± 0.14
UNS S32750	*Ferrite*	26.07 ± 0.22	4.83 ± 0.27	5.29 ± 0.16	0.25 ± 0.17
	Austenite	23.71 ± 0.10	3.02 ± 0.19	8.31 ± 0.20	0.20 ± 0.06

Table 3 : Cr, Mo, Ni and Si content in ferrite and austenite (wt %) obtained by EDS analysis

The parameter σ_{eq} has been calculated using eq. (1):

σ_{eq} (UNS S31803) = 40.51

σ_{eq} (UNS S32750) = 48.18

It can be seen that the σ_{eq} value for the super duplex grade (UNS S32750) is higher, so it results to be more prone to sigma phase formation, according to the theory proposed by Ramirez-Londoño.

Isothermal heat treatments

Fig. 3 shows some micrographs referred to isothermally heat treated specimens, for both the materials. The average amount of sigma phase detected with LOM analysis, and the related standard deviations are summarized in Table 3.

	UNS S31803	*UNS S32750*
800°C, 5 min		
850°C, 420 min		
900°C, 30 min		
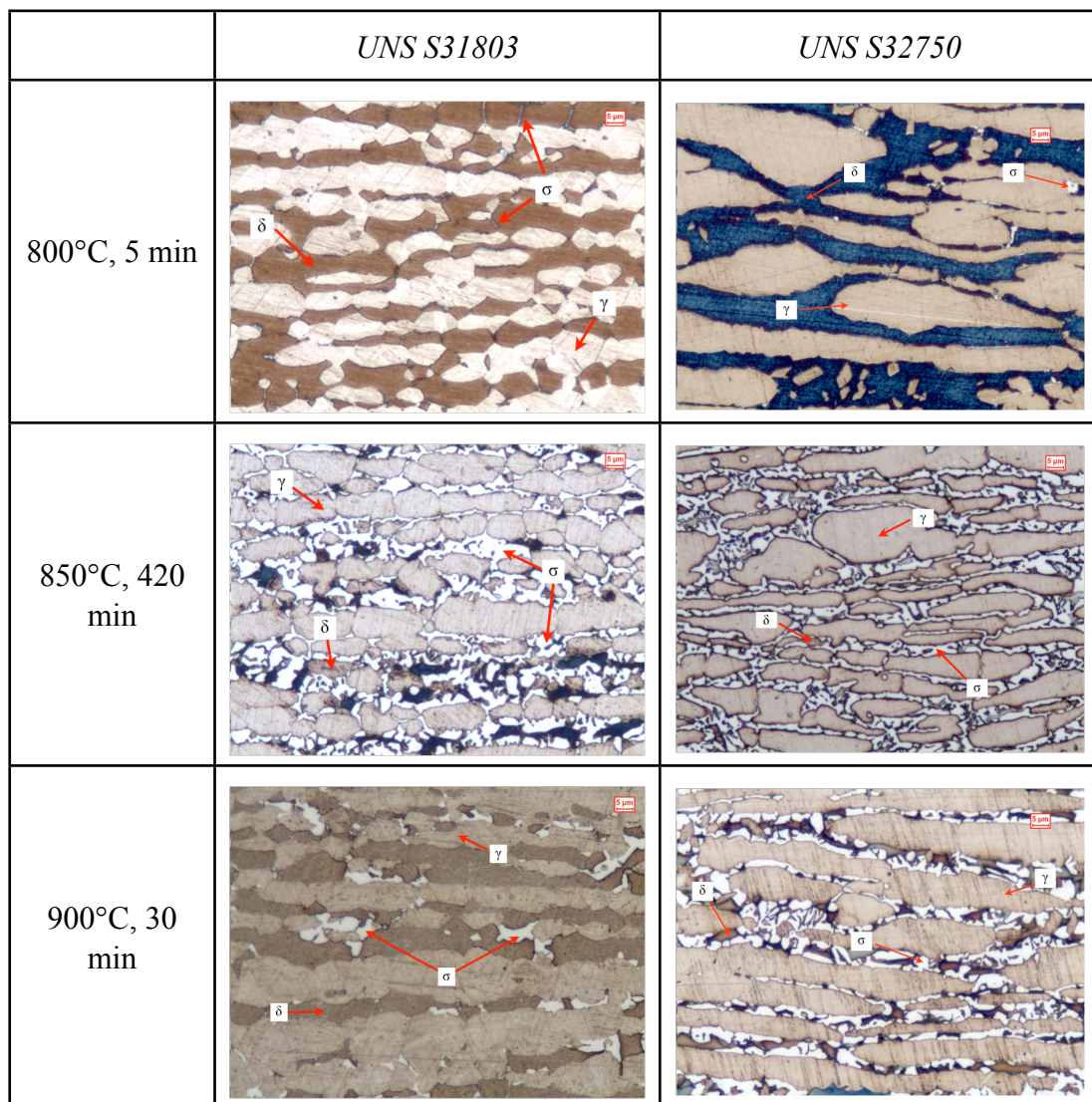
Fig. 3: Microstructure of the isothermally heat-treated specimens (500x), Beraha's etching.

	UNS S31803			UNS S32750			
	800°C	**850°C**	**900°C**	**800°C**	**850°C**	**900°C**	**950°C**
1 min		0.9 ± 0.3			0.04 ± 0.03	0.4 ± 0.1	
5 min	1.1 ± 0.3	2.1 ± 0.3	1.9 ± 0.6	0.2 ± 0.1	0.4 ± 0.3	7.0 ± 1.7	7.2 ± 2.6
10 min	1.9 ± 0.3	3.2 ± 0.5		8.1 ± 1.5	13.4 ± 1.7	19.4 ± 2.9	10.4 ± 3.7
30 min	5.5 ± 0.5	9.5 ± 1.9	6.1 ± 1.2	14.1 ± 1.7	33.9 ± 2.0	31.3 ± 1.7	24.7 ± 1.9
180 min	12.7 ± 1.4	22.9 ± 1.4	21.9 ± 1.8	36.3 ± 4.9	35.5 ± 2.9	38.5 ± 2.2	27.2 ± 2.2
420 min		23.8 ± 2.3			41.1 ± 1.9	40.1 ± 2.2	

Table 3: Volume fraction of sigma phase for isothermal treatments detected with LOM analysis

It can be seen that the precipitation kinetic of sigma phase, regarding isothermal heat treatments in the range 800-900°C, results to be faster for the UNS S32750. For this material, the precipitation rate is the highest at 900°C, and after 10 minutes the sigma phase volume fraction reaches values close to 20%. Regarding the DSS grade (UNS S31803) the sigma phase precipitation is slower in the range considered, and the most critical temperature results to be 850°C, at which only after 3 hours the volume fraction of sigma phase reaches values above 20%.

In addition to that, it can be found that the equilibrium volume fraction (which is taken as the volume fraction of sigma phase at 420 minutes) is close to 40% for the superduplex grade, and slightly below 25% for the duplex 2205.

Continuos cooling treatments

Some continuos cooling treatments has been carried out to compare the σ-phase amounts formed in the materials analyzed; these treatments are aimed to simulate coolings resulting from welding operations or after solubilization of large components.

The experimental σ-phase amounts obtained by different anisothermal heat treatments are collected in Table 4, while some significant microstructures are shown in Fig. 4.

UNS S31803		UNS S32750	
Mean cooling rate (°C/s)	**% sigma phase formed**	**Mean cooling rate (°C/s)**	**% sigma phase formed**
-0.3	0.8 ± 0.5	-0.5	0.2 ± 0.12
-0.11	5.9 ± 1.8	-0.3	1.6 ± 0.4
-0.0811	6.7 ± 1.4	-0.12	13.9 ± 2.1
-0.033	13.1 ± 1.5	-0.033	41.5 ± 4.6

Table 4: Volume fraction of sigma phase formed at room temperature after anisothermal heat treatments

	UNS S31803	UNS S32750
0.3°C/s		
0.033°C /s		
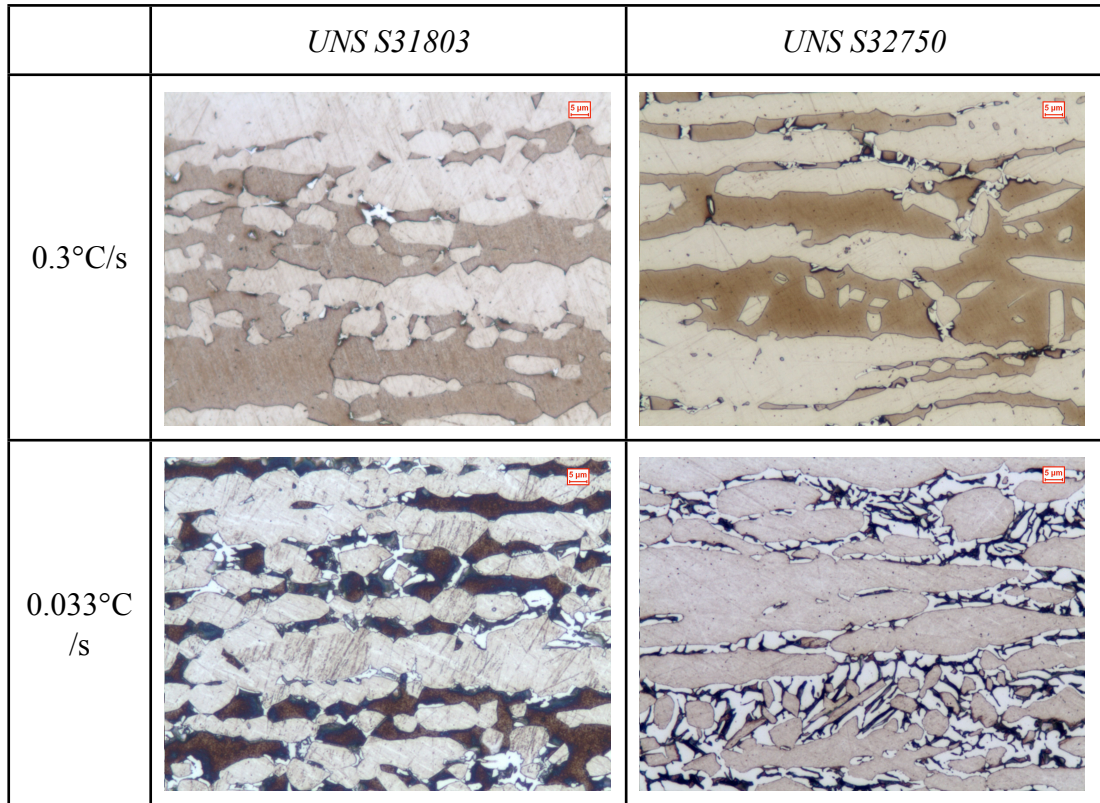
Fig. 4: Microstructure of the heat-treated materials (continuous cooling, 500x) Beraha's etching (dark phase: ferrite, white phase: austenite, light white phase: sigma phase).

The fact that the Super Duplex grade is more prone to sigma formation is more evident after anisothermal heat treatments: for cooling rates equal to 0.3°C/s and 0.11-0.12°C/s, the volume fractions of sigma phase detected in the UNS S32750 are double than the corresponding values of the UNS S31803. For the lowest cooling rate (0.033°C/s) the volume fraction detected in the superduplex grade is almost four times the volume fraction obtained in the duplex one.

It has been demonstrated [29] that the critical cooling rate for the formation of sigma phase in UNS S31803 is equal to 0.3°C/s; the corresponding volume fraction of sigma phase obtained in the present study is 0.8%. Concerning the UNS S32750, a cooling rate of 0.5°C/s is already critical for sigma phase precipitation, and the corresponding volume fraction results to be 0.2%. These values could be useful to set the welding parameters (in terms of current, voltage and travel speed) which determine the cooling rate, and then to avoid the formation of undesired phases in the heat affected zone of welded components made in DSS or SDSS.

4. NUMERICAL MODELS

The experimental data presented above have been used to set up and verify two numerical models predicting the σ-phase amount formed during isothermal and anisothermal heat treatments on both the materials analyzed.

Johnson-Mehl-Avrami equation (4) have been used to model the σ-phase precipitation during isothermal heat treatments:

$$P_i \ (T,t) = P_m \ (1 - \exp(-t/\tau)^n) \tag{4}$$

In equation (4), P_i is the current proportion of phase i according to time t and for a given temperature T; P_m is the phase proportion obtained after an infinite time, τ is the delay time associate with the reaction and n is an exponent illustrating the reaction rate.

When the temperature varies, it can be considered the P_i derivative with respect to time at constant temperature, with temperature-dependent transformation parameters P_m, τ and n. For σ-phase transformation this derivative has been also multiplied for a heating-cooling rate dependent function (F(dT/dt)):

$$\frac{dP_i}{dt} = n(T)\left(\frac{P_m(T) - P_i}{\tau(T)}\right)\left(Ln\left(\frac{P_m(T)}{P_m(T) - P_i}\right)\right)^{\frac{n(T)-1}{n(T)}} F(\dot{T})$$

$$\tag{5}$$

It should be noted that when n = 1, equation (3) is identical to the Avrami-Leblond equation [30].

The value of P_m has been set according to the experimental data, while τ and n were calculated, for each temperature, by interpolating the values of Table 3. Table 5 reports these parameters, while Fig. 4 shows the comparison among experimental, numerical and analytical results, regarding isothermal heat treatments for both the materials.

Temperature (°C)	UNS S31803			UNS S32750		
	P_m	τ	n	P_m	τ	n
800	25%	1.35E4	0.8	40%	2.50E+03	1.45
850	25%	3.9E3	0.97	40%	1.05E+03	1.8
900	25%	5.5E3	1.05	40%	1.20E+03	1.05
950	-	-	-	30%	1.00E+03	1.2

Table 5: Parameters of Eq. (4) (τ, n) calculated starting from experimental data
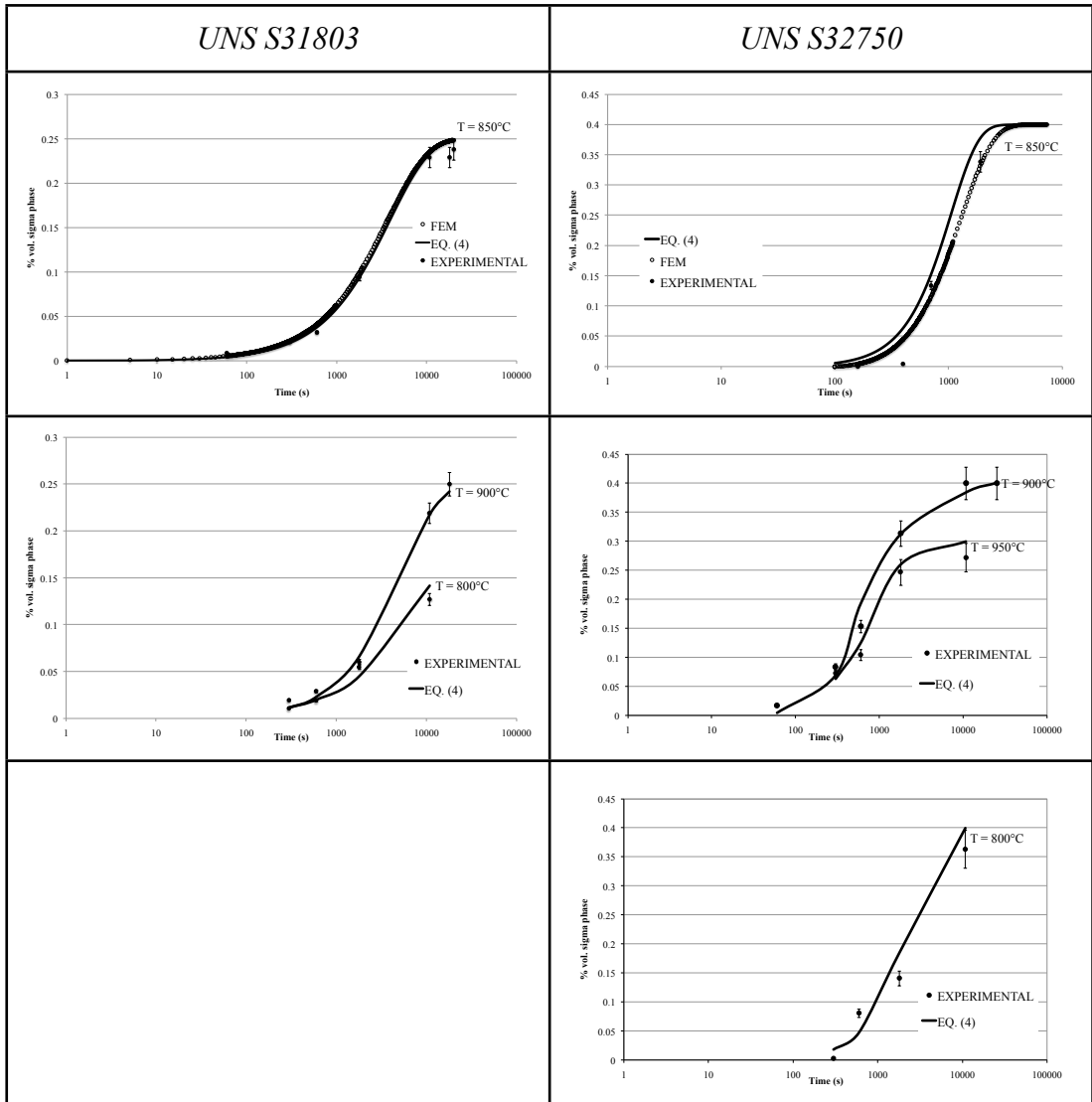
UNS S31803	UNS S32750

Fig. 4: Comparison among experimental, numerical and analytical results:
isothermal σ-phase precipitation

The F function of Eq. (5) has been calibrated using the corresponding measured σ-phase proportions and the corresponding values are reported in Table 6.

UNS S31803		UNS S32750	
dT/dt (°C/sec)	F(dT/dt)	dT/dt (°C/sec)	F(dT/dt)
-0.3	0.28	-0.5	0.2
-0.11	1.8	-0.3	0.3
-0.0811	0.85	-0.12	1
-0.033	-	-0.033	9

Table 6: Values of F function obtained by means of experimental measurements

By using the parameters of Tables 5 and 6, and Eq. (5), implemented in SYSWELD 11.0® numerical code, the TTT and CCT diagrams for σ-phase precipitation have been obtained (Fig. 5). A good correspondence with literature data can be observed [2,29].

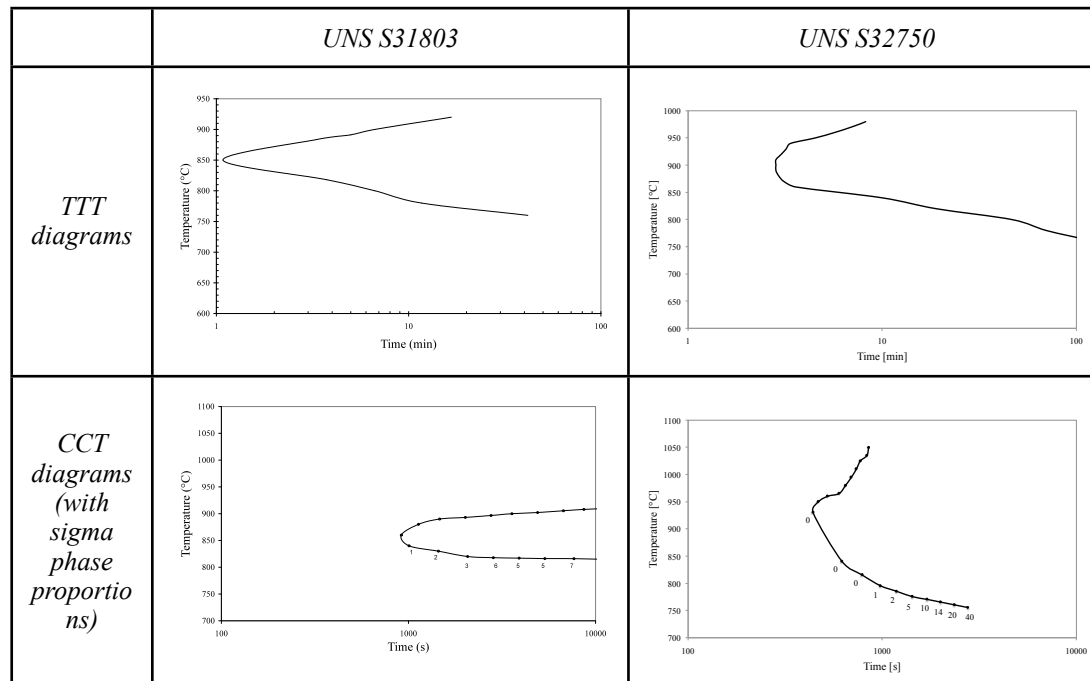|	UNS S31803	UNS S32750
TTT diagrams		
CCT diagrams (with sigma phase proportions)		

Fig. 5: TTT and CCT diagrams related to σ-phase precipitation of UNS S31803 and UNS S32750

It must be noted that the nose of TTT curve of UNS S32750 is at higher temperatures than the nose of UNS S31803, because of its higher content of alloying elements (cf. fig. 1). Nevertheless, unlike expected, the nose of duplex grade is placed at lower times than the nose of the superduplex one. This fact could be attributed to the error related to experimental measurements, which is higher for short holding times and low sigma phase fractions.

Concerning the CCT diagrams, the UNS S32750 curve is placed at short times if compared with the UNS S31803 curve; therefore, like expected, the superduplex grade results to be more prone to sigma phase precipitation in relation to anisothermal treatments.

5. CONCLUSIONS

In this work the σ-phase precipitation in UNS S31803 duplex stainless steel and UNS S32750 super duplex stainless steel has been studied; in addition, a method for the calibration of the precipitation kinetics of sigma phase in these steels has been described.

Starting from isothermal heat treatments in the temperature range 800-950°C, the parameters τ and n of the Avrami's equation have been obtained by interpolating the analytical and the experimental values at several holding times. Different

anisothermal heat treatments have been also performed and the temperature histories have been measured. Starting from the corresponding σ-phase proportions at room temperature the function F has been calibrated. Finally, these results have been implemented in SYSWELD 11.0® code, to calculate and plot the TTT and CCT diagrams related to σ-phase precipitation. The superduplex grade results to be more prone to sigma phase precipitation, both for isothermal and anisothermal heat treatments.

The obtained results are in good agreement with those found in literature, however, more experimental points are probably needed for a better description of the TTT and CCT curves.

Further developments of this work will be the use of the model elaborated for the prediction of the sigma phase precipitation in industrial heat treatments of DSS and SDSS.

REFERENCES

[1]   IRIS ALVAREZ-ARMAS, "Duplex Stainless Steels: Brief History and Some Recent Alloys", Recent Patents on Mechanical Engineering 2008, 1, 51-57

[2]   J.-O. NILSSON, "Super duplex stainless steels", Materials Science and Technology 8 (1992), 685-700

[3]   M.R. EL KOUSSY, I.S. EL MAHALLAWI, W. KHALIFA, M.M. AL DAWOOD, M. BUECKINS, Mater.Sci. Technol. 20 (2004), p.375.

[4]   Y.S. AHN, J.P. KANG, Mater.Sci. Technol. 16 (2000), p.382.

[5]   T.H. CHEN, K.L. WENG, J.R. YANG, Mater. Sci. Eng. A338 (2002), p.259.

[6]   L.SCOPPIO, M.BARTERI, Proceedings of the Applications of Stainless Steel, Stockholm, Sweden (1992), p. 260.

[7]   L.KARLSSON, L.BENGSSTON, U. ROLANDER, S.PAK, Proceedings of the Applications of Stainless Steel, Stockholm, Sweden (1992) p. 335.

[8]   C.-J. MADERUD, J.-O. ANDERSSON, M.LILIJAS, Proceedings of the Applications of Stainless Steel, Stockholm, Sweden (1992) p. 370.

[9]   T.H. CHEN, J.R. YANG, Mater. Sci. Eng. A311 (2001), p. 28.

[10]   L.KARLSSON, Proceedings of the Duplex Stainless Steel, Maastricht, The Netherlands (1997) p. 43.

[11]   L.KARLSSON, S.RIGADL, F.LAKE, Proceedings of the Duplex America 2000, Houston, USA (2000), p. 257.

[12]   J.-O. NILSSON, A. WILSON, B.JOSEFSSON, T.THORVALDSSON, Proceedings of the Applications of Stainless Steel, Stockholm, Sweden (1992), p. 280.

[13]   S.HERTZMAN, B. LEHTINEN, E.SYMNIOTIS-BARRDAHL, Proceedings of the Applications of Stainless Steel, Stockholm, Sweden (1992), p. 345.

[14]   H.SIEURIN, R. SANDSTRÖM, Eng. Fract. Mech. 73 (2006), p. 377.

[15]   A.DHOOGE, E. DELEU, Weld. World 39 (1997), p. 47.

[16]   C.S. WIESNER, Proceedings of the Duplex Stainless Steel 1997, Maastricht, The Netherlands (1997), p.979.

[17] YOON-JUN KIM, L. SCOTT CHUMBLEY, and BRIAN GLEESON, "Determination of Isothermal Transformation Diagrams for Sigma-Phase Formation in Cast Duplex Stainless Steels CD3MN and CD3MWCuN" METALLURGICAL AND MATERIALS TRANSACTIONS A, VOLUME 35A, NOVEMBER 2004, 3377

[18] RAMIREZ LONDONO, A.J., Estudo da precipitação de nitreto de cromo e fase sigma por simulação térmica da zona afetada pelo calor na soldagem multipasse de aços inoxidáveis duplex, M.Sc. Thesis 1997, University of São Paulo (USP).

[19] H. SIEURIN, R. SANDSTRÖM, Mater. Sci. Eng. A 444 (2007), p.271.

[20] CHI-SHANG HUANG, CHIA-CHANG SHIH, Mater. Sci. Eng. 402 (2005), p. 66.

[21] A. REDJAIMIA, G. METAUER, M.GANTOIS, Proceedings of the Duplex Stainless Steel 1991, Beaune, France (1991), p. 119.

[22] L.DUPREZ, B.C. DE COOMAN, N.AKDUT, Steel Res. 72 (2001), p. 311.

[23] L.H. CHIU, W.C. HSIEH, C.H. WU, Mater. Sci. Eng. A354 (2003), p. 82.

[24] T.KURODA, K.NAKADE, K.IKEUCHI, Weld. World 44 (2000), p. 17.

[25] F. BONOLLO, A. TIZIANI, P. FERRO, La Metallurgia Italiana 2 (2005), p. 27.

[26] M.AVRAMI, Journal of Chemical Physic 7 (1939), p. 1103.

[27] M.AVRAMI, Journal of Chemical Physic 8 (1939), p. 212.

[28] L.DUPREZ, B.C. DE COOMAN, N.AKDUT, Proceedings of the Duplex Stainless Steel 2000, Venice, Italy (2000), p.355.

[29] G. MELOTTI, R. BERTELLI, M. ZANESCO, I. CALLIARI, E. RAMOUS, La Metallurgia Italiana 4, 2005, p.39.

[30] P.FERRO, H. PORZNER, A. TIZIANI, F. BONOLLO, Modelling Simul. Mater. Sci. Eng. 14 (2006), p. 117.

OTHER ACTIVITIES

In this final part of the thesis, other activities connected to the researches previously presented and carried out during the PhD work are presented.

1. Numerical modeling of welding: Ahrengot model

The study and modeling of temperature distribution in relation to welding processes, could be useful to predict the formation of secondary phases in the heat-affected zone of Duplex Stainless Steels welded joints.

A first thermal model has been developed by Grong [1], and the heat flow around an arc weld can be described by the solution proposed by him, after a model by Rosenthal.

An expression of the cooling time from 800 to 500°C ($\Delta t_{8/5}$) has been derived by Hannerz (2-D) and Ahrengot (3-D), based on the work by Rosenthal and Rykalins. The cooling times given by these expressions are independent of the distance from the weld centre line, which was experimentally verified. 3-D heat distribution is applied at small values of $\Delta t_{8/5}$ and at large dimensions. The 3-D solution by Ahrengot has been applied in the present study with thick specimens and relatively fast cooling times:

$$\Delta t_{12/8} = \frac{Q_n}{2\pi\lambda}\left[\frac{1}{773-T_0} - \frac{1}{1073-T_0}\right]$$

(1)

where Q_n is the net heat input (eq. 2), λ is the thermal conductivity and T_0 is the interpass temperature of welding in Kelvin.

$$Q_n[kJ/mm] = \eta\frac{I[A]*U[V]}{v[mm/s]*1000}$$

(2)

where η is the efficiency (dependent on welding process), I is the current, V the voltage and v the travel speed.

The value of $\Delta t_{8/5}$ can be used to obtain a time–temperature relation:

$$T = T_0 + \frac{k_1}{\tau}\exp\left(-\frac{k_2}{(T_{max}-T_0)\tau}\right)$$

(3)

where:

$$k_1 = \frac{(1073-T_0)(773-T_0)}{300}$$

(4)

$$k_2 = \frac{(1073 - T_0)(773 - T_0)}{e \times 300} \qquad (5)$$

$$\tau = \frac{t}{\Delta t_{8/5}} \qquad (6)$$

where e is equal to 2.718.

The cooling time between 800 and 500°C can be then correlated to the cooling time between 1200 and 800°C ($\Delta t_{12/8}$), which is more relevant for Duplex Stainless Steels, since this interval is where the major austenite reformation and intermetallic phase precipitation occur (cf. §2.3 of section "State of the art").

$$\Delta t_{12/8} = \Delta t_{8/5} \frac{\dfrac{1}{1073 - T_0} - \dfrac{1}{1473 - T_0}}{\dfrac{1}{773 - T_0} - \dfrac{1}{1073 - T_0}} \qquad (7)$$

Therefore, the presented model has been implemented in Microsoft Excel® and MatLab®, and it has been applied to the submerged-arc welding of two DSS plates of different thickness (30 mm and 50 mm) [2].

Other experimental and calculated parameters are reported in the following table:

Type of process	SAW	
Plate thickness	30 mm	50 mm
η	0.95	
v [m/s]	0.01	0.007
V [V]	29	30
I [A]	600	495
Q_n [J/m]	1653000	2015357
λ [W/(m°K)]	20	
T_0 [°C]	150	
$\Delta t_{8/5}$ [s]	17.4	21.2
$\Delta t_{12/8}$ [s]	7.7	9.4
T_{max} [°C]	1350	
k_1	758	
k_2	279	

Table 1 - Parameters of the Ahrengot model

It can be seen that, using this welding technology and the present parameters, the resulting cooling times in the HAZ (1200/800°C) are very short, 7.7 s for the 30 mm thick plate, and 9.4 s for the thicker plate. The corresponding temperature distribution is reported in figure 1:

Temperature distribution - Model of Ahrengot
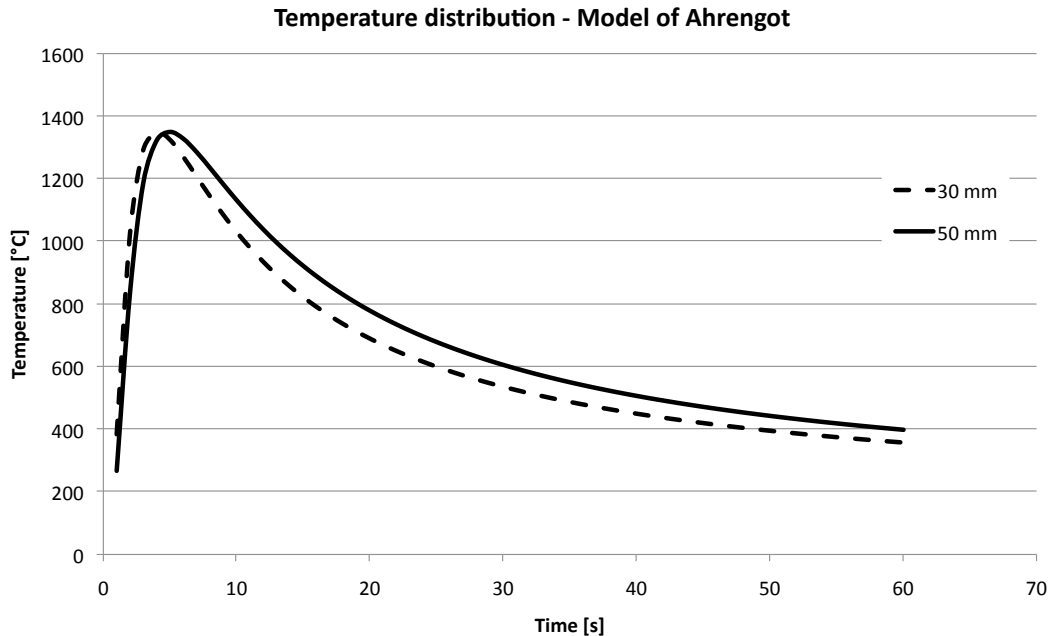
Fig. 1 - Temperature distribution in the HAZ of the 30 and 50 mm materials, evaluated using the model of Ahrengot.

Examining figure 1, it can be noted that the thicker specimen generates a lower cooling rate, with the considered parameters.

It also must be keep in mind that, for Duplex Stainless Steels, a higher cooling rate inhibits the formation of austenite, while a slower cooling rates promotes the formation of secondary phases (cf. §3.3 of section "State of the art").

For example, in <u>Article V</u>, it has been obtained that the critical cooling rate for the sigma phase precipitation is equal to 0.3°C/s for the UNS S31803 and 0.5°C/s for the UNS S32750. Comparing these data with the calculated cooling times, $\Delta t_{12/8}$, using the Ahrengot model, it can be concluded that the final welded joints will not be affected by the presence of sigma phase in the HAZ, both in the case of UNS 31803 and UNS S32750.

2. Influence of welding heat input on corrosion properties of UNS S32750 GTA welded joints

With reference to <u>Article II</u>, other weldings have been performed using the same filler metal (indicated as "Filler A"), but different welding parameters.

The results of this study has been analyzed between the drafting of <u>Article II</u> and <u>Article III</u>. The aim of this work has been to study the influence of heat input on corrosion properties of UNS S32750 GTA welded joints, to consider the hypothesis

that the partitioning of elements could have a valuable influence on corrosion properties of Super Duplex welded joints. In fact, a higher heat input implies a slower cooling rate, which affect the diffusion and the partitioning of elements in the fusion zone, and consequently the resulting pitting corrosion properties.

Travel speed of the three passes has been reduced, and the new welding parameters results to be:

| Run | Process type | Filler metal | Current | | Voltage range [V] | Travel speed [mm/s] | Heat input [kJ/mm] |
		Ø [mm]	Polarization type	Intensity range [A]			
1st	GTAW	1.2	DC-SP	140 ± 5	15.8 ± 0.5	2.5	0.35
2nd	GTAW	1.2	DC-SP	135 ± 5	17.5 ± 0.5	1.33	0.71
3rd	GTAW	1.2	DC-SP	140 ± 5	14.8 ± 0.5	1.33	0.62

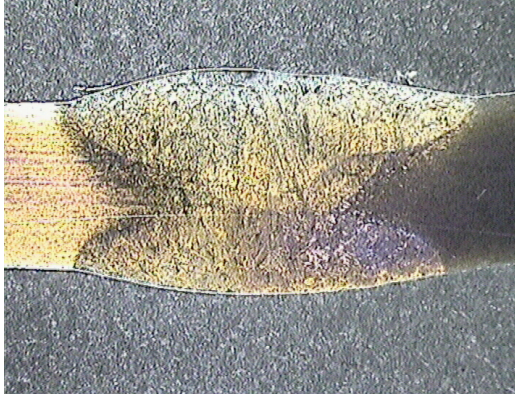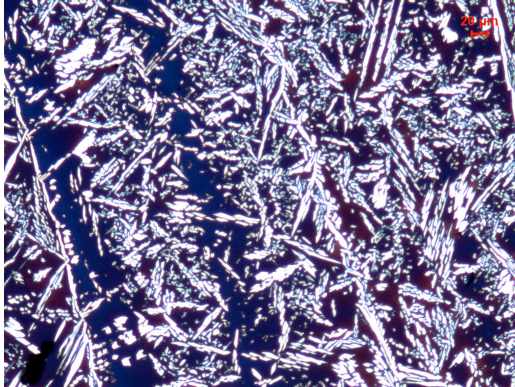*Table 2 - Welding parameters of the new weldings*

The welding parameters considered in Article II are reported in Table 3 for comparison:

| Run | Process type | Filler metal | Current | | Voltage range [V] | Travel speed [mm/s] | Heat input [kJ/mm] |
		Ø [mm]	Polarization type	Intensity range [A]			
1st	GTAW	1.2	DC-SP	185 ± 5	13.5 ± 0.5	4.7	0.21
2nd	GTAW	1.2	DC-SP	205 ± 5	17.7 ± 0.5	2.5	0.58
3rd	GTAW	1.2	DC-SP	200 ± 5	15.4 ± 0.5	4.2	0.29

Table 3 - Welding parameters considered in Article II

It can be seen that the new weldings are characterized by a higher heat input than the weldings considered in Article II.

Results of microstructural analysis on weldings with higher heat input are summarized in the following table, and the corresponding analysis of weldings considered in Article II (Filler A) are reported for comparison:

Low heat input (__Article II__)	High heat input
Cross sections	
Micrographs of fusion zone, Beraha's etching (100x)	
Austenite volume fraction %	
27	32

Table 4 - Results of microstructural analysis on GTA welded joints with different heat input

By examining the results reported in table 4, it can be noted that a higher welding heat input (obtained by a lower travel speed) assures a greater austenite amount in the fusion zone.

Specimens pertaining to the welded joints characterized by higher heat input have been subjected to post welding heat treatments (PWHT), like illustrated in __Article II__. The corresponding austenite volume fractions in function of annealing treatments are summarized in the following table, which contains also the data obtained in __Article II__ for comparison:

Annealing Temperature [°C]	Holding time [min]	Low heat input	High heat input
-	-	27.2	32.0
1050	4	41.2	34.4
	11	41.6	35.2
	18	43.9	36.2
	27	46.8	36.5
1075	4	42.2	34.8
	11	41.0	37.7
	18	43.7	37.9
	27	45.9	40.5
1100	4	42.7	34.9
	11	44.0	37.4
	18	45.5	38.7
	27	47.0	42.9

Table 5 - Austenite volume fractions detected in the fusion zone of the considered specimens

By examining table 5, it can be seen that the fusion zone of specimens welded with higher heat input contains less austenite if compared with the specimens welded using minor heat input. This fact is due to the lower austenite precipitation in relation to post welding heat treatment. In fact, a higher heat input assures a slower cooling and a better partitioning of elements, and the resulting ferrite is more stable and less prone to austenite precipitation.

The corrosion properties have been evaluated by gravimetric tests using ASTM G48 standard. After post welding heat treatment, specimens have been pickled (5 minutes in a 5% HF and 20% HNO_3 solution at 60°C), weighed and immersed in a 6% $FeCl_3$ solution at 50°C for 24 hours. After that, the specimens have been rinsed in water, dried, and weighed again; weight losses have been calculated using equation 8:

$$Corrosion\ Rate = \frac{Wt_i - Wt_f}{A} \tag{8}$$

where Wt_i is the initial weight, Wt_f is the final weight and A is the specimen area.

Figure 2 shows a comparison between the weight losses of the specimens annealed at 1100°C (which has been indicated as the best temperature for the annealing of welded joints considered in Article II), both for the high heat input and the low heat input welded joints. Weight losses for the as-welded specimens results to be equal to 109 g/m² for the high heat input specimen and 175 g/m² for the low heat input one:
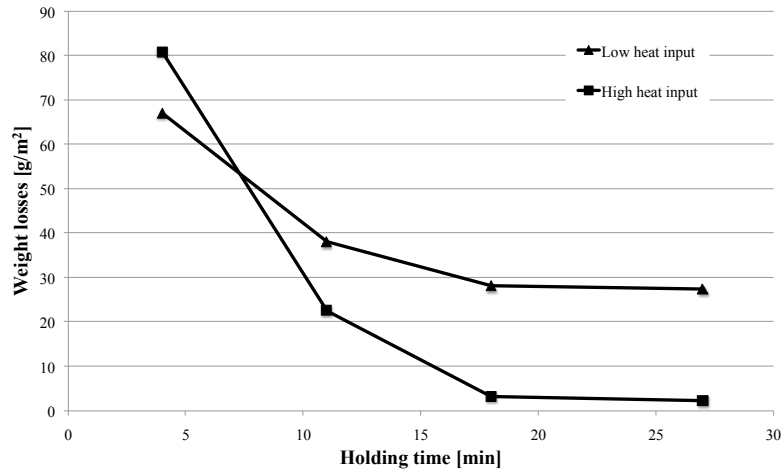
*Fig. 2 - Weight losses of the annealed specimens at 1100°C,
after gravimetric test using ASTM G48 standard*

The weight losses diagrams follow the trend described in Article II: increasing the holding times of PWHT, the pitting corrosion resistance of the welded joints tends to improve.

In addition, the obtained weight losses confirm the assumption that a higher heat input guarantees a better pitting corrosion behavior. In fact, the as-welded specimen exhibits lower weight losses and after heat treatment, the pitting corrosion behavior is better for the joints characterized by a higher heat input, especially for holding times of 11, 18 and 27 minutes.

3. Experimental and numerical analysis of laser welding process on Advanced High Strength Steels

Several new commercial advanced high-strength steels (AHSS) exhibit high strength and enhanced formability. These steels have the potential to affect cost and weight saving while improving performance.

The fusion welding processes have historically been, and they are today, commonly used in manufacturing of automotive structures. Recently, the increased use of AHSS in automotive design posed a desire to evaluate the application of fusion welding processes relative to the joining of AHSS.

Starting from experimental analysis, a numerical model describing the laser welding process of dual-phase (DP) steels has been implemented in this work.

The base material analyzed has been a DP600 steel, having a chemical composition reported in table 6:

C	Mn	Si	S	P	Cr	Ni	Mo	Al	Cu
0.08	1.21	0.29	0	0.01	0.42	0.1	0.25	0.03	0.15

Table 6 - Chemical composition of the base material considered

The considered welding process has been laser welding, using nitrogen as shielding gas and the following parameters: beam power: 1800 and 3000 W, travel speed: 1 and 3 m/min.

3.1 Microstructural analysis

The corresponding macrographs of the cross sections of the welded joints with the calculated fusion zone (FZ) area are reported in figure 3:
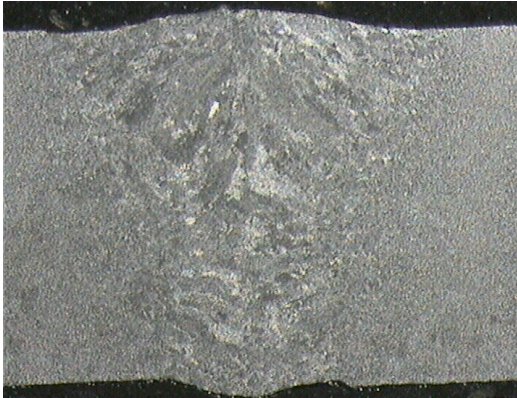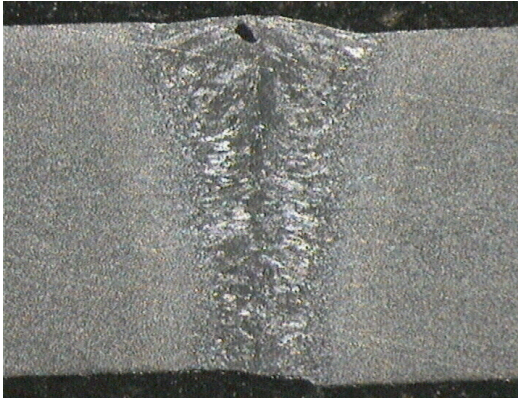
Beam power: 1800W Travel speed: 1 m/min	Beam power: 3000W Travel speed: 3 m/min
Area (FZ) = 2.76 mm²	*Area (FZ) = 1.93 mm²*

Fig. 3 - Cross sections of the laser welded joints

Because of its higher heat input, the fusion zone of the first welded joint results to be wider, like showed by figure 3. Some gas porosities have been found in the fusion zone of the considered weldings, especially in the specimen welded with minor heat input. Metallographic analyses have been carried out by means of Light Optical Microscope and Environmental Scanning Electron Microscope, to establish suitable laser welding parameters. Similar structures have been observed, and the following figures illustrates the metallurgy of the considered welded joints:
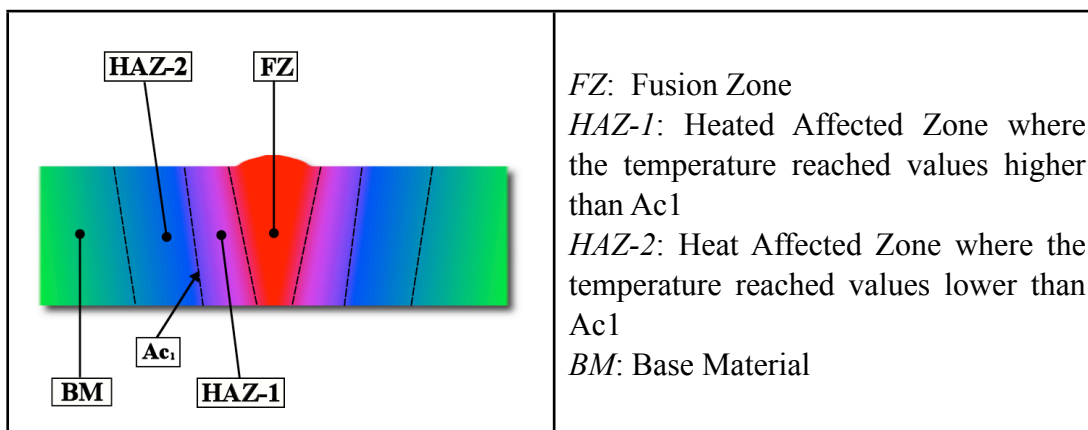

FZ: Fusion Zone
HAZ-1: Heated Affected Zone where the temperature reached values higher than Ac1
HAZ-2: Heat Affected Zone where the temperature reached values lower than Ac1
BM: Base Material

Fig. 4 - Schematic representation of the different zones modified by the welding process, with reference to the work of Mingsheng et al. [3]

Figure 5 shows some optical micrographs of different zones of the welded joint (power 1800W, speed 1m/min), while figure 6 summarizes the corresponding SEM micrographs of the zones identified in figure 4, for both the welding parameters:
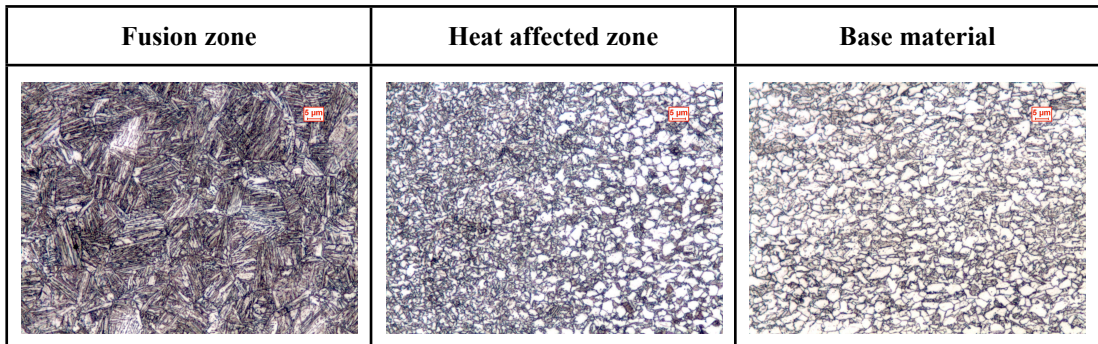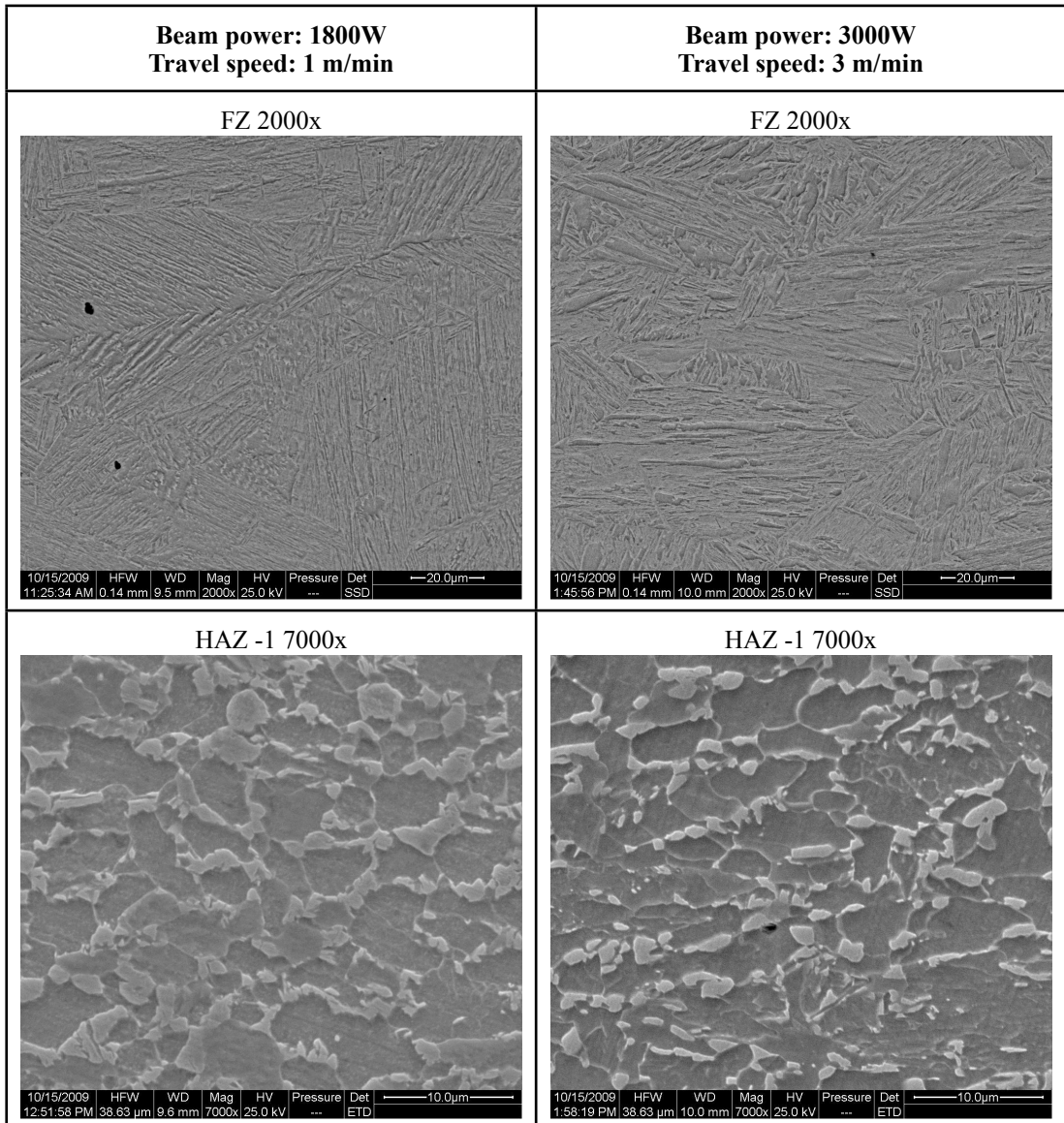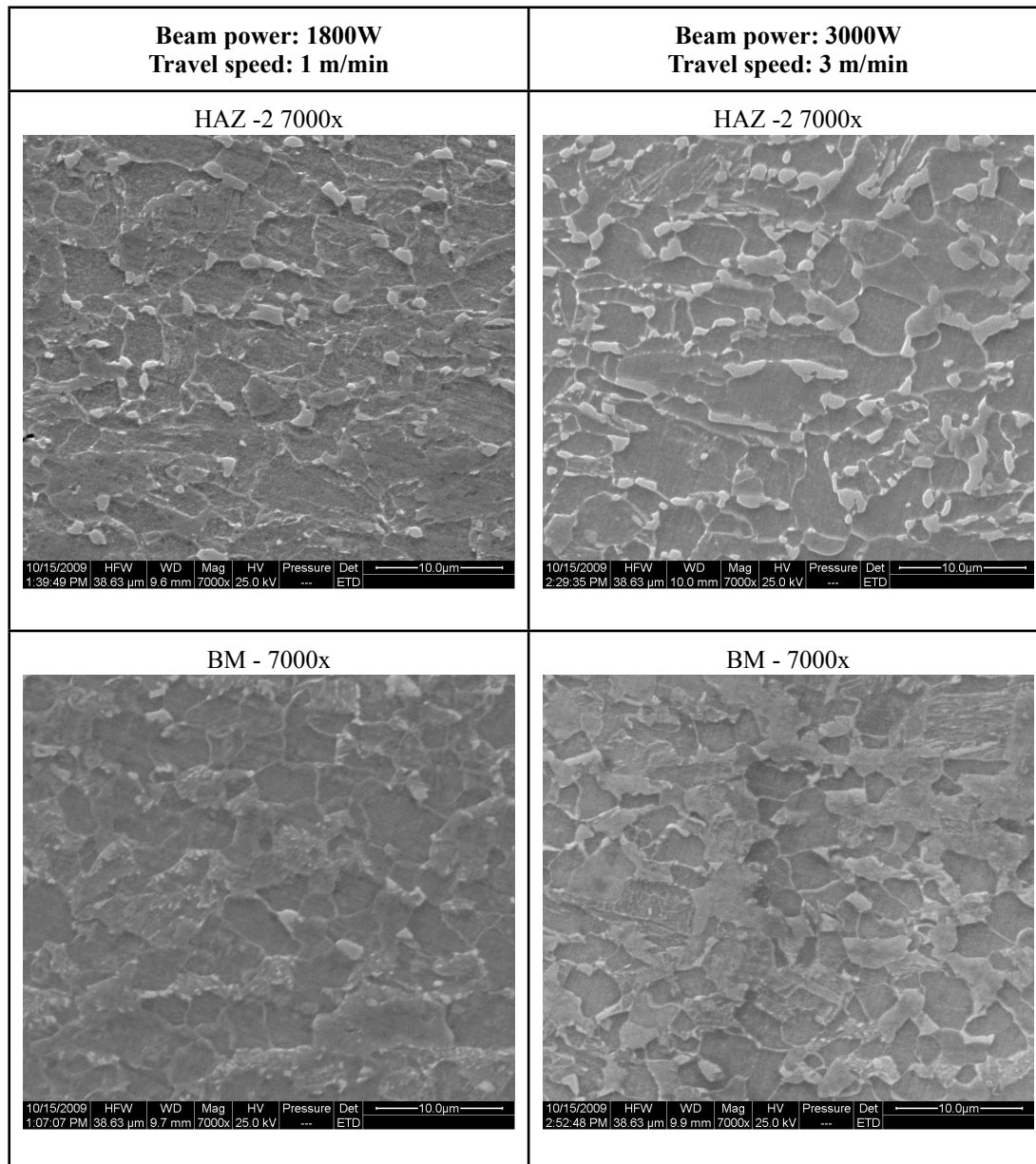
Fusion zone	Heat affected zone	Base material

Fig. 5 - Microstructures of different zones of the welded joints, Nital etching (500x)

Beam power: 1800W Travel speed: 1 m/min	Beam power: 3000W Travel speed: 3 m/min
FZ 2000x	FZ 2000x
HAZ -1 7000x	HAZ -1 7000x

Beam power: 1800W Travel speed: 1 m/min	Beam power: 3000W Travel speed: 3 m/min
HAZ -2 7000x	HAZ -2 7000x
BM - 7000x	BM - 7000x

Fig. 6 - Scanning electron microscope images of the zones identified in fig. 4

By examining figure 5 and 6, it can be observed that the fusion zone (FZ) results fully martensitic, in all the analyzed samples.

The heat affected zone (HAZ-1 and HAZ-2) microstructure is ferritic with martensite islands; the martensite volume fraction decreases with increasing the distance from the fusion zone. The base material results to be constituted by ferrite, with martensite and bainite islands.

The corresponding phase volume fractions and grain size (expressed by equivalent diameter) have been obtained by image analysis of SEM micrographs, and the results are summarized in the following diagrams:
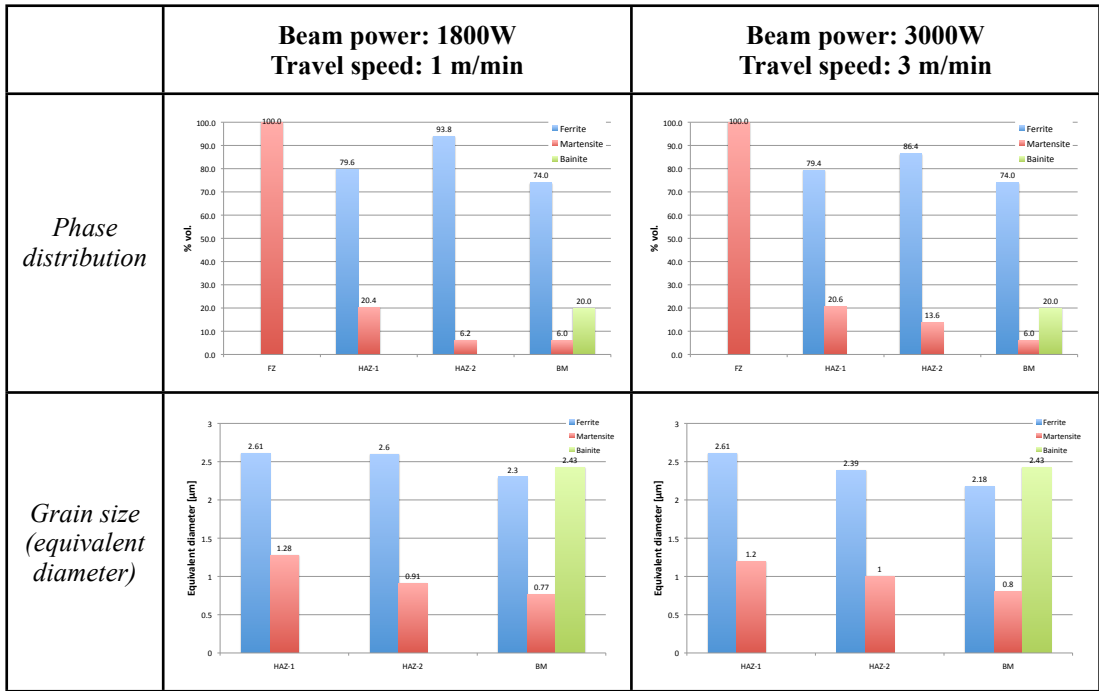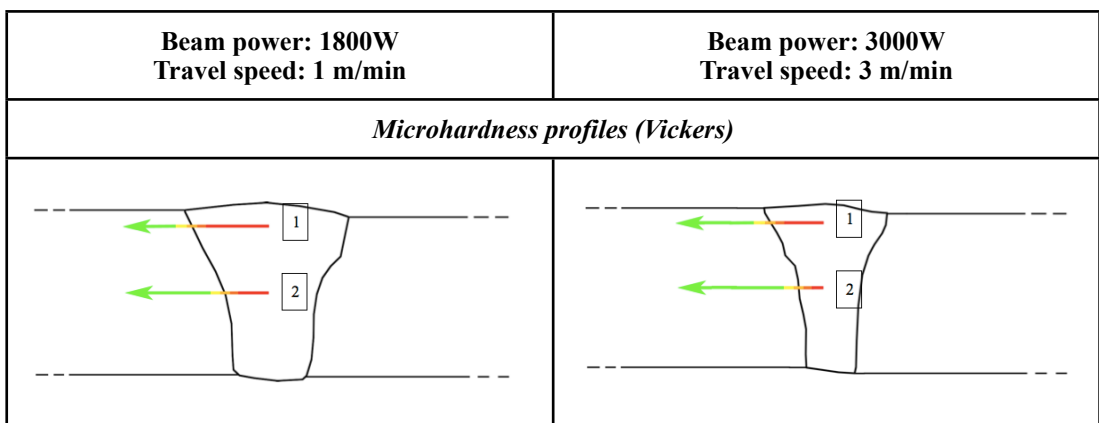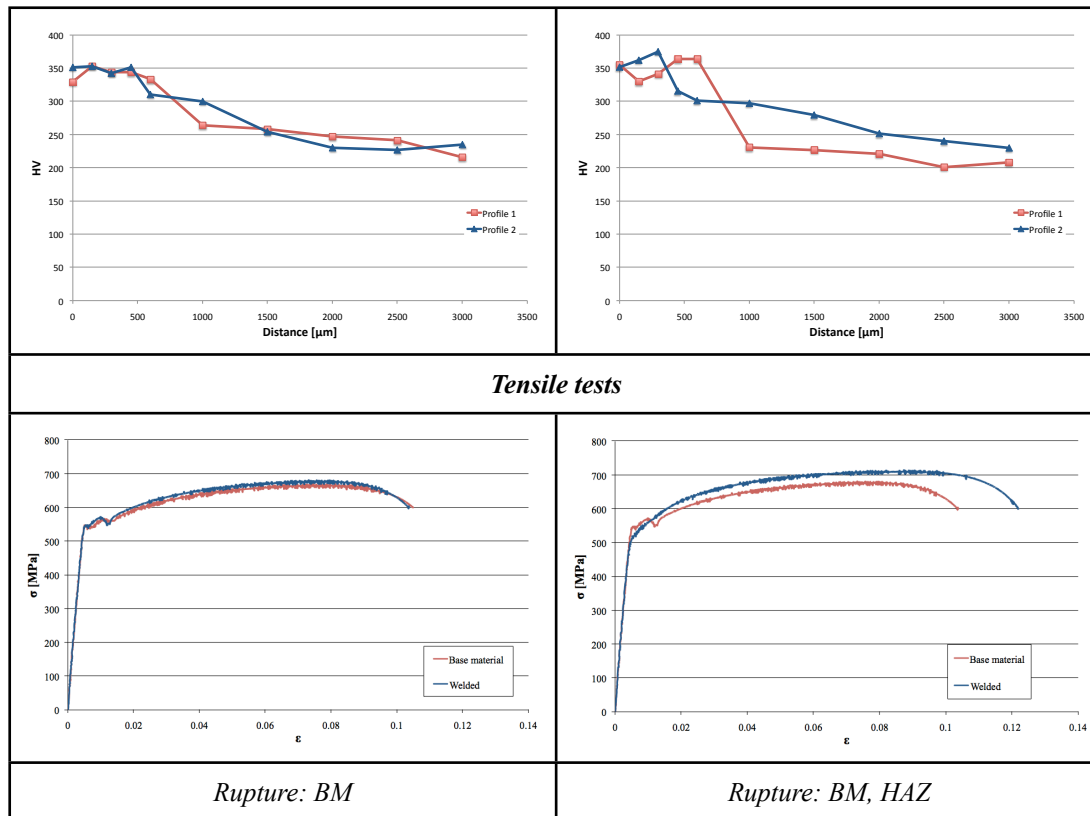
Beam power: 1800W Travel speed: 1 m/min	Beam power: 3000W Travel speed: 3 m/min
Phase distribution	
Grain size (equivalent diameter)	

Fig. 7 - Results of microstructural analysis on DP600 welded joints

It can be seen that the joint welded with higher heat input is characterized by a lower martensite volume fraction in the HAZ, and a coarser ferritic and martensitic grain. In the case of minor heat input, which implies a higher cooling rate, the martensite proportion is higher, and the grain results to be less altered by the welding operation.

3.2 Mechanical properties

The results of Vickers microhardness and tensile tests on DP600 welded joints are summarized in the following figure:

Beam power: 1800W Travel speed: 1 m/min	Beam power: 3000W Travel speed: 3 m/min
Microhardness profiles (Vickers)	

Fig. 8 - Results of mechanical tests on DP600 welded joints

It can be noted that the Vickers microhardness of the fusion zone of the specimen welded with lower heat input is slightly higher than the other specimen, probably for the higher cooling rate which inhibits the diffusion and tends to form a harder martensite. The typical HAZ softening [3] due to the tempered martensite was not observed. In addition, the tensile properties are slight different: the elongation and the ultimate tensile stress (UTS) of the specimen welded with lower heat input is higher if compared with the base material, while the specimen welded with higher heat input shows a tensile behavior similar to the base material. The major percentage of gas porosities found in the specimens welded with the minor heat input is considered the main cause of rupture in HAZ.

3.3 Numerical models

The thermo-metallurgical analysis has been performed by means of the numerical code SYSWELD 2009®. The welding source has been modeled by the superposition of two power density distributions (conical and spherical). The spherical heat source has been used to simulate the plume effect on FZ shape. A good agreement between measured and predicted fusion profile has been obtained, like shown by the following figure:
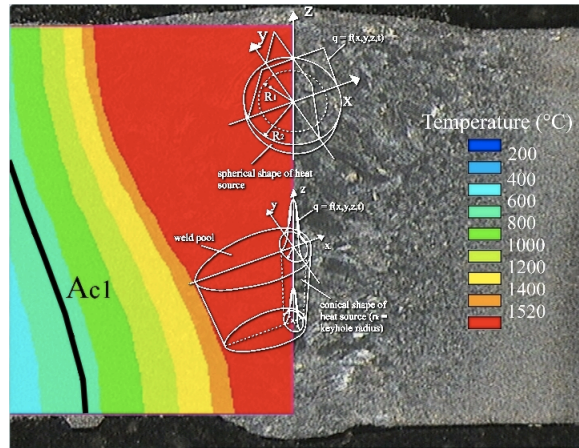
Fig. 9 - Comparison between experimental and calculated fusion profile (welding parameters: travel speed 1 m/min, beam power 1.8 kW)

The metallurgical model has been implemented using Leblond (for ferrite, eq. 9) and Kosten-Marburger's (for martensite, eq. 10) equations, in order to take into account of phase transformations:

$$\frac{dP}{dt} = f\left(\dot{T}\right)\frac{P_{eq}(T) - P}{\tau(T)} \tag{9}$$

$$P(T) = 1 - \exp\left(-b\bullet\left(M_s - T\right)\right) \tag{10}$$

where P is the phase proportion, t is the time, $\dot{T}$ is the heating or cooling rate, T is the temperature, P_{eq} is the phase proportion at equilibrium and τ is the delay time, M_s is the martensite start temperature and b is a law parameter (0.011).

The equation's parameters have been determined using the data found in ref. [4] and the experimental data obtained in this study.

The resulting Continuos-Cooling-Transformation (CCT) curves regarding ferrite and martensite transformations are reported in the following figure:
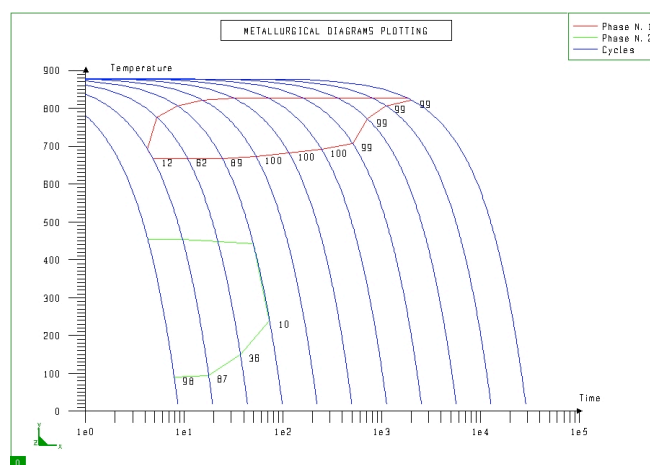

Fig. 10 - CCT curves (Phase 1 = Ferrite, Phase 2 = Martensite) obtained using Leblond and Koisten-Marburger's equations

CCT curves and metallurgical model constitute a useful tool to determine the phase proportions of the welded joint in function of welding parameters.

Thermal and metallurgical simulation of the laser welding process are in good agreement with the experimental tests and finally, optimal laser welding parameters have been found on the basis of microstructure, defects and tensile tests investigation (power beam: 1.8 kW, speed 1 m/min).

REFERENCES

[1] Ø. Grong, "Metallurgical Modelling of Welding", The Institute of Materials, 1994.

[2] H. Sieurin, R. Sandström "Austenite reformation in the heat-affected zone of duplex stainless steel 2205", Mat. Sc. Eng. A418, 2006, 250.

[3] Mingsheng Xia, Elliot Biro, Zhiling Tian and Y. Norman Zhou, "Effects of Heat Input and Martensite on HAZ Softening in Laser Welding of Dual Phase Steels", ISIJ International, Vol. 48, 6 (2008) 809.

[4] Chunling Zhang, Dayong Cai, Yuhui Wang, Mingqing Liu, Bo Liao and Yunchang Fan "Effects of deformation and Mo, Nb, V, Ti on continuous cooling transformation in Cu–P–Cr–Ni–Mo weathering steels", Materials Characterization, Vol. 59, 11 (2008), 1638.